VOL. 16 NO. 1 JANUARY 1968
PUBLISHED MONTHLY

JOURNAL OF

ELECTROANALYTICAL CHEMISTRY

AND INTERFACIAL ELECTROCHEMISTRY

International Journal devoted to all Aspects of Electroanalytical Chemistry, Double Layer Studies, Electrokinetics, Colloid Stability, and Electrode Kinetics.

ELSEVIER

GENERAL INFORMATION

See also Suggestions and Instructions to Authors which will be sent free, on request to the Publishers.

Types of contributions

(a) Original research work not previously published in other periodicals.
(b) Reviews on recent developments in various fields.
(c) Short communications.
(d) Bibliographical notes and book reviews.

Languages

Papers will be published in English, French or German.

Submission of papers

Papers should be sent to one of the following Editors:
Professor J. O'M. BOCKRIS, John Harrison Laboratory of Chemistry, University of Pennsylvania, Philadelphia 4, Pa. 19104, U.S.A.
Dr. R. H. OTTEWILL, Department of Chemistry, The University, Bristol 8, England.
Dr. R. PARSONS, Department of Chemistry, The University, Bristol 8, England.
Professor C. N. REILLEY, Department of Chemistry, University of North Carolina, Chapel Hill, N.C. 27515, U.S.A.

Authors should preferably submit two copies in double-spaced typing on pages of uniform size. Legends for figures should be typed on a separate page. The figures should be in a form suitable for reproduction, drawn in Indian ink on drawing paper or tracing paper, with lettering etc. in thin pencil. The sheets of drawing or tracing paper should preferably be of the same dimensions as those on which the article is typed. Photographs should be submitted as clear black and white prints on glossy paper. Standard symbols should be used in line drawings, the following are available to the printers:

All references should be given at the end of the paper. They should be numbered and the numbers should appear in the text at the appropriate places.
A summary of 50 to 200 words should be included.

Reprints

Fifty reprints will be supplied free of charge. Additional reprints (minimum 100) can be ordered at quoted prices. They must be ordered on order forms which are sent together with the proofs.

Publication

The *Journal of Electroanalytical Chemistry and Interfacial Electrochemistry* appears monthly and has four issues per volume and three volumes per year.
Subscription price: £ 18.18.0 or $ 52.50 or Sfr. 228.00 per year; £ 6.6.0 or $ 17.50 or Sfr. 76.00 per volume; plus postage. Additional cost for copies by air mail available on request. For advertising rates apply to the publishers.

Subscriptions

Subscriptions should be sent to:

ELSEVIER SEQUOIA S.A., P.O. Box 851, 1001 Lausanne 1, Switzerland

JOURNAL OF ELECTROANALYTICAL CHEMISTRY AND INTERFACIAL ELECTROCHEMISTRY

VOL. 16 (1968)

JOURNAL
of
ELECTROANALYTICAL CHEMISTRY
and
INTERFACIAL ELECTROCHEMISTRY

AN INTERNATIONAL JOURNAL DEVOTED TO ALL ASPECTS OF ELECTROANALYTICAL CHEMISTRY, DOUBLE LAYER STUDIES, ELECTROKINETICS, COLLOID STABILITY AND ELECTRODE KINETICS

Vol. 16 1968

ELSEVIER SEQUOIA S.A.
LAUSANNE

PRINTED IN THE NETHERLANDS

ELECTROANALYTICAL CHEMISTRY AND INTERFACIAL ELECTROCHEMISTRY
Elsevier Sequoia S.A., Lausanne – Printed in The Netherlands

CORRECTIONS FOR DOUBLE-LAYER CHARGING IN CHRONOPOTENTIOMETRY*

ROBERT S. RODGERS† AND LOUIS MEITES††
Department of Chemistry, Polytechnic Institute of Brooklyn, Brooklyn, N.Y. (U.S.A.)
(Received March 1st, 1967)

Chronopotentiometric analyses of dilute solutions and investigations of fast coupled chemical reactions are complicated by the necessity of correcting for the charging of the electrical double layer. In deriving the Sand equation[1] it is assumed that the current is entirely consumed by the faradaic process that is of interest. This can never be exactly true: because the potential of the working electrode varies continuously with time, some fraction of the total current must be devoted to double-layer charging at every instant. This has two effects. Because the faradaic current is always smaller than the total current, the transition time always exceeds that computed from the Sand equation; because the charging and faradaic currents are time-dependent, the chronopotentiogram does not have the ideal shape. The magnitudes of these effects depend on the concentration of the electroactive substance and the current density. They are imperceptible if the concentration is not too small and the current density not too great. Transition times are then easy to measure and interpret. At low concentrations or high current densities, the difficulty of measurement increases and deviations from the Sand equation become more pronounced.

The problem was first discussed by GIERST[2], who stressed the ratio of the quantity of electricity, Q_c, consumed in double-layer charging to that, Q_f, consumed in the faradaic process. He described these by equations that may be written:

$$Q_c = i_c \tau = \bar{\varkappa} A \Delta E \tag{1}$$

$$Q_f = i_f \tau = \tfrac{1}{2} \pi^{\frac{1}{2}} n F D^{\frac{1}{2}} A C \tau^{\frac{1}{2}} \tag{2}$$

where $\bar{\varkappa}$ is the average differential capacity of the double layer over the range of potentials, ΔE, included between $t = 0$ and $t = \tau$, i_c and i_f represent charging and faradaic currents, and the other symbols have their usual significances. To account for the effects of anodic oxide-film formation on platinum and other solid electrodes, LINGANE[3] wrote an equation analogous to eqn. (1):

$$Q_{ox} = i_{ox} \tau \tag{3}$$

where Q_{ox} is the quantity of electricity consumed in the formation (or reduction) of

* This paper is based on a thesis submitted by ROBERT S. RODGERS to the Faculty of the Polytechnic Institute of Brooklyn in partial fulfilment of the requirements for the M.S. degree in June, 1966.
† National Science Foundation Undergraduate Research Participant, summer, 1965.
†† To whom correspondence and requests for reprints should be addressed.

the oxide film over the range of potentials, ΔE. BARD[4] included the effect of adsorption of electroactive material by writing

$$Q_{\text{total}} = i\tau = Q_f + Q_c + Q_{ox} + Q_{ads} \tag{4}$$

where Q_{ads}, the quantity of electricity consumed in the oxidation or reduction of the adsorbed material, is given by

$$Q_{ads} = i_{ads}\tau = nF\Gamma \tag{5}$$

Γ being the number of moles of that material adsorbed onto the electrode surface.

It has been assumed that i_c, i_{ox}, and i_{ads} are all constant throughout the electrolysis. If this were so, the occurrence of these extraneous processes would merely cause i_f to be smaller than the total current i, so that

$$i_f = i - (i_c + i_{ox} + i_{ads}) = \frac{\pi^{\frac{1}{2}} nFD^{\frac{1}{2}} AC}{2\tau^{\frac{1}{2}}} \tag{6}$$

The assumption is invalid. The charging current at any instant, given by

$$i_c = -\bar{\varkappa} A\,(\mathrm{d}E/\mathrm{d}t) \tag{7}$$

is large at $t = 0$, passes through a minimum at the point where the slope of the chronopotentiogram is smallest, and increases again as the concentration of the electroactive substance at the electrode surface approaches zero. Hence i_f varies, and eqn. (6) is incorrect. The behaviors of i_{ox} and i_{ads} are qualitatively different, as is discussed in a subsequent paragraph, but their values, too, are time-dependent. In this paper, attention is confined to the charging-current problem. The discussion is based on chronopotentiograms synthesized by numerical solutions of partial differential equations that include the effects of double-layer charging. Both reversible and totally irreversible couples are considered. A procedure is described for the evaluation of the transition time from a single chronopotentiogram that includes a substantial contribution from double-layer charging.

THEORY AND COMPUTATIONAL PROCEDURE

We shall consider the cathodic chronopotentiogram obtained for the half-reaction $O + ne = R$. Fick's second law,

$$\frac{\partial C}{\partial t} = D\frac{\partial^2 C}{\partial x^2} \tag{8}$$

may be transformed into a difference equation by writing

$$C_O(x, t) = C(I, K); \quad x = (I-1)\Delta x; \quad t = K\Delta t \tag{9}$$

so that, for example, the concentration of O at the electrode surface at time t is represented by C(1, K). Replacing $\partial C/\partial t$ by $\Delta C/\Delta t$ and $\partial^2 C/\partial x^2$ by $\Delta(\Delta C/\Delta x)/\Delta x$, eqns. (8) and (9) may be combined to give

$$C(I, K+1) = G[C(I+1, K) - 2C(I, K) + C(I-1, K)] + C(I, K) \tag{10}$$

where

$$G = D\Delta t/(\Delta x)^2 \tag{11}$$

FELDBERG AND AUERBACH[5], who computed chronopotentiograms by a similar pro-

cedure (but without taking double-layer charging into account), found that the condition $G < \frac{1}{2}$ must be satisfied to produce convergence; in these computations we used $G = 0.474$. Concentration profiles were computed by assuming C(I, K) to be constant and equal to $C_O{}^b$, the initial bulk concentration of O, at all K when $I \geq 500$. This is equivalent to restricting the concentration gradient to 500 Δx-intervals. Identical potentials were obtained on doubling this number.

The concentration gradient at the electrode surface is described by

$$i = nFDA \left(\frac{\partial C_O}{\partial x}\right)_{x=0} - \varkappa A \frac{dE}{dt} \tag{12}$$

If the half-reaction is reversible, a description of dE/dt may be obtained by differentiating the Nernst equation:

$$\frac{dE}{dt} = \frac{RT}{nF}\left[\left(\frac{1}{C_O}\frac{\partial C_O}{\partial t}\right)_{x=0} - \left(\frac{1}{C_R}\frac{\partial C_R}{\partial t}\right)_{x=0}\right] \tag{13}$$

Assuming that the diffusion coefficients of O and R are identical, the concentrations of O and R at any x and t will be related by

$$C_R(x,t) + C_O(x,t) = CT \tag{14}$$

where CT is the sum of their concentrations in the bulk of the solution. Accordingly eqn. (12) becomes

$$i = \frac{nFDA}{\Delta x}\left[C(2, K+1) - C(1, K+1)\right] - \frac{RT\varkappa A}{nF\Delta t}\left[\frac{C(1, K+1)}{C(1, K)} - \frac{CT - C(1, K+1)}{CT - C(1, K)}\right] \tag{15}$$

Replacing Δx by $(D\Delta t/G)^{\frac{1}{2}}$ from eqn. (11), dividing through by i, and replacing $nFAD^{\frac{1}{2}}/i$ by $2\tau_s{}^{\frac{1}{2}}/\pi^{\frac{1}{2}}C_O{}^b$, where τ_s is the Sand-equation transition time, we obtain

$$\begin{aligned} 1 = {} & \frac{2G^{\frac{1}{2}}}{(\Delta t/\tau_s)^{\frac{1}{2}}}\left[\frac{C(2, K+1) - C(1, K+1)}{C_O{}^b}\right] \\ & - \frac{RT\varkappa A}{nFi\tau_s}\left(\frac{1}{\Delta t/\tau_s}\right)\left[\frac{C(1, K+1)}{C(1, K)} - \frac{CT - C(1, K+1)}{CT - C(1, K)}\right] \end{aligned} \tag{16}$$

The ratio $\Delta t/\tau_s$ was usually taken as 1/3000. In some cases, however, the rate of change of potential was so small that the computations had to be carried far beyond $t = \tau_s$. The value of $\Delta t/\tau_s$ was then quadrupled, while that of Δx was doubled to maintain G constant. Because values of C(I,K) appear only as ratios, the shape of the chronopotentiogram depends only on the values of G, $\Delta t/\tau_s$, and $\varkappa A/ni\tau_s$. The first and second of these affect only the accuracy of the numerical solution; it is the third that is of physical interest.

Most of the computations were performed with $CT = 1.0005\, C_O{}^b$, so that the initial potential was $195/n$ mV more positive than the formal potential; a few were performed with $CT = 1.001\, C_O{}^b$ and a few with $CT = 1.01\, C_O{}^b$. Starting with C(0,0) = C(1,0) = $C_O{}^b$, eqn. (16) was used to compute C(0, 1), the concentration of O at the electrode surface when $t = \Delta t$. The surface concentration of R was then obtained from eqn. (14), and the potential was computed by combining these concentrations with the Nernst equation. Subsequent computations employed eqns. (10) and (16) in straightforward fashion.

If the half-reaction is totally irreversible, eqn. (15) must be replaced by

$$i = \frac{nFDA}{\Delta x}[C(2, K+1) - C(1, K+1)]$$

$$- \frac{RT\varkappa A}{\alpha n_a F \Delta t}\left[\frac{C(1, K+1)}{C(1, K)} - \frac{C(2, K+1) - C(1, K+1)}{C(2, K) - C(1, K)}\right] \quad (17)$$

so that the fundamental normalizing parameter is $\varkappa A/\alpha n_a i\tau_s$.

Most of the calculations were performed with constant values of the appropriate normalizing parameters, which is equivalent to assuming $\varkappa$ to be independent of potential. A sub-routine was developed to remove this assumption; it involves the use of an empirical equation or set of equations relating $\varkappa$ to the potential throughout the range of interest. GRAHAME's data[6] on the differential capacities at mercury electrodes over the range of potentials from +0.03 to −1.85 V *vs.* S.C.E. in 0.1 *F* potassium chloride could not be reproduced to our satisfaction by any single polynomial, and a set of three parabolas, obtained by least-squares techniques, was used instead.

To obtain an estimate of the reliability of the transition times resulting from these calculations, a similar computation was performed with $\kappa = 0$. The transition was found to occur at $t = 2931\ \Delta t$ rather than at the theoretical $t = \tau_s = 3000\ \Delta t$. The error is comparable with that obtained by FELDBERG AND AUERBACH[5]. Inordinate amounts of computer time would have been needed to obtain significantly better results. The ratios of times, which are alone of real interest, are felt to be considerably more reliable than the absolute values.

Programs written in Fortran IV are given in full in the junior author's thesis.

RESULTS AND DISCUSSION

Figures 1 and 2 show typical curves for reversible and totally irreversible couples, drawn for $n = 1$ and $\alpha n_a = 0.5$, respectively, over wide ranges of the appropriate normalizing parameters. Their most prominent features—the initial nearly linear portion, in which most (though, as is shown below, by no means all) of the current is consumed in double-layer charging, and the final curvature resulting from the slow decrease of the faradaic current as depletion of the diffusion layer becomes more and more extensive—have been recognized for a long time and discussed in several reviews[7,8]. More fundamental descriptions of these features are provided by Fig. 3, which is drawn for a reversible couple in circumstances that are not at all extreme.

The faradaic current efficiency rises rapidly at the start of the chronopotentiogram, and in this case reaches 0.20 at a potential $100/n$ mV more positive than the half-wave potential (*i.e.*, the theoretical quarter-transition-time potential). Even though the initial portion of the chronopotentiogram may appear to be linear, its slope will be considerably smaller than the value $(-i/\varkappa A)$ that would represent pure double-layer charging unless the initial potential is much more positive than $E_{\frac{1}{4}} + 100/n$ mV. This is illustrated by Fig. 4. The faradaic current efficiency rises to a maximum value, which decreases as $\varkappa A/ni\tau_s$ increases, at a potential that is always more negative than the half-wave potential and that becomes more negative as $\varkappa A/ni\tau_s$ increases. Increases of $\varkappa A/\alpha n_a i\tau_s$ have the same effects in the irreversible case. Beyond the

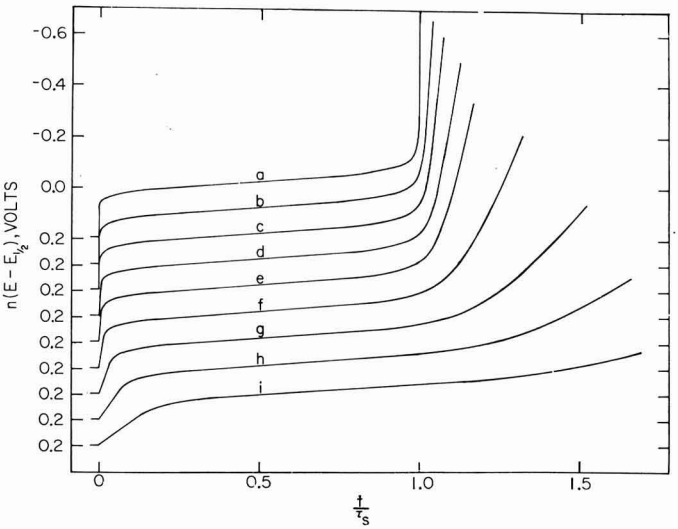

Fig. 1. Calcd. chronopotentiograms for a reversible couple with $\varkappa A/ni\tau_s$ = (a), 0; (b), 0.00648; (c), 0.0130; (d), 0.0259; (e), 0.0415; (f), 0.1037; (g), 0.259; (h), 0.518; (i), 1.037 V^{-1}. The potential, $E_{\frac{1}{4}}$, is the quarter-transition-time potential in the absence of double-layer charging. The initial potential is assumed to be $195/n$ mV more +ve than $E_{\frac{1}{4}}$.

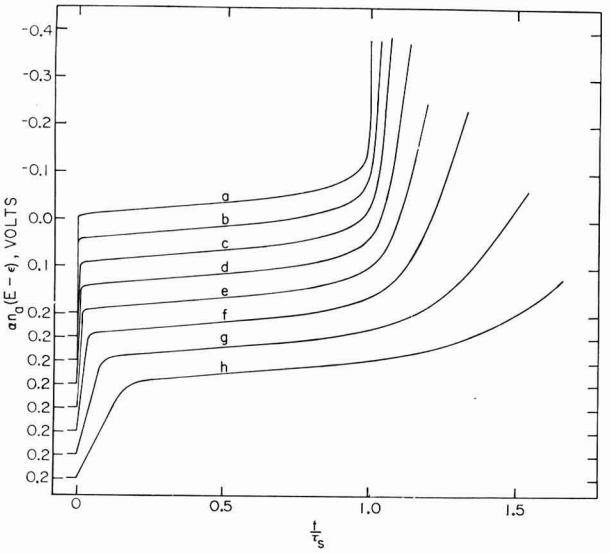

Fig. 2. Calcd. chronopotentiograms for a totally irreversible couple with $\varkappa A/\alpha n_a i\tau_s$ = (a), 0; (b), 0.00782; (c), 0.01564; (d), 0.0391; (e), 0.0782; (f), 0.1564; (g), 0.391; (h), 0.782 V^{-1}. The potential, ε, is the quarter-transition-time potential in the absence of double-layer charging.

maximum, the faradaic current efficiency decreases very slowly, and finally becomes almost constant. This is why, as was noted by RUSSELL AND PETERSON[9], chronopotentiograms generally appear to become linear at very negative potentials.

Graphical procedures for the evaluation of transition times are quite unable to cope with the distortion resulting from this dependence of faradaic current efficiency

on potential. The behavior of REINMUTH's procedure[10], for example, is shown in Fig. 5: in this case it overestimates the transition time by 13.2%. It is interesting to note that KUWANA's procedure, which was found both by RUSSELL AND PETERSON[9] and by HAWLEY AND ADAMS[11] to yield better results than REINMUTH's in other circumstances, is very much inferior to it here: for the curve of Fig. 5, KUWANA's

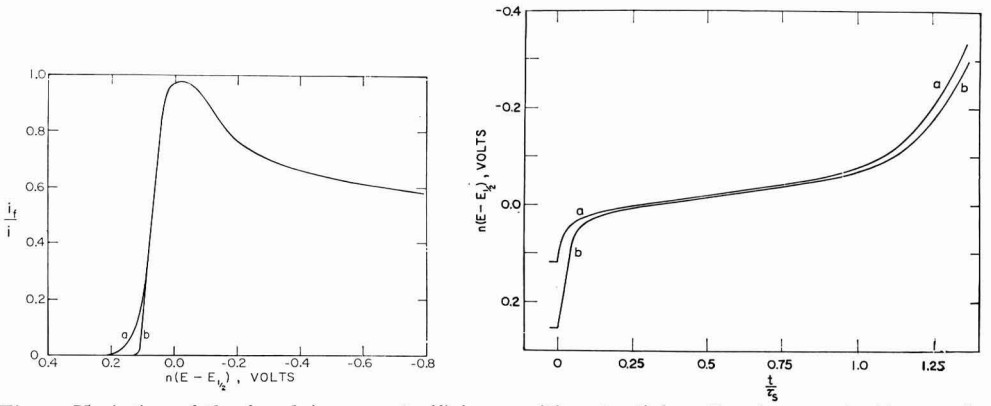

Fig. 3. Variation of the faradaic current efficiency with potential on the chronopotentiogram for a reversible couple when $\varkappa A/ni\tau_s = 0.1037\ V^{-1}$ and when the initial potential is: (a), $200/n$; (b), $120/n$ mV more +ve than $E_{\frac{1}{4}}$.

Fig. 4. Calcd. chronopotentiograms for a reversible couple when $\varkappa A/ni\tau_s = 0.1037\ V^{-1}$ and when the initial potential is: (a), $120/n$; (b), $240/n$ mV more +ve than $E_{\frac{1}{4}}$.

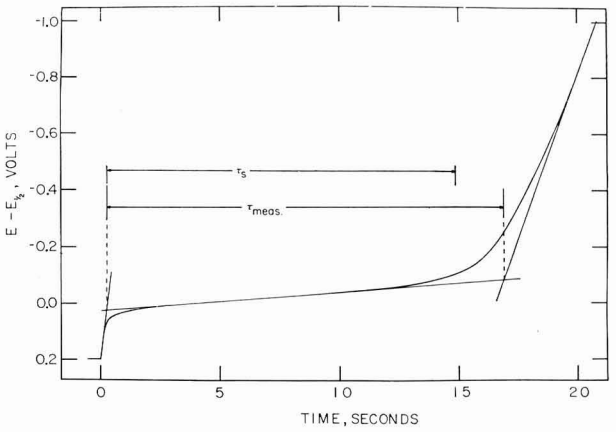

Fig. 5. Comparison of the transition time, $\tau_{meas.}$, obtained by applying REINMUTH's procedure to curve (f) of Fig. 1, with the Sand-equation transition time, τ_s. The time-scale was obtained by arbitrarily letting $\Delta t = 5$ msec, so that the value of τ_s obtained from the computer solution was $2931 \times 0.005 = 14.66$ sec.

procedure overestimates the transition time by 22.6%. This is simply because it is equivalent to measurement at a more negative potential. The procedure of DELAHAY AND MATTAX[12] is equivalent to measurement at the apparent quarter-transition-time potential, which is more positive than that employed in REINMUTH's procedure, and therefore it yields a slightly better result. However, the difference of potential is so

small that the error is decreased only to 11.1% in this case. Even if the distance between the extrapolated lines is measured at the initial potential, an error of 7.1% is still incurred. The last of these techniques tends to underestimate the transition time because the current consumed in double-layer charging in the apparently linear final section of the chronopotentiogram is larger than the average value. However, this is overbalanced by the fact that the double-layer charging increases the time required to attain that section, so that much more O is reduced than would have to be reduced to attain the same range of potentials in the absence of double-layer charging.

From such considerations it is clear that no graphical technique can yield an accurate value of the transition time when the charging current is appreciable. The approximate values of $\varkappa A/ni\tau_s$ and $\varkappa A/\alpha n_a i\tau_s$ below which each of these techniques leads to errors not exceeding 1% in τ, are listed in Table 1. Although this analysis is formally equivalent to that given by GIERST[2] and DELAHAY[7], the values in Table 1 are much more restrictive. These authors took $\Delta E = 0.1$ V for the range of potentials covered by the chronopotentiogram, but Fig. 5 shows that this is far too small, and that $\Delta E = 0.5/n$ V is a more realistic figure for a reversible couple (as is $\Delta E = 0.5/\alpha n_a$ V for a totally irreversible one).

TABLE 1

VALUES OF THE NORMALIZING PARAMETERS YIELDING ERRORS OF 1% IN TRANSITION-TIME MEASUREMENTS BY VARIOUS GRAPHICAL TECHNIQUES

For both reversible and totally irreversible couples, this table gives estimates of the values of the normalizing parameters that lead to measured transition times exceeding the theoretical values by 1%. Because all of these procedures involve the construction of more or less arbitrary extrapolations, the estimates are correspondingly arbitrary.

Technique	*Maximum value of the normalizing parameter for an error not exceeding 1%*	
	$\varkappa A/ni\tau_s$	$\varkappa A/\alpha n_a i\tau_s$
REINMUTH[10]	0.0028	0.021
KUWANA[9,11]	0.0016	0.0036
DELAHAY–MATTAX[12]	0.0037	0.071
Extrapolation to initial potential	0.0065	0.0047

The evaluation of the transition time must therefore be based on a measurement of the time τ_m required to attain some definite preselected potential, as was suggested by LINGANE[3] and BARD[4]. BARD proposed two procedures, both based on eqn. (6) in the form

$$i\tau_m = (i_c + i_{ox} + i_{ads})\tau_m + (\pi^{\frac{1}{2}} nFD^{\frac{1}{2}} AC/2\tau_s^{\frac{1}{2}})\ \tau_m \qquad (18)$$

Over any fixed range of potentials, the first term on the right-hand side represents a constant quantity of electricity Q, which is equal to the value of Q_c described by eqn. (1) if double-layer charging is the only extraneous process involved. Equating τ_s and τ_m as a first approximation, one may write either

$$i\tau_m = Q + k\tau_m^{\frac{1}{2}} \qquad (19)$$

where k is the chronopotentiometric constant $\pi^{\frac{1}{2}} nFD^{\frac{1}{2}} AC/2 = i\tau_s^{\frac{1}{2}}$, or

$$i\tau_m^{\frac{1}{2}} = Q/\tau_m^{\frac{1}{2}} + k \qquad (20)$$

Figures 6 and 7 show the behaviors of plots based on eqns. (19) and (20) for both reversible and irreversible couples over most of the ranges of values of the normalizing parameters covered by Figs. 1 and 2. For convenience, these figures are drawn for $i\tau_s^{\frac{1}{2}} = 100\ \mu A\ sec^{\frac{1}{2}}$. The straight line in Fig. 6 and line (e) in Fig. 7 are drawn with the theoretical slopes. In Fig. 7 the values of ΔE were fixed by measuring τ_m from $E_{\frac{1}{2}} + 100$ mV to $E_{\frac{1}{2}} - 200$ mV (curve *a*) or $E_{\frac{1}{2}} - 400$ mV (curve *b*) in the reversible case; this choice of initial potential leads to an error of only -0.05% in τ when $\varkappa A/ni\tau_s = 0$. In the irreversible case, with $\alpha n_a = 0.5$ (curves *c* and *d*), each of these numerical values was doubled.

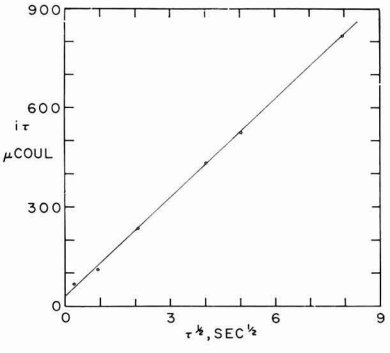

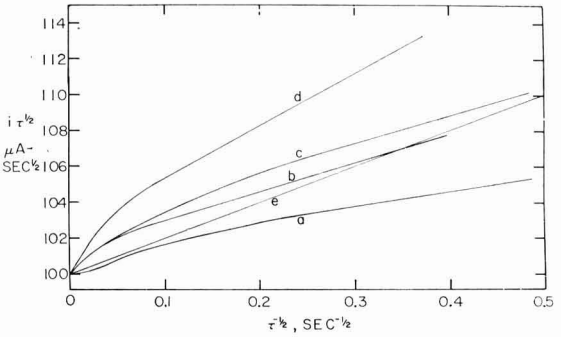

Fig. 6. Variation of $i\tau_m$ with $\tau_m^{\frac{1}{2}}$ for the data of Fig. 1, taking τ_m as the time that elapses between the instants at which $E = E_{\frac{1}{2}} + 195$ mV and $E = E_{\frac{1}{2}} - 400$ mV. Here and in Fig. 7, the coordinate scales were obtained by arbitrarily letting $i\tau_s^{\frac{1}{2}} = 100\ \mu A\ sec^{\frac{1}{2}}$, $\varkappa A = 20\ \mu F$, and $n = 1$.

Fig. 7. Variations of $i\tau_m^{\frac{1}{2}}$ with $\tau_m^{-\frac{1}{2}}$ for the data of Figs. 1 and 2, taking τ_m as the time that elapses between the instants at which: (a), $E = E_{\frac{1}{2}} + 100$ mV and $E = E_{\frac{1}{2}} - 200$ mV for a reversible couple; (b), $E = E_{\frac{1}{2}} + 100$ mV and $E = E_{\frac{1}{2}} - 400$ mV for a reversible couple; (c) $E = \varepsilon + 200$ mV and $E = \varepsilon - 400$ mV for a totally irreversible couple; (d), $E = \varepsilon + 200$ mV and $E = \varepsilon - 800$ mV for a totally irreversible couple. In curves (c) and (d) the value of αn_a is arbitrarily assumed to be 0.5. Curve (e) represents the prediction of eqn. (20) under the conditions of curve (d).

Although the plot in Fig. 6 appears to be much the more satisfactory of the two, the difference between them is largely illusory. When $i\tau_s^{\frac{1}{2}}$ and ΔE are fixed, larger values of $\varkappa A/ni\tau_m$ for a reversible couple, or of $\varkappa A/\alpha n_a i\tau_m$ for an irreversible one, correspond to smaller values of τ_m and thus to higher current densities. Most of Fig. 6 is therefore taken up by the range in which $\varkappa A/ni\tau_m$ is small. The proper value of $i\tau_s^{\frac{1}{2}}$ is obtained from the slope of the line, not because the proper correction is made for the effect of double-layer charging, but because the line is based on data obtained under such conditions that this effect is imperceptibly small.

The intercept of a plot can usually be evaluated more precisely than its slope, but an extrapolation based on Fig. 7 would inspire little confidence. Here the normalizing parameter is negligible only in the lower left-hand corner, and the failure of eqn. (20) and its ancestors to provide an adequate correction for double-layer charging becomes clearly evident. A plot of this type must always lead to an overestimate of $i\tau_s^{\frac{1}{2}}$, and the overestimate must be appreciable unless the data are confined to the region where double-layer charging is really unimportant.

Whichever form it takes, the Lingane–Bard treatment owes its success to its

reliance on data obtained when τ_m is relatively large. To achieve such conditions may not always be feasible even in purely analytical work, for convection may begin to become important before a sufficiently large value of τ_m is attained, and may be even more seriously disadvantageous in attempts to investigate the rates and mechanisms of fast reactions.

For such purposes, and also to obviate the necessity of recording a number of chronopotentiograms at different current densities, as must be done before the Lingane–Bard treatment can be applied, it would be desirable to be able to make a direct correction for the effect of double-layer charging on a single chronopotentiogram. Because the shape of a chronopotentiogram is uniquely defined by the value of $\varkappa A/ni\tau_s$ or $\varkappa A/\alpha n_a i\tau_s$, the relation between τ_m/τ_s and the appropriate normalizing parameter is single-valued for any pair of potentials—$E_{\frac{1}{4}}+x/n$ mV and $E_{\frac{3}{4}}-y/n$ mV for a reversible couple, or $\varepsilon+x/\alpha n_a$ mV and $\varepsilon-y/\alpha n_a$ mV for an irreversible one—between which τ_m is measured. The symbol ε denotes the quarter-transition-time potential for the irreversible process in the absence of double-layer charging. Large-scale plots of these relations are easily constructed from the interpolated values given in Tables 2 and 3, and are easily used to obtain τ_s from a measured value of τ_m, using known values of n (or αn_a) and i, together with an estimate of $\varkappa A$. Chronopotentiograms calculated by taking the actual potential-dependence of $\varkappa$ into account are only insignificantly different from those calculated with a constant average value of $\varkappa$. It is therefore appropriate to evaluate $\varkappa A$ by recording the chronopotentiogram of the supporting electrolyte alone at a suitably low current density, measuring the

TABLE 2

VALUES OF τ_m/τ_s FOR REVERSIBLE COUPLES FOR VARIOUS RANGES OF POTENTIAL AND VALUES OF $\varkappa A/ni\tau_m$

The values in the body of this table and in that of Table 3 were obtained by interpolation on large-scale plots. The value of τ_m is defined as the time that elapses between the instant at which the potential is $E_{\frac{1}{4}} + 100/n$ mV and that at which it is $E_{\frac{3}{4}} - y/n$ mV.

$\varkappa A/ni\tau_m$ (V^{-1})	*Value of* τ_m/τ_s *when* $y =$		
	200	*300*	*400*
0			
0.010	1.012	1.024	1.035
0.025	1.031	1.054	1.078
0.050	1.061	1.106	1.132
0.075	1.090	1.154	1.185
0.100	1.119	1.195	1.236
0.125	1.146	1.233	1.287
0.150	1.171	1.270	1.338
0.175	1.196	1.306	1.389
0.200	1.221	1.343	1.441
0.250	1.270	1.415	1.544
0.300	1.319	1.487	1.646
0.350	1.368	1.559	
0.400	1.418	1.631	
0.450	1.467		
0.500	1.516		
0.550	1.565		
0.600	1.614		
0.650	1.663		

time required to traverse the range of potentials, ΔE, employed in measuring τ_m, and computing $\varkappa A$ from eqn. (1).

A brief investigation of the effect of double-layer charging on the ratio of the reverse to the forward transition times in current-reversal chronopotentiometry led to the results shown in Fig. 8. Both O and R were assumed to be soluble and to have

TABLE 3

VALUES OF τ_m/τ_s FOR TOTALLY IRREVERSIBLE COUPLES FOR VARIOUS RANGES OF POTENTIAL AND VALUES OF $\varkappa A/\alpha n_a i\tau_m$

The value of τ_m is defined as the time that elapses between the instant at which the potential is $\varepsilon + 100/\alpha n_a$ mV and that at which it is $\varepsilon - y/\alpha n_a$ mV.

$\varkappa A/\alpha n_a i\tau_m$, ($V^{-1}$)	*Value of* τ_m/τ_s *when* $y =$		
	200	*300*	*400*
0			
0.005	1.010	1.016	1.022
0.010	1.018	1.030	1.040
0.020	1.032	1.054	1.070
0.030	1.046	1.074	1.096
0.040	1.059	1.092	1.118
0.050	1.070	1.108	1.137
0.060	1.080	1.122	1.156
0.070	1.089	1.135	1.175
0.080	1.098	1.149	1.194
0.090	1.108	1.163	1.212
0.100	1.117	1.176	1.231
0.120	1.135	1.204	1.268
0.140	1.154	1.232	1.305

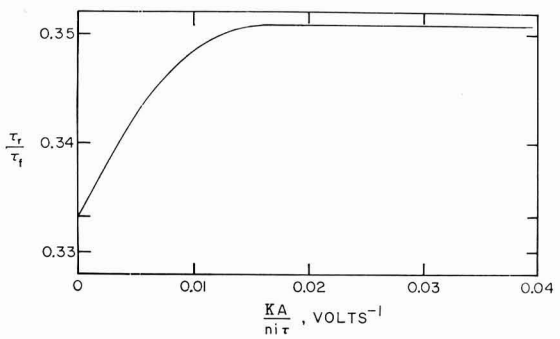

Fig. 8. Effect of $\varkappa A/ni\tau_s$ on the ratio τ_r/τ_f in current-reversal chronopotentiometry for a reversible couple. The quantity τ_s is the Sand-equation transition time for the forward transition; τ_r and τ_f are the measured times for the traversal of the range of potentials given in the text.

equal diffusion coefficients. It was assumed that the current was reversed at $E_{\frac{1}{4}} - 400/n$ mV, and τ_f is the time required to reach this point from an initial potential of $E_{\frac{1}{4}} + 200/n$ mV. The reverse transition time, τ_r, is the additional time then required to reach the original potential again. With $\varkappa = 0$ the computations yielded $\tau_r/\tau_f = 0.325$ instead of the expected value[13], $\frac{1}{3}$, and therefore the values plotted in Fig. 8 have been corrected for computational error by multiplying them by 0.333/0.325. The

quantity of electricity consumed by double-layer charging is the same for the reverse process as for the forward process, but because τ_r is smaller than τ_f, the average charging current is larger in the reverse process. Hence, although increasing $\varkappa A/ni\tau_s$ increases both τ_r and τ_f, it increases the former much more rapidly than the latter.

The results and conclusions described here are valid only when the extraneous consumption of electricity is wholly due to double-layer charging. When this is so, the current efficiency for the process of interest passes through a maximum at some potential between the start of the chronopotentiogram and the potential at which the transition time is measured, as is shown by Fig. 3. If, on the other hand, the extraneous consumption of electricity is due to the anodic formation or cathodic reduction of an oxide or other film, to the oxidation or reduction of adsorbed material, or to any other faradaic process, the current efficiency for the process of interest may pass through either a maximum or a minimum or may even fortuitously remain nearly constant. Its behavior will depend on how the rates of the competing electron-transfer processes vary with potential. Unless these variations are identical, which will not often be the case, it seems evident that the Lingane–Bard treatment can succeed only to the extent that it can be based on data obtained at transition times so long that the extraneous process consumes only an insignificant fraction of the total quantity of electricity.

SUMMARY

Numerical computations of linear-diffusion chronopotentiograms distorted by double-layer charging are used to show that previously proposed corrections are erroneous in principle and to devise a simple empirical procedure for evaluating the Sand-equation transition time from a measurement of the time required for the traversal of an arbitrary range of potentials on a single chronopotentiogram. The effect of double-layer charging in current-reversal chronopotentiometry is to increase the ratio of the reverse transition time to the forward one. Double-layer charging and extraneous faradaic processes have different effects on the time-dependence of the current efficiency for the process of interest, and corrections for them must therefore be made in different ways.

REFERENCES

1 H. J. S. Sand, *Phil. Mag.*, 1 (1901) 45.
2 L. Gierst, Thesis, Université Libre de Bruxelles, 1952.
3 J. J. Lingane, *J. Electroanal. Chem.*, 1 (1960) 379.
4 A. J. Bard, *Anal. Chem.*, 35 (1963) 340.
5 S. Feldberg and C. Auerbach, *Anal. Chem.*, 36 (1964) 505.
6 D. C. Grahame, *J. Am. Chem. Soc.*, 71 (1949) 2975; *J. Electrochem. Soc.*, 98 (1951) 343.
7 P. Delahay, *New Instrumental Methods in Electrochemistry*, Interscience Publishers, Inc., New York, 1954, pp. 208–9.
8 L. Meites, *Polarographic Techniques*, Interscience Publishers, Inc., New York, 2nd ed., 1965, pp. 563–6.
9 C. D. Russell and J. M. Peterson, *J. Electroanal. Chem.*, 5 (1963) 467.
10 W. H. Reinmuth, *Anal. Chem.*, 33 (1961) 485.
11 D. Hawley and R. N. Adams, *J. Electroanal. Chem.*, 10 (1965) 376.
12 P. Delahay and C. C. Mattax, *J. Am. Chem. Soc.*, 76 (1954) 874.
13 T. Berzins and P. Delahay, *J. Am. Chem. Soc.*, 75 (1953) 4205.

ELECTROANALYTICAL CHEMISTRY AND INTERFACIAL ELECTROCHEMISTRY
Elsevier Sequoia S.A., Lausanne – Printed in The Netherlands

DETERMINATION OF THE DOUBLE-LAYER CAPACITY IN THE PRESENCE OF A DEPOLARIZER

DIETER BRITZ AND HENRY H. BAUER
C.S.I.R.O. Division of Food Preservation, Box 43, Ryde, N.S.W. (Australia)
Department of Chemistry, University of Kentucky, Lexington, Kentucky 40506 (U.S.A.)
(Received January 27th, 1967)

INTRODUCTION

In faradaic-admittance studies, the measured quantity is always the total cell-impedance, which can be represented as in Fig. 1; R_x is the sum of all circuit resistances (usually the resistances of the solution and of the capillary, in the case of studies at the dropping mercury electrode, DME), C_H is the double-layer capacity and Y_f the faradaic admittance. The magnitude and phase of the faradaic admittance are then obtained by vectorial subtraction of the values of R_x and C_H, which are obtained from measurements of the cell impedance in the absence of the depolarizing substance, *i.e.*, for $Y_f = 0$.

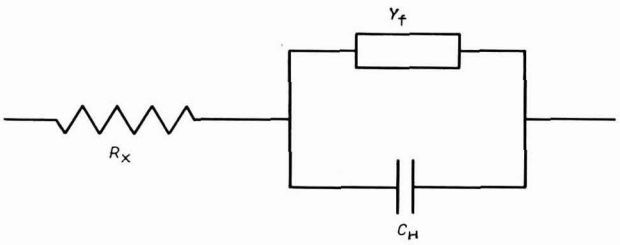

Fig. 1. Equiv. circuit of the polarographic cell; (R_x), total series resistance; (C_H), capacity of the double layer; (Y_f), faradaic admittance.

This method relies on the assumption that the parameters R_x and C_H are not altered by the presence of the depolarizer, an assumption that is probably valid for most inorganic species (with the exception of thallium, for which anomalous behaviour was noted by TAMAMUSHI AND TANAKA[1] and SALIE AND LORENZ[2]).

In general, one can always expect that R_x will not be affected by depolarizers at usual concentrations because R_x is a function only of the conductivity of the solution (determined by the relatively high concentration of the supporting electrolyte) and of the radius of the mercury drop (*c.f.* ILKOVIČ[3]). If the depolarizer is surface-active, it may alter the drop-time of the DME and hence the radius of the drop; such changes are usually small, however, and the corresponding change in the series resistance can, if necessary, be calculated sufficiently accurately by using the treatment[3] referred to above.

The double-layer capacity, on the other hand, is determined by the constitution of the double-layer and this may be markedly affected by the presence in the solution of quite small concentrations of adsorbable species.

Tensammetric studies[4,5] have shown that many organic substances are adsorbed at the DME and it is generally believed that the anomalous electrochemical behaviour of many organic depolarizers can be attributed to adsorption; such adsorption will affect both the faradaic admittance and the double-layer capacity. Theoretical predictions (*e.g.*, RANDLES AND SOMERTON[6]; LAITINEN AND RANDLES[7]; MATSUDA[8]; KASTENING, GARTMANN AND HOLLECK[9]) have been made regarding the behaviour of the faradaic admittance under these conditions, but experimental verification necessitates accurate measurements of the magnitude and phase of the faradaic admittance and this, in turn, requires accurate knowledge of the double-layer capacity in the presence of the adsorbed depolarizers.

An attempt to obtain this was made by SLUYTERS-REHBACH[10]. However, in this method it was assumed that the faradaic admittance is "normal", *i.e.*, that it obeys the equation[11]

$$\cot\phi = 1 + (\tfrac{1}{2}\omega D)^{\frac{1}{2}}/k \qquad (1)$$

where ϕ is the faradaic phase-angle, k the heterogeneous rate-constant, D the diffusion coefficient, and ω the angular frequency. In view of the above-mentioned studies[6-9], however, it is evident that precisely in many cases where we wish to measure the double-layer capacity in the presence of the depolarizer, we cannot make any such definite assumptions about the faradaic admittance. This objection applies also to the work of SLUYTERS AND DE LOEUWE[12], who assumed that $\cot\phi = 1$.

It should be noted that, when we speak of "faradaic admittance", we are referring to alternating-current conditions. There is no special difficulty involved in measuring the double-layer capacity at potentials where only direct current can flow as a result of a redox process—*e.g.*, at the plateau of a d.c. polarographic step; the difficulties arise in the region of the alternating-current wave, where the faradaic processes give rise to a.c. admittance in parallel with the double-layer admittance. This distinction is important when considering the recent paper by ROBBINS AND ENKE[13], the title of which is similar to that of the present article; however, the method of ROBBINS AND ENKE fails in the region of an a.c. wave whereas the present method enables measurements to be made at these potentials.

A method that does not suffer from the above-mentioned restrictions was developed by DE LEVIE[14]. Here, the only two assumptions made are that the faradaic admittance is negligibly small compared with the double-layer admittance at a sufficiently high frequency and that the double-layer capacity, at high frequencies at least, is itself independent of frequency. Both are quite reasonable assumptions and the latter has been verified up to 32 kHz in our own work, using the apparatus previously described[15]. We believe that any observed frequency-dependence of the double-layer capacity at frequencies from a few hundred hertz into the radio-frequency region is likely to be an experimental artifact, perhaps of the sort discussed by SUSBIELLES[16] (see further discussion below).

In DE LEVIE's technique[14], a curved plot is obtained which has to be extrapolated to infinite frequency to give the double-layer capacity. In using this method, we have found that the extrapolation can be quite uncertain, because the plots curve

strongly in critical regions, *viz.* at points corresponding to high-frequency measurements. The technique we shall describe overcomes this problem to a considerable extent and therefore improves the certainty with which the double-layer capacity can be determined.

DISCUSSION

We make the two above-mentioned assumptions: (1) that the faradaic admittance, Y_f, is negligibly small in magnitude compared with that of the double-layer capacity (ωC_H) at sufficiently high frequencies, *i.e.*,

$$\lim_{\omega \to \infty} (Y_f/\omega C_H) = 0 \tag{2}$$

and (2) that, at high frequencies at least, the double-layer capacity, C_H, is independent of frequency (at frequencies below a few hundred hertz, frequency dispersion has often been observed—*e.g.* GRAHAME[17]; the processes responsible have not as yet been identified with certainty).

The first assumption suggests that one might simply measure the total cell-impedance, Z_t, at a sufficiently high frequency, resolve Z_t into its resistive and capacitive (series) components and thereby obtain, respectively, R_x and C_H. This can, in fact, be done quite successfully for slow (irreversible) electrode processes, where the faradaic admittance becomes essentially resistive, small, and constant, at quite low frequencies. If the electrode process in question is fast (reversible), however, it becomes impracticable to use a frequency sufficiently high that eqn. (2) holds accurately; furthermore, at these frequencies, the series resistance is usually large compared with the double-layer impedance, so that the total cell-impedance is almost entirely resistive and the accuracy of determination of the magnitude of C_H becomes intolerably low.

A better approach, again similar to that of DE LEVIE[14], is to measure Z_t over a range of frequencies and, at each frequency, to resolve Z_t into the resistive and capacitive (series) components, Z' and Z'', respectively, with

$$Z' = Z_t \cos \theta \tag{3}$$

$$Z'' = Z_t \sin \theta \tag{4}$$

where θ is the phase-angle of the cell impedance, Z_t. The values of Z'' are then expressed as capacities, C, by the transformation

$$C = (\omega Z'')^{-1} \tag{5}$$

and these are plotted as a function of the inverse of frequency and extrapolated to zero (*i.e.*, to infinite frequency; *cf.* Fig. 2). With this method, a curve that can be extrapolated quite well provided the faradaic process is fairly slow is obtained, but the uncertainty of the extrapolation becomes very great for electrode processes that are quite fast—in fact, whose speed makes them suitable for study by faradaic-impedance methods.

We believe that the best approach is one in which a family of curves is generated with the condition that all curves extrapolate to the same point at infinite

frequency. In this way, the uncertainties resulting from variations in the rate of curvature of the individual curves can be minimized. The procedure for generating the desired family of curves is described below.

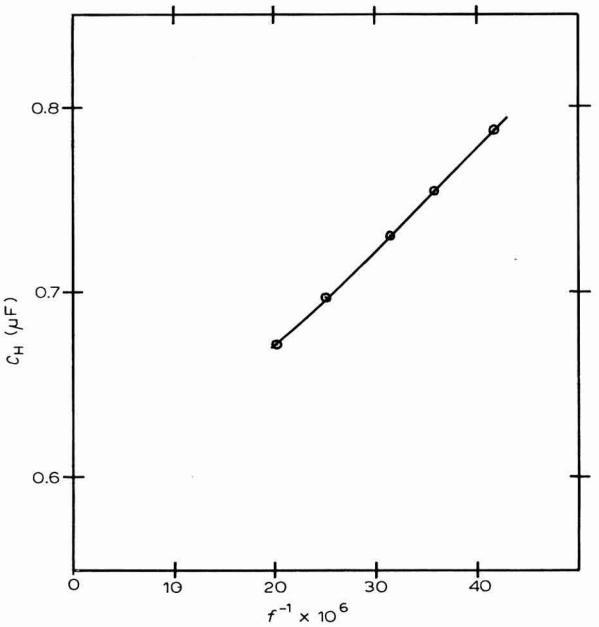

Fig. 2. Extrapolation to obtain double-layer capacity (0.6 μF) by plotting the total series capacity *vs.* inverse of the frequency. The system is a fast one, similar to *e.g.* 10^{-3} M cadmium ions.

PROPOSED PROCEDURE

Consider the parallel admittances, Y_1 and Y_2, having phase-angles, θ_1 and θ_2, respectively. If the magnitude, Y, and the phase-angle, θ, of the total parallel-network admittance Y are known, together with the values of the phase-angles, θ_1 and θ_2, then the magnitudes, Y_1 and Y_2, can be calculated. This is evident from the vector diagram in Fig. 3. Points A and B on the diagram give the vectors, Y_1 and Y_2, respectively, and the lengths OA and OB are the magnitudes, Y_1 and Y_2, respectively. The following equations apply:

$$\left.\begin{aligned} Y \sin\theta &= Y_1 \sin\theta_1 + Y_2 \sin\theta_2 \\ Y \cos\theta &= Y_1 \cos\theta_1 + Y_2 \cos\theta_2 \end{aligned}\right\} \quad (6), (7)$$

These are simultaneous equations for Y_1 and Y_2 and yield the symmetrical solutions

$$Y_1 = Y \frac{\sin(\theta - \theta_1)}{\sin(\theta_2 - \theta_1)} \quad (8)$$

$$Y_2 = Y \frac{\sin(\theta - \theta_2)}{\sin(\theta_1 - \theta_2)} \quad (9)$$

Consider now Fig. 1. If we subtract the value of R_x from the total cell-impedance

Z_t, there remains the parallel network of the two admittances, ωC_H and Y_f, the total admittance and impedance of which we shall designate, Y_{el} and Z_{el}, respectively (terminology as used by DE LEVIE[14]). We know that the phase-angle of the double-layer capacity is $\pi/2$ and we know the magnitude, Y_{el}, and phase-angle, θ_{el}, and

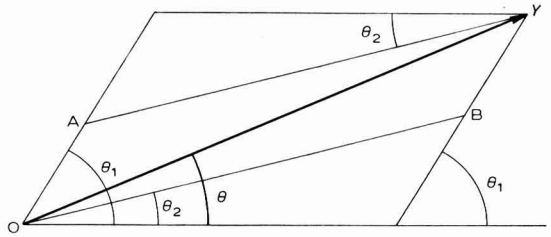

Fig. 3. Vector diagram showing the relationships between the magnitudes of the vectors, Y_1 and Y_2, the phase angles, θ_1 and θ_2, and the total admittance, Y, and its phase angle, θ.

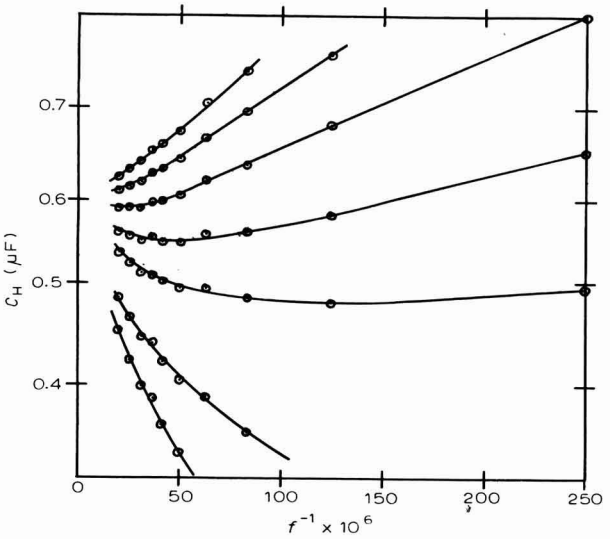

Fig. 4. Extrapolation to obtain the double-layer capacity (0.6 μF) from a family of curves generated so as to extrapolate to the same value.

thus, designating the faradaic phase-angle by the symbol ϕ, and using relations analogous to eqns. (8) and (9), we obtain for ωC_H

$$\omega C_H = Y_{el} \cdot \frac{\sin(\theta_{el}-\pi/2)}{\sin(\phi-\pi/2)} = Y_{el} \cdot \frac{\cos\theta_{el}}{\cos\phi} \tag{10}$$

or

$$C_H = \frac{Y_{el}}{\omega} \cdot \frac{\cos\theta_{el}}{\cos\phi} \tag{11}$$

In practice, we do not know the value of the faradaic phase-angle ϕ—in fact, this is one of the quantities we wish to determine. We proceed by assigning an ar-

bitrary value to ϕ and calculate "C_H" by using eqn. (11), for a series of measurements of Z_t over a range of frequencies; then, we plot these "C_H"-values against the inverse of frequency, obtaining a curve that extrapolates to the correct value of C_H at zero inverse frequency (and with less curvature than the previous plot in Fig. 2, obtained by simply ignoring Y_f). Further, by assigning to ϕ a series of arbitrary values, we obtain a family of curves, all extrapolating to the same C_H-value, but from different directions. Such a family of curves enables good extrapolated values of C_H to be obtained even for extremely fast electrode reactions (*cf.* Fig. 4).

This technique obviously involves a large number of calculations for each single estimation of C_H, but this is quite easily programmed for an electronic computer. The full equation is

$$C_H = \frac{Z_t \sin \phi' - \tan \phi (Z_t \cos \phi' - R_x)}{(Z_t^2 - 2Z_t R_x \cos \phi' + R_x^2)} \qquad (12)$$

where ϕ' is the phase-angle of the total cell-impedance, all other symbols having their previous significance. For the computer programme used in our work, we assigned the values cot $\phi = 0.8$, 1, 1.5, 2, 3, 5, 7, and 10; each value gives a separate curve. This range was found to be generally useful although, if desired, it could of course be part of the data input and therefore readily variable.

RESULTS

To test this method, we calculated artificial cell-impedance and phase-angle values over a wide range of high frequencies, corresponding to a fast system such as Cd(II)/Cd(Hg); the following values, typical for a conventional polarographic cell, were used:

$R_x = 20\ \Omega$

$C_H = 0.6\ \mu F$

$\Theta = 15\ \Omega$

$\sigma = 3000\ \Omega\ \text{sec}^{-\frac{1}{2}}$

$f = 4, 8, 12, 16, 20, 24, 28, 32, 40, 50$ kHz

where Θ is the activation-polarization resistance, f the frequency, and σ the Warburg coefficient describing the so-called Warburg impedance, *i.e.*, that (series) component of the faradaic impedance that is determined by diffusion processes and has a phase-angle of 45°. These calculations produced a series of values of Z_t and ϕ' over the frequency range, simulating a series of such measurements. These were then processed according to eqn. (12), each for the given range of cot ϕ-values, and the resulting plots of "C_H" against inverse frequency are shown in Fig. 4.

It is seen that the extrapolation to $C_H = 0.6\ \mu F$ is relatively easy, even if one disregards the points above 32 kHz, our practical frequency limit. A comparison with the plot in Fig. 2, derived from the same system, clearly shows the advantage of our proposed technique over that illustrated in Fig. 2.

It may be noted, in conclusion, that we have used this method successfully on actual systems; the results of that work will be published elsewhere.

SUMMARY

A method is described by which the double-layer capacity can be measured at potentials where an a.c. polarographic wave (faradaic admittance) is present. No special assumptions are made about the nature of the faradaic admittance and the latter can therefore be measured and studied in cases where it is "anomalous", *e.g.*, in systems involving adsorbed depolarizers.

REFERENCES

1 R. TAMAMUSHI AND N. TANAKA, *Z. Physik. Chem. Frankfurt*, 28 (1961) 158.
2 G. SALIE AND W. LORENZ, *Z. Physik. Chem. Frankfurt*, 29 (1961) 408.
3 D. ILKOVIČ, *Collection Czech. Chem. Commun.*, 4 (1932) 480.
4 B. BREYER AND S. HACOBIAN, *Australian J. Sci. Res.*, A5 (1952) 500.
5 B. BREYER AND H. H. BAUER, *Alternating Current Polarography and Tensammetry*, Interscience Publishers, Inc., New York, 1963.
6 J. E. B. RANDLES AND K. W. SOMERTON, *Trans. Faraday Soc.*, 48 (1952) 937.
7 H. A. LAITINEN AND J. E. B. RANDLES, *Trans. Faraday Soc.*, 51 (1955) 1954.
8 H. MATSUDA, *J. Phys. Chem.*, 64 (1960) 339.
9 B. KASTENING, H. GARTMANN AND L. HOLLECK, *Electrochim. Acta*, 9 (1964) 741.
10 M. SLUYTERS-REHBACH, Doctoral Thesis, Utrecht State University, 1963.
11 J. E. B. RANDLES, *Discussions Faraday Soc.*, 1 (1947) 11.
12 J. H. SLUYTERS AND R. DE LOEUWE, *Rec. Trav. Chim.*, 83 (1964) 657.
13 G. D. ROBBINS AND C. G. ENKE, *J. Electroanal. Chem.*, 12 (1966) 102.
14 R. DE LEVIE, *Electrochim. Acta*, 10 (1965) 395.
15 D. BRITZ AND H. H. BAUER, submitted for publication.
16 G. G. SUSBIELLES, *J. Electroanal. Chem.*, 12 (1966) 230.
17 D. C. GRAHAME, *J. Am. Chem. Soc.*, 68 (1946) 301.

ELECTROANALYTICAL CHEMISTRY AND INTERFACIAL ELECTROCHEMISTRY
Elsevier Sequoia S.A., Lausanne – Printed in The Netherlands

PHASE SELECTIVE SAMPLING IN A.C. POLAROGRAPHY AND APPLICATION TO DIRECT MEASUREMENT OF DOUBLE-LAYER CAPACITY

T. F. RETAJCZYK AND D. K. ROE

Department of Chemistry and Laboratory for Nuclear Science, Massachusetts Institute of Technology, Cambridge, Massachusetts 02139 (U.S.A.)

(Received January 20th, 1967; in revised form, April 17th, 1967)

The full potentialities of a.c. polarography can only be realized when both amplitude and phase of the current from the electrochemical cell are measured. This is because there are two components of the cell current that must be resolved: a capacitive current from the electrical double layer with a phase angle of 90° relative to the applied sinusoidal potential, and a faradaic current having a phase angle of 45° if the electrode process is diffusion-controlled, and approaching 0° for charge-transfer control. Although the exact phase angle may not be known for the electrode reaction, rejection of the 90° or quadrative component is always possible by some type of synchronous rectification[1–3] so that an essentially zero base-line can be obtained. The output of the rectifier contains a direct current component having a fixed relation to the peak amplitude of the faradaic current and this is measured in the familiar polarogram. Many accounts of these techniques are available; especially noteworthy is the recent and very thorough survey of operational amplifier circuits for a.c. polarography[4].

The method described in this paper employs a gating circuit for phase-sensitive detection instead of a synchronous rectifier. The gating circuit allows the amplitude of the a.c. current signal to be measured at essentially any selected point of a cycle. The point generally selected is where the capacitive current passes through zero, which occurs in phase with the potential maximum. Of course, other components of the a.c. current signal can be similarly resolved and the technique therefore suggests applications other than conventional a.c. polarography. The extension to measurements of capacity currents is included here.

Several methods have been proposed for measuring the double-layer capacitance in the presence of a faradaic reaction; most of them require a graphical analysis of individually obtained data points[5–9]. Automatic recording of double-layer capacity *versus* potential curves has been reported, but these techniques are limited to potential regions where no reaction is occurring[10,11], or where the reaction current is nearly constant[12] (*i.e.*, in the limiting current plateau). Because of the importance of the double-layer capacity in electrode reactions, a new technique has been developed in this laboratory which permits continuous and direct recording of double-layer capacity *versus* potential curves in the presence of a reversible faradaic process, even for potential regions in which the current changes markedly with potential and time.

PRINCIPLE OF THE METHOD

The processes occurring in the vicinity of an electrode–solution interface are usually represented in terms of an equivalent circuit (Fig. 1A) consisting of a resistance, R_x, in series with a network composed of a capacitor, C, in parallel with a complex impedance, Z_f. Here, R_x represents the ohmic resistance of the solution, electrode, etc., C the double-layer capacity, and Z_f the faradaic impedance due to an electro-

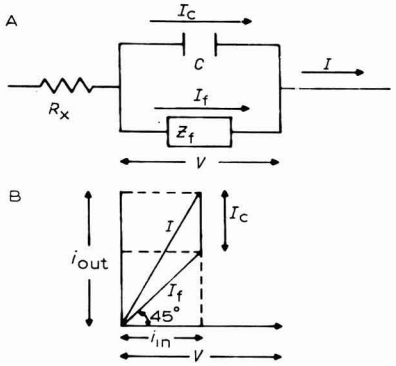

Fig. 1. A. Equivalent circuit of solution–electrode interface. B. Current–voltage phase relationship when R_x is negligible: C = double-layer capacity; Z_f = faradaic impedance; R_x = resistance in series with interface; I = total alternating current; I_f = faradaic current; I_c = double-layer current; i_{in} = current in-phase with V; i_{out} = current 90° out-of-phase with V; V = applied alternating voltage across electrode–solution interface.

chemical process. If R_x can be made negligible and if the faradaic process is assumed to be completely diffusion-controlled[13] ($\varphi = 45°$) then the vector diagram for the resulting equivalent circuit can be represented as in Fig. 1B. It can be seen from this diagram that if the amplitude of the current vector is measured only at the moment when the alternating voltage is at its maximum value, then only i_{in} is recorded and I_c is rejected. For the phase angle as given in Fig. 1B, $i_{in} = I_f/\sqrt{2}$. If the electrode process exhibits some other phase angle, the proportionality constant between i_{in} and I_f is cos φ. In terms of a.c. polarography, the phase angle may be any value between 0 and 45°; the important point is the rejection of I_c. The success of this rejection is related to the accuracy with which the gating circuit can be synchronized with the phase of the applied potential and to the duration of the gate opening, usually 10–100 μsec. An empirical adjustment with a capacitor in place of the cell proved to be the most accurate and the simplest method. Details are given in the section on instrumentation.

Double-layer capacities were obtained from sampling of the a.c. current signal at two points. Referring again to Fig. 1B, it can be seen that, if the in-phase (i_{in}) and quadrature (i_{out}) current components are measured simultaneously, the difference between them is I_c which is directly proportional to the double-layer capacity in the presence of a reversible faradaic process. In general,

$$I_c = i_{out} - i_{in} \tan \varphi \qquad (1)$$

so that this procedure is directly possible when $\varphi = 45°$.

If R_x is not negligible, it introduces a voltage drop in phase with the overall resulting current, I. Therefore i_{in} and i_{out} are not measured with respect to the alternating voltage across the electrode solution interface but with respect to the total applied voltage. Hence, i_{in} now has a capacity component and i_{out} no longer equals I_c plus i_{in}. Therefore, for these measurements it is necessary that R_x be kept as small as possible so that unwanted phase shifts are avoided. Values of 2–10 Ω resulted in phase shifts of less than 1 degree.

Subtraction of i_{in} from i_{out} gives exactly I_c if $\varphi = 45°$, but when $\varphi < 45°$, the difference is less than the actual I_c. Any faradaic process that is not diffusion-controlled in its rate (the large class of "quasi-reversible" processes) will have a phase angle of less than 45° and the value of the angle will vary with potential[3,4,7], *i.e.*,

$$\varphi = \cot^{-1}\left\{1 + \frac{(2D\omega)^{\frac{1}{2}}}{k_s[\exp(-\alpha f(E-E_{\frac{1}{2}})) + \exp(\beta f(E-E_{\frac{1}{2}}))]}\right\}$$

where

D = diffusion coefficient
ω = angular frequency
k_s = apparent heterogeneous rate constant
α = transfer coefficient and $\beta = 1-\alpha$
$f = nF/RT$

The minimum value of φ is

$$\varphi_m = \cot^{-1}\left\{1 + \frac{(2\omega D)^{\frac{1}{2}}}{k_s[(\alpha/\beta)^{-\alpha} + (\alpha/\beta)^{\beta}]}\right\} \qquad (2)$$

and occurs at $E_{\varphi m} = E_{\frac{1}{2}} + (RT/nF)\ln(\alpha/\beta)$.

From these equations a very good assessment of the importance of quasi-reversibility can be obtained if values of k_s and α are available or estimatable. In the absence of kinetic information, ω can be varied and experimental values of C should be independent of ω if the above effect is negligible. Point-by-point measurements of I_c are, of course, possible at any known value of φ. In all the measurements reported here, the gating circuit was adjusted to sample as if φ was 45° although this angle was not exactly attained in any case. The actual phase angles were then calculated from available kinetic data and several points on each curve were corrected according to eqn. (1). This procedure was followed in order to assess the measurement method. In general, the gating circuit can be adjusted for any phase angle.

INSTRUMENTATION

The circuit diagram for the phase-sensitive detector is shown in Fig. 2. The oscillator is a Wien-bridge design[14], the active element being a K2-XA Philbrick operational amplifier. The frequency of the sine-wave produced is determined by the relation:

$$f = \tfrac{1}{2}\pi R_1 R_2 C_1 C_2 \qquad (3)$$

The frequency of the oscillator can therefore be varied by using a multiposition two-pole switch to change simultaneously the values of the frequency-determining resistors. In this manner, the oscillator was set to operate at any one of nine different frequencies ranging from 25–900 Hz.

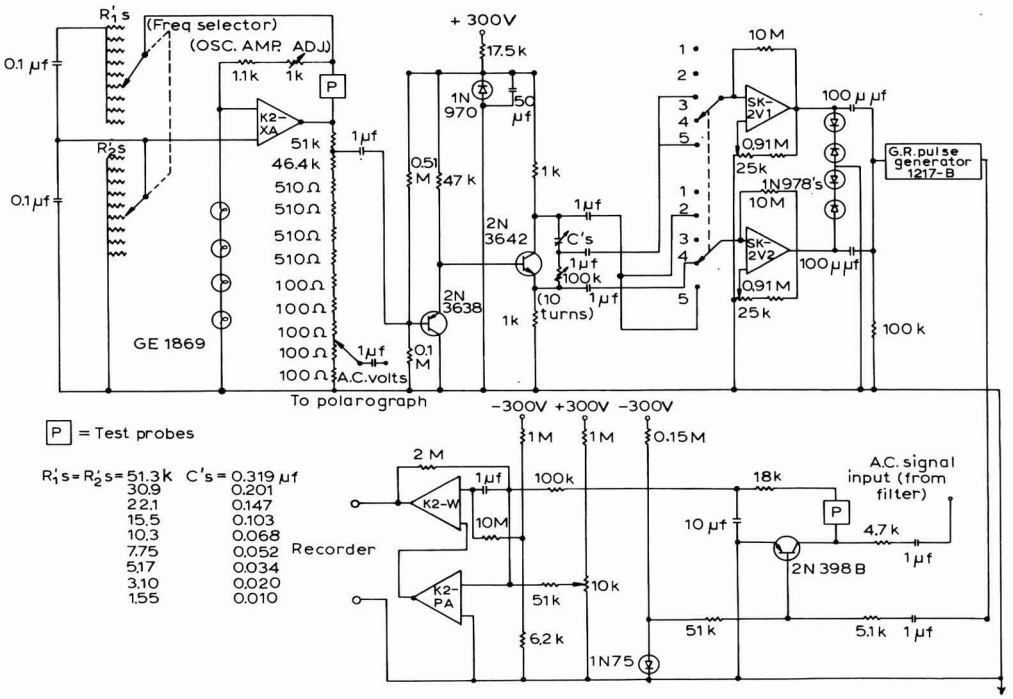

Fig. 2. Circuit diagram of oscillator and sampling circuit of a.c. polarograph.

The oscillator output was fed to a phase-shift network consisting of a two-stage transistor amplifier with a variable RC network across the emitter-collector of the 2N3692 transistor. Since the signals at the emitter and collector were equal in amplitude, but differed in phase by 180°, a phase shift variable over about 180° was possible simply by changing the values of R and/or C in this RC network. In practice, the value of C was changed only with frequency, since the values for C were chosen so that the amount of phase shift introduced at a given R-setting was the same at each frequency.

The signals at the emitter and collector of the 2N3642 transistor, as well as the output of the RC phase-shift network, were capacitively coupled to a multi-position two-pole switch, each pole of which was connected to a Philbrick SK-2V operational amplifier set up to operate as a zero-crossing detector. The signal outputs of the detectors were then differentiated to give a series of spikes which were fed to the external trigger input of a General Radio Corporation Unit Pulse Generator, type #1217-B, which produced one positive pulse of adjustable height and width for each spike fed into the input.

The pulse train was fed into the negatively-biased base of a PNP transistor which functioned as a gate. Hence, in the absence of any positive pulse, there was no appreciable *IR*-drop across the emitter-collector. The positive pulses produced a counter-bias which was sufficient to reverse bias the transistor so that it became non-conducting, or open, between the emitter-collector. Thus the incoming alternating current signal from the electrochemical cell produced an *IR*-drop across the RC

series combination which was proportional to the magnitude of the current during the duration of the pulse. This signal was then amplified and recorded.

Subsequent to the construction of this gating circuit a six-diode gate was tried as a series switch. It is significantly superior in all respects and approaches the ideal as a gate[15].

By changing the setting of the five-position, two-pole switch at the inputs to the two zero-crossing detectors, it was possible to sample the alternating current either 0°, 90°, or 180° out-of-phase individually, or 90° and 180° out-of-phase simultaneously. This latter setting was used to measure double-layer capacity and it was achieved by connecting the output of the collector of the 2N3642 transistor to the input of the #2 zero-crossing detector *via* one pole of the switch, and the output of the RC phase-shift network to the input of the #1 zero-crossing detector *via* the other pole of the switch. The #2 zero-crossing detector was then adjusted *via* the hysteresis control so that the pulses sampled the current exactly 180° out-of-phase with the voltage signal.

In practice, this procedure was carried out using a capacitor in place of the electrochemical cell and adjusting the phase so that the current output to the recorder was zero. Likewise, the RC phase-shift network was adjusted so that the pulses sampled exactly 90° out-of-phase to the voltage signal when the output of the RC network was connected to the #1 zero-crossing detector. In this case, a resistor was used in place of the electrochemical cell and, once again, the phase was adjusted for zero recorder response.

At the output of the oscillator was an attenuating switch which allowed alternating voltages of various amplitudes to be applied to the input of a summing amplifier of a controlled-potential polarograph of fairly conventional operational amplifier design[16,17]. The alternating current signal from the electrochemical cell, after being amplified by a current amplifier in the polarograph, was fed through a SKL Variable Electronic Filter Model 302. This made it possible to select a high and a low band pass so that only the desired frequency was passed. The output of the filter was then capacitively coupled to the collector of the transistor switch in the phase-sensitive detector.

Operation of the instrument was checked by sampling the current from an equivalent circuit of a resistor and capacitor in parallel. The voltage signal was selected to have a frequency of 94 Hz and an amplitude of 10 mV peak-to-peak. When the total current was sampled in phase with the peak voltage, a signal was obtained which was due only to the current through the resistor. A precision of better than 1% was obtained between values of resistance and recorder response from 200 Ω–10 kΩ with parallel capacitances of up to 1 μF. These tests show that the sampling had very nearly the intended phase relation to the applied signal.

In a similar way, the out-of-phase sampling, 90° from the peak voltage, was tested by measuring recorder response for values of standard capacitors in parallel with resistors down to 500 Ω. Response was again linear to 1% for values of 0.02–2 μF. Below 500 Ω parallel resistance, some error became measurable, especially at small capacitance. In general, the errors were within limits of normal recorder accuracy provided the total current was not greater than about ten times the current to be measured. Also, the operating range of the instrument was suitable for signals normally expected from polarographic cells.

EXPERIMENTAL

Cell and electrodes

The cell consisted of a 250-ml wide-mouth jar fitted with a sulfur-free vinyl stopper. Through this stopper were inserted a low resistance DME (effective capillary resistance $\sim 1\ \Omega$) similar in nature to that already described[18], a platinum-foil counter electrode, and a commercial asbestos-wick SCE. In order to reduce solution resistance to a minimum, the SCE was positioned close to the DME *via* a Luggin-type capillary arrangement. The cell also contained a fritted-glass gas dispersion tube which was used to deliver pre-purified nitrogen for deoxygenation of the solution, a thermometer, and a drop collector. Triply-distilled mercury was used in the DME. All measurements were carried out in an air-conditioned room at $24 \pm 1°$. All the data reported here were obtained using an applied alternating voltage of 94 Hz and 10 mV p–p and a sampling pulse width of 100 μsec. Potential scans were in the negative direction at a rate of 0.05 V/min.

Materials

Individual 1 *M* stock solutions of sodium fluoride, potassium nitrate, and potassium chloride, and 0.1 *M* stock solutions of cadmium chloride, cadmium nitrate, zinc chloride, and thallium nitrate were prepared. The supporting electrolyte solutions contained about 10^{-2} *M* acid to prevent precipitation of any basic salts and/or hydroxides. All solutions were prepared from reagent-grade chemicals, except for thallium nitrate which was C.P.-grade, and water which was first put through a mixed-bed deionizer, then distilled once in the presence of potassium permanganate, and finally redistilled in a quartz still. Prior to actual use, each of the supporting electrolyte solutions was mixed with purified activated charcoal and vacuum-filtered through a medium porosity fritted funnel.

RESULTS AND DISCUSSION

Figure 3 shows typical results obtained from measurements of the double-layer capacity in the absence of a faradaic process. Here, a plot of the double-layer capacity of a DME at the end of drop life in 0.66 *M* sodium fluoride *versus* potential

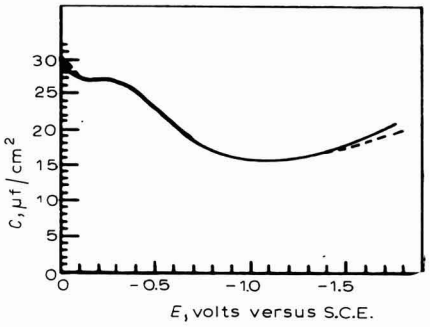

Fig. 3. Recorded double-layer capacity of mercury electrode: (---), in 0.66 *M* NaF; (—), GRAHAME's[19] data.

is compared with a plot obtained by GRAHAME[19] under similar conditions. As can be seen, the agreement is in accord with the specifications of the instrument.

Measurements of a.c. polarograms and of the double-layer capacity in the presence of a faradaic process were carried out using thallium, cadmium, and zinc as the electroactive species and 1 *M* potassium chloride and 1 *M* potassium nitrate as supporting electrolytes. Results for cadmium are shown in Figs. 4 and 5 and similar curves for zinc in Fig. 6. Thallous ion gave a different result as shown in Figs. 7 and 8. In all cases, the capacity current was measured for the supporting electrolyte alone (i_{out}), and then the reducible ion was added and $i_{out}-i_{in}$ recorded. The latter is seen as a dashed line where different from i_{out}. A third measurement was also made of i_{in} alone, which gave an a.c. polarogram drawn inverted in the lower part of the Figures.

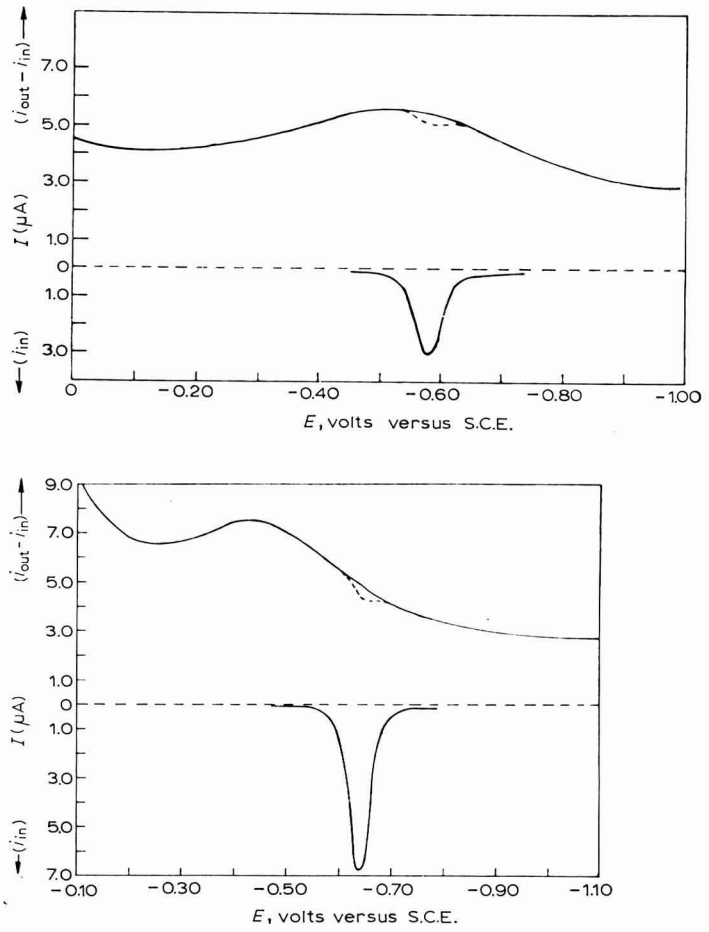

Figs. 4-5. Capacity currents *vs.* potential of mercury electrode: (4) (—), in 1 *M* KNO_3; (---), with $5\cdot10^{-5}$ *M* Cd^{2+}; (5) (—), in 1 *M* KCl; (---), with 10^{-4} *M* Cd^{2+}. Lower curves are a.c. polarograms (i_{in}) of Cd^{2+} in same soln.

Pertinent data for these metal ion–amalgam electrodes are collected in Table 1, including the phase angle of the faradaic current near the maximum of i_{in} calculated from these data. The variation in the value of φ_m is surprising at first in view of the magnitudes of k_s. None of the systems is seen to have a phase angle of 45°; however, the measurements of $i_{out}-i_{in}$ were made on the assumption that $\varphi=45°$. With the data at hand, it can be reasonably shown that the differences between $i_{out}-i_{in}$ measurement in the absence and presence of reduction of cadmium and zinc ions is due to the phase angle of I_f being less than 45°.

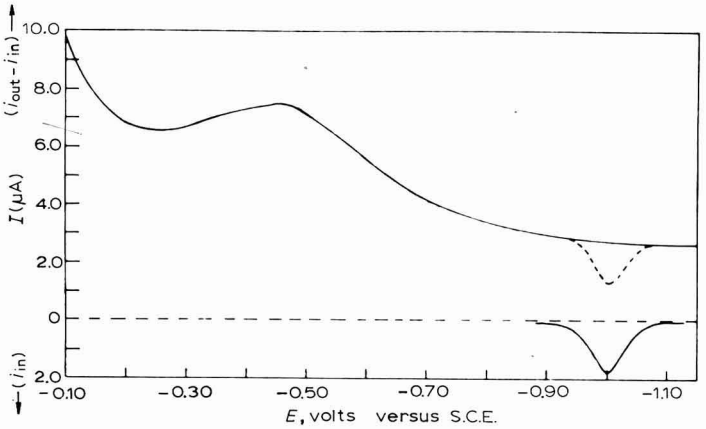

Fig. 6. Capacity current *vs.* potential of mercury electrode: (—), in 1 *M* KCl; (---), with $2\cdot10^{-4}$ *M* Zn^{2+}. Lower curve is a.c. polarogram (i_{in}) of Zn^{2+} in same soln.

From the Figures, $i_{out}-i_{in}$ and i_{in} were obtained at the peak value of i_{in}. Equation (1) and the calculated values of φ_m (which occurs close enough to the potential of the peak value of i_{in} to be used for this purpose) were then used to calculate the tabulated charging currents, I_c. These currents are what would have been measured had the instrument been adjusted to compensate for the proper values of φ. Also listed in the Table are values of capacity currents (i_{out}) for the supporting electrolyte alone at the same potential. It is apparent that the charging currents in the case of cadmium and zinc (in the last two columns) are in much better agreement than are the curves in Figs. 4, 5, and 6. Since the differences in capacity currents in the vicinity of the reduction processes appear to be accountable to phase angle variations, it can be suggested that there was no measurable change in the double-layer capacity of the mercury electrode due to the occurrence of the reduction of cadmium and zinc ions.

The effects of thallium on measurements of $i_{out}-i_{in}$ in potassium nitrate and potassium chloride (Figs. 7 and 8) are quite different from those of cadmium and zinc. Measurements of $i_{out}-i_{in}$ in potassium nitrate show a decrease at values of potential just anodic to the in-phase peak maximum and then a subsequent increase at potentials just cathodic to the peak maximum. Measurements of $i_{out}-i_{in}$ in potassium chloride show an overall increase at potentials anodic to the thallium discharge process, a decrease near the peak maximum, and then a subsequent large increase at potentials just cathodic to the peak maximum. Beyond the reduction wave at

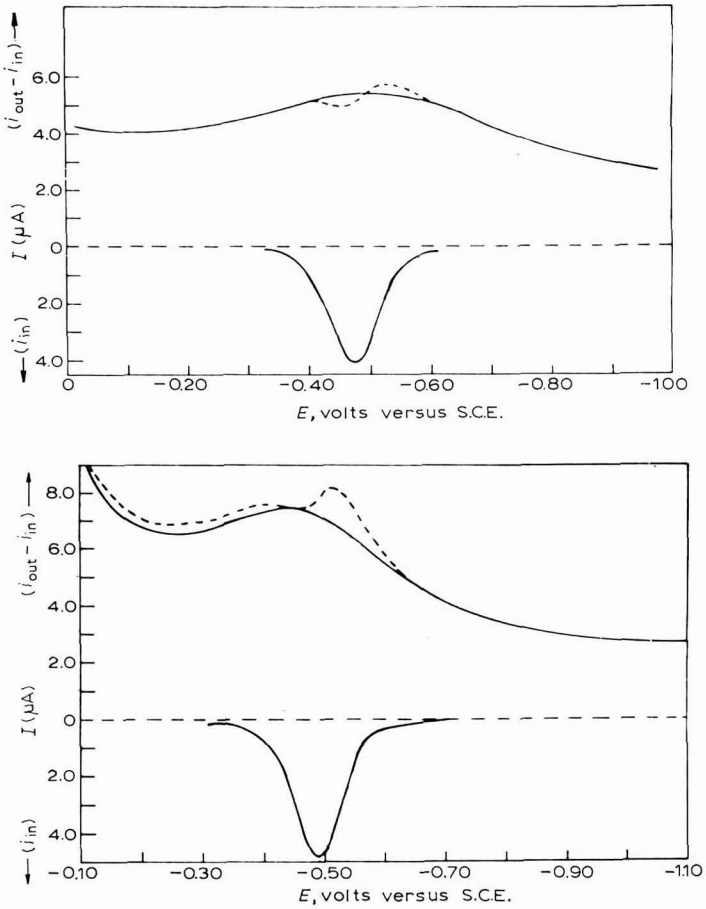

Figs. 7-8. Capacity currents *vs.* potential of mercury electrode: (7) (—), in 1 *M* KNO_3; (---), with $2 \cdot 10^{-4}$ *M* Tl^+; (8) (—), in 1 *M* KCl; (---), with $2 \cdot 10^{-4}$ *M* Tl^+. Lower curves are a.c. polarograms (i_{in}) of Tl^+ in same soln.

TABLE 1

	k_s[a] *(cm sec^{-1})*	α[a]	D[b] *($10^6 \times$ cm^2 sec^{-1})*	φ_m[c]	I_c[d] *(μA)*	i_{out}[e] *(μA)*
Cd^{2+} (in KNO_3)	0.6	0.15	6.3	42.0°	5.3	5.4
Cd^{2+} (in KCl)	2.9	0.78	8.7	44.6°	4.7	5.0
Zn^{2+} (in KCl)	0.004	0.3	7.9	4.0°	2.8	2.7
Tl^+ (in KNO_3)	0.3	0.8	20	37.5°	6.1	5.5
Tl^+ (in KCl)	0.15	0.9	10	29.8°	9.7	7.2

[a] From TANAKA AND TAMAMUSHI[20].
[b] From polarographic diffusion current constants given by MEITES[21].
[c] Calculated from eqn. (2) for a frequency of 94 Hz.
[d] Calculated from eqn. (1) and φ_m using i_{in} and $i_{out}-i_{in}$ of Figs. 4, 5, 6, 7 and 8 at the peak value of i_{in}.
[e] Capacity current of supporting electrolyte at the potential of peak value of i_{in}.

negative potentials, $i_{out}-i_{in}$ decreases to values obtained in the absence of thallium.

If the subtraction of i_{in} from i_{out} is again made with eqn. (1) and the phase angles listed in Table 1, then the capacity current at the peak of i_{in} in the presence of thallous ion reduction is found to be larger than the capacity current in the absence of the reduction at the same potential. That is, the actual phase angle was less than 45° and this caused the measured $i_{out}-i_{in}$ to be low; the corrected value of I_c in Table 1 is higher than i_{out} of the supporting electrolyte at the peak potential of i_{in}. Inspection of the curves of Figs. 7 and 8 certainly suggests that the use of a phase angle of 45° resulted in a negative error in $(i_{out}-i_{in})$, particularly in the region where i_{in} is large. Even so, there is clear evidence of an increase of capacity current and therefore of double-layer capacity caused by the addition of thallous ion.

It is interesting to compare the results obtained here with thallium with those obtained by BARKER AND FAIRCLOTH[10]. They found that the addition of $5\cdot10^{-4}$ *M* thallous ion to 1 *M* potassium chloride produced an increase in the double-layer capacity at potentials anodic to the thallous ion discharge process. This increase was fairly constant in the potential range of about -0.12 – -0.26 V *versus* the SCE and amounted to about 1.8 μF/cm^2. This compares with an average value of about 1.7 μF/cm^2 obtained here for $2\cdot10^{-4}$ *M* thallium in acidified 1 *M* potassium chloride over the same potential range.

Since BARKER AND FAIRCLOTH did not compensate for the faradaic current, they were unable to study the changes of the double-layer capacity in the immediate vicinity of the thallous ion discharge process. However, it is interesting to note that the large increase in the double-layer capacity at potentials just cathodic to the in-phase peak maximum of thallium (Fig. 8) coincides with the d.c. maximum observed for thallium in 1 *M* potassium chloride and which BARKER AND FAIRCLOTH attribute to specific adsorption.

SLUYTERS-REHBACH *et al.*[7] also measured changes in the double-layer capacity during the thallous ion discharge process *via* a complex plane analysis of a.c. impedance measurements at different frequencies. They found that the double-layer capacity increased with increasing thallous ion concentration and that the highest increase was not found at the in-phase current maximum (-0.580 V *vs.* 0.1 N.C.E.), but at -0.620 V *vs.* 0.1 N.C.E., a potential close to the electrocapillary maximum. In most respects, the curves of Figs. 7 and 8 agree with the more precise results of the bridge measurements[7]. There is one distinct difference, however, and that is in the value of the phase angle for the faradaic current. SLUYTERS-REHBACH *et al.* concluded that the experimental angle was 45° when the solution contained 1 *M* KNO_3 + 0.1 *M* KCl and thallous ion. It is suggested by the kinetic data of Table 1 that pure diffusion control would not be found for this particular supporting electrolyte unless the a.c. frequency were made very low (say 10 Hz as opposed to the 220–8000 Hz actually used[7]). Indeed, if φ was 45°, then these results should agree exactly with their measurements.

Double-layer capacity measurements obtained on the cathodic side of reduction waves where the faradaic process is completely diffusion-controlled would be expected to be the same as measurements obtained in the absence of any faradaic process because the concentration of the electroactive species at the electrode surface is zero and Z_f is very large, infinite in the limit. The fact that values of $i_{out}-i_{in}$ obtained with thallium, zinc, and cadmium at the same cathodic potentials

where each discharge process is completely diffusion-controlled, coincide exactly with the values of i_{out} obtained in the absence of any of these species, indicates that the measurements are independent of the d.c. diffusion current and thereby provides additional evidence for the validity of this technique.

As a detector for a.c. polarography, the gating circuit offers high sensitivity and excellent noise rejection. The limit of application to trace amounts of Cd^{2+} appeared to be met at about 10^{-6} M, which is comparable to the results reported for other phase-sensitive methods. In principle, there should be some improvement in signal-to-noise ratio due to the restricted band-width of the sampled signal, and because the signal is measured only when it is near its maximum value. This is probably a second-order improvement because the output stage in all a.c. polarographs contains a low-pass filter which brings about a very large change in signal band-width and, consequently, a significant improvement in signal-to-noise ratio. The feature that is unique to this method is the multiple sampling capability which is so easily accomplished and which invites a variety of measurements.

ACKNOWLEDGEMENTS

The authors are grateful to Professor D. N. HUME for helpful discussions during the course of this work. The work was supported in part through funds provided by the U.S. Atomic Energy Commission under Contract AT(30-1)-905.

SUMMARY

A phase-selective a.c. polarograph is described which operates on a sampling principle using a gating circuit. Conventional a.c. polarograms are obtained, but, in addition, direct measurement of the electrode double-layer capacity *vs.* potential is possible, even in the presence of a diffusion-controlled faradaic process. Results show that the double-layer capacity is not measurably altered by the presence of Cd^{2+} or Zn^{2+} but that Tl^{+} is adsorbed strongly in the vicinity of its reduction wave.

REFERENCES

1 B. BREYER AND H. H. BAUER, *Alternating Current Polarography and Tensammetry*, in *Chemical Analysis*, Vol. 13, edited by P. J. ELVING AND I. M. KOLTHOFF, Wiley (Interscience), New York, 1963.
2 G. JESSOP, British Patents, 640,768 (1950) and 776,543 (1957).
3 D. E. SMITH, *Anal. Chem.*, 35 (1963) 1811.
4 D. E. SMITH, *Electroanalytical Chemistry*, Vol. 1, edited by A. J. BARD, Marcel Dekker, Inc., New York, 1966, Ch. 1.
5 J. J. MCMULLEN AND N. J. HACKERMAN, *J. Electrochem. Soc.*, 106 (1959) 341.
6 B. D. CAHAN AND P. RÜETSCHI, *J. Electrochem. Soc.*, 106 (1959) 543.
7 M. SLUYTERS-REHBACH, B. TIMMER AND J. H. SLUYTERS, *Rec. Trav. Chim.*, 82 (1963) 525, 535, 553; 83 (1964) 67.
8 R. DE LEVIE, *Electrochim. Acta*, 10 (1965) 395.
9 J. N. BUTLER AND M. L. MEEHAN, *J. Phys. Chem.*, 69 (1965) 4051.
10 G. C. BARKER AND R. L. FAIRCLOTH, *Advances in Polarography*, Vol. 1, edited by I. S. LONGMUIR, Pergamon Press, New York, 1960, p. 313.
11 Z. KOWALSKI AND J. SRZEDNICKI, *J. Electroanal. Chem.*, 8 (1964) 399.
12 G. D. ROBBINS AND C. G. ENKE, *J. Electroanal. Chem.*, 12 (1966) 102.
13 D. C. GRAHAME, *J. Electrochem. Soc.*, 98 (1952) 370C.

14 G. A. Philbrick Researches, Inc., Boston, *Applications Manual for Computing Amplifiers*, 1966, p. 69.
15 F. FALLSIDE AND N. THEDCHANAMOORTHY, *Electron. Eng.*, 38 (1966) 246.
16 M. T. KELLEY, D. J. FISHER AND H. C. JONES, *Anal. Chem.*, 32 (1960) 1262.
17 C. G. ENKE AND R. A. BAXTER, *J. Chem. Educ.*, 41 (1964) 202.
18 J. E. B. RANDLES AND K. W. SOMERTON, *Trans. Faraday Soc.*, 48 (1952) 937.
19 D. C. GRAHAME, *J. Am. Chem. Soc.*, 76 (1954) 4819.
20 N. TANAKA AND R. TAMAMUSHI, *Electrochim. Acta*, 9 (1964) 963.
21 L. MEITES, *Polarographic Techniques*, Interscience Publishers Inc., New York, 2nd ed., 1965.

ELECTROANALYTICAL CHEMISTRY AND INTERFACIAL ELECTROCHEMISTRY
Elsevier Sequoia S.A., Lausanne – Printed in The Netherlands

NEW INDICATING SYSTEM: TWIN ELECTRODES, AT ZERO CURRENT. II. THE CHOICE OF ELECTRODES

E. KIROWA-EISNER, A. GOLOMBEK AND M. ARIEL

Laboratory of Analytical Chemistry, Department of Chemistry, Technion—Israel Institute of Technology, Haifa (Israel)

(Received August 20, 1966)

INTRODUCTION

Potentiometric titrations with twin electrodes[1-3] exploit an indicating system consisting of two identical, smooth electrodes, positioned in two differently-stirred regions of the titrated solution; continuous titrant addition and recording of the potential difference between the two electrodes are essential. Whenever the fundamental requirements enumerated below are fulfilled by the system, very low concentrations may be conveniently determined by this method[1,4].

Admittedly, any single electrode fulfilling these criteria may be employed in the classical potentiometric method (i.e. *vs.* a suitable reference electrode), with significantly higher sensitivity; on the other hand, as is widely appreciated, the titration of trace amounts is often harassed by various factors impairing the functioning of the indicating electrode in the midst of a determination and causing severe distortion of the potentiometric curve[5]. In the case of potentiometric titrations with identical twin electrodes, the width of the PDP (potential difference peak) serves as a convenient and immediate criterion for the proper functioning of the indicating system.

The rates of the chemical reaction, of the mass transfer to the diffusion layer and of the electrochemical reaction (charge transfer) at the electrode surface must all be rapid compared to the rate of titration progress; the passage of the reactants through the diffusion layer must be rate determining (although sufficiently rapid to prevent undue spreading of the potential difference peak); in addition, the diffusion layers at the twin indicating electrodes must be of different width.

In view of the above, certain limitations immediately become apparent: the method will be inapplicable to titrations of slowly-reacting species (a limitation common to many methods employing continuous recording). Efficient magnetic stirring, coupled with the proper layout of the titration cell will ensure sufficiently rapid mass transfer for titration times of 1 min or more.

Since the diffusion coefficients of most species are of the same order of magnitude, the rate of their passage through the diffusion layer will be determined chiefly by the latter's width; this, in turn, depends on the rate of stirring and on the roughness factor of the electrode surface. Beyond the maximum decrease of the diffusion layer effectable by efficient stirring, increased roughness will increase its width; it is, therefore, desirable to employ highly-polished electrode surfaces. Rough surfaces cause lagging of the observed end-point with regard to the equivalence point, increasing with increased roughness factor.

The rate of electrochemical reactions is governed by the reaction itself and by the character (material and surface condition) of the electrode. The influence of electrode cleanliness on the rate of electron transfer has been mentioned (e.g. in ref. 6); among others, surface-active substances, adsorbed at the electrode surface and films (e.g. oxide films) formed on it affect it significantly; as a result, even in systems characterized by high current densities, the presence of surface-active substances must be guarded against, and the formation of surface films avoided. Proper electrode treatment becomes crucial; passage of currents through the electrode during titration, liable to result in surface oxidation, should be avoided.

The experimental cell (100 ml approximately) described[1] was found suitable for this method, allowing the convenient positioning of the indicating electrodes; no efforts have been made to investigate smaller cells or volumes below 30 ml. The authors are aware that the proper lay-out for a particular cell must be determined by experiment, to ensure the sharpest indication achievable; however, due to the variety of parameters (e.g. electrode size and shape, rate and method of stirring, rate and site of titrant introduction, etc.), no general recommendations can be given.

ACID–BASE TITRATIONS AND THE MECHANISM OF INDICATING ELECTRODES WITH UNCOUPLED REDOX REACTIONS

An electrode system for acid–base titrations has been described: a pair of mercury-coated silver wire electrodes[1]. Part of the experiments were carried out with rigorous precautions to prevent the oxide coating of the electrode surface; in spite of this, a linear relationship between the potential of each electrode and the pH of the solution in which it is dipped was found in the pH range 5–9. This relationship ensures the response of the electrodes to the progress of the acid–base titrations (Fig. 1). These results agree with those reported[7] where this relationship was investigated in a most rigorous system. In both cases no experimental proof of the absence of a thin (monomolecular-layer) oxide film on the electrode was produced; such a film, obviously,

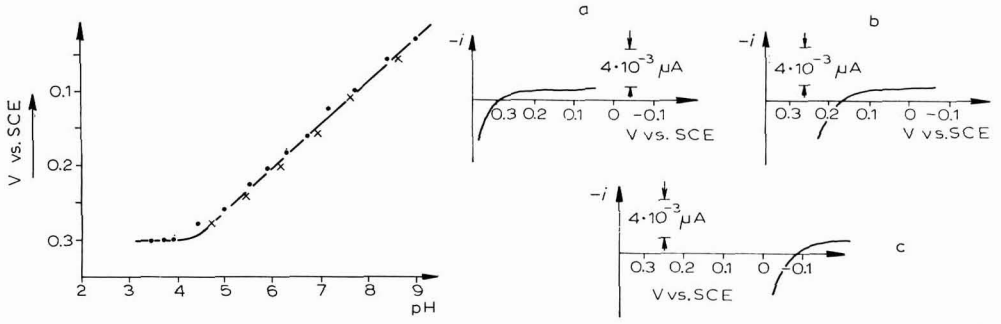

Fig. 1. pH–potential curve for the Hg–H_2O system (in the absence of O_2 and mercury ions). Hg electrodes: (●)HMDE according to KEMULA[17];(×) HMDE according to SHAIN[15].

Fig. 2. Current–potential curves of the Hg–H_2O system (in the absence of mercury ions), at various stages of the acid–base titration. Radiometer polarograph Polariter, Type PO 4d; initial soln. composition: KNO_3, 3% + HNO_3, $5 \cdot 10^{-4} N$; after thorough deaeration, and with passage of N_2 over the test solution throughout the experiments. Electrodes: HMDE according to KEMULA[17] *vs.* SCE. (a) $\lambda = 0$; (b) $\lambda = 1$; (c) $\lambda = 2$.

could provide an explanation of its Nernstian response to pH. However, in the absence of a film, another explanation of this response, based on the presence of a mixed potential (at zero current) may be proposed, the two partial reactions defining this potential being: (i) the anodic reaction of the oxidation of mercury, which is pH-dependent ($Hg \rightarrow Hg^{2+}$ in acid, $Hg \rightarrow HgO$ in basic media): (ii) the cathodic reaction, determined by the residual current (independent of pH).

Current–potential curves, recorded at various states of the titration (Fig. 2), support the possibility of the potential (at zero current) being determined not by a redox couple, but rather by the residual current coupled with a pH-dependent electrochemical reaction. The residual current remains virtually unchanged throughout the titration; the potential of mercury dissolution, on the other hand, changes and is responsible for the variation in the resulting mixed potential.

The proposed mechanism, which requires further corroboration, does not preclude the possible contribution of a reduction current due to the reduction of an oxide (mercury oxide) film, should such a film be present; however, this reduction will not be potential determining as long as the residual current due to other sources exceeds it.

To sum up: potentiometric titrations, at zero current, seem feasible in systems containing uncoupled redox reactions. A number of such electrodes have been reported, but, as far as the authors are aware, without a reasonable explanation of their mechanism (e.g. platinum electrodes for argentometry and platinum or mercury (in the absence of mercury ions) for complexometry).

Whatever the potential determining mechanism might be (mixed potential or thin oxide film), one may state that any metal of sufficient chemical and electrochemical stability in a given medium, may serve as a pH electrode, provided at least one of the electrochemical reactions is pH-dependent ($M \rightarrow MO$ or the redox reaction of water at noble metals). A number of electrodes have been tested: Ni, Sb, Ag, Au, Pt, Cu and graphite. Each responds to pH changes, but the rate of potential stabilization varies; graphite and antimony respond very slowly and are, therefore, entirely unsuited for use in twin electrode systems (in this case, the rate of the electrochemical process decreases with increased electrode polish)[10]. New smooth nickel electrodes function satisfactorily, but deteriorate rapidly after a few titrations.

The pH response of gold and silver electrodes has been demonstrated without polishing them especially; polished platinum electrodes*, while unsuitable for acidimetry (wide potential-difference peak and considerable lag), may be effectively employed in some redox determinations[11].

The authors are fully aware of the imperative need for pure solutions and clean electrodes to be employed in attempts at elucidating the difficult problems of electrodics and of the importance of the fundamental insights to be gained from such experiments; on the other hand, most analytical determinations cannot be carried out under such stringent conditions. The proposed method in a way, makes a virtue out of necessity, exploiting the non-ideality of the solution (i.e. the residual current due to slight impurities) as an aid to achieving end-point indication.

COPPER ELECTRODES

Copper electrodes were successfully employed in acid–base determinations of

* The polishing of the platinum electrodes parallels that described below for copper electrodes.

acetic and perchloric acid solutions, down to 10^{-5} *M*. Since their effectiveness and robustness were exemplary, a detailed description of their preparation is given here.

A copper wire (2 mm diameter) is soldered to a short copper rod (diameter 8 mm; length 30–40 mm), and both wire and rod are tightly bandaged with Teflon tape, so that only the base of the rod is left exposed. This base, the intended indicating surface, is polished on a lathe, at about 2000 rev./min, using increasingly finer grain carborundum paper, pressed against the copper surface by means of a flexible support (this ensures gradual removal of surface roughness, with equal pressure being effected throughout the polished area). No reconditioning is necessary; between titrations the electrodes are kept in a closed vessel containing a dehydrant (silica gel).

The influence of the generating current and of the roughness factor on the width of the potential difference peak (PDP) was tested for the smoothest electrodes, in a series of experiments; the width at half-peak height changed as follows:

Generating current (mA)	10	3	1
Width at half-peak (sec)	8	15	30

The changes in peak width were investigated, for varying degrees of indicating surface roughness at a generating current of 10 mA. The six degrees of roughness were produced by employing 5 kinds of carborundum paper, of various grain and, for the roughest electrode, a rough grinding stone (this differed appreciably from the rest). The results obtained are summarized below.

Electrode*	1	2	3	4	5	6
Width at half-peak (sec)	8	8	8	—	10	12

As may be seen, in the case of copper electrodes, changes in half-peak width remain moderate and the sharpness of the peaks is maintained in spite of the wide range of surface roughness tested. This, of course, makes them attractive for any system in which their chemical stability is satisfactory.

POTENTIOMETRIC TITRATIONS WITH TWIN ELECTRODES IN OTHER SYSTEMS

The method is not limited to acid–base titrations, but may also be applied to monitoring suitable complexometric and redox titrations; it will, probably, be inapplicable to precipitation titrations, since the adsorption of precipitates on the electrode surfaces affects their functioning.

Since there is no need for the electrode system to form a redox couple with the ion determined in solution, the choice of electrodes—at least in principle—is rather wide.

COMPLEXOMETRIC TITRATIONS

The exploitation of mercury electrodes in the presence of mercury ions for complexometry has been described[12]. In the present work, the applicability of the twin mercury electrode system (without the addition of mercury ions) to the titration of copper and EDTA has been investigated. A linear calibration curve was obtained for the determination of EDTA; for a 2.4×10^{-4} *M* soln. the standard deviation was 1%.

* The roughness of the electrode surface increased from 1→6.

ADVANTAGES AND LIMITATIONS

The method is suited to systems in which the rate of electrode response is relatively rapid (as compared to the rate of change in the composition of the titrated solution).

The instrumentation is simple, except for the IMU (impedance matching unit), which is easily constructed[13]. Due to its rapidity, the method is useful for routine determinations and for the monitoring of reaction kinetics; the recorded titration curves lend themselves easily to quantitative analytical interpretation. No reference electrode is required (this is important in the case of non-aqueous media or titrations in fused salts). The method is highly sensitive, precise and accurate. Surface-active agents must be absent.

Due to the difference in potential measurement, the method does not suffer from the disadvantages inherent in classical zero-current potentiometry (in spite of the fact that here, too, measurements are made at zero current). The classical method involves the measurement of equilibrium potentials; potential stabilization near the end-point is always slow and is also slow throughout the course of titrations in very dilute solutions. Potentiometry with twin electrodes, on the other hand, involves the measurement of non-equilibrium potentials[3], thus greatly shortening total titration time. This advantage is shared by the well-known potentiometric titrations with polarization current (dead-stop, etc.); however, twin electrode potentiometry at zero current has the distinct advantage of better electrode surface conservation, due to the absence of deleterious effects attributable to the passage of the polarizing current through the electrodes.

On the other hand, every system requires the development of a suitable electrode, including the method of its reconditioning to ensure proper functioning (the distortion of the titration curves indicates malfunctioning, but provides no clues to the best treatment for restoring the electrode surface to the desired state).

ACCURACY

In trace amount determination, the systematic error, resulting from the residual current and increasing with progressing sample dilution, must be taken into account and evaluated. The relationship between the residual current and the magnitude of the titration error may be illustrated by delineating the theoretical and experimental current–potential curves (Fig. 3) at the equivalent point of the reaction:

$$Red' + Ox'' \rightarrow Ox' + Red''$$

As a result of the superposition of the residual current curve on the theoretical curve, the experimental curve, obtained at the equivalent point, is shifted and made to appear as if this point had been passed, i.e. the end-point precedes the equivalent point and a negative error results. According to the nature of the impurities present, the end-point may precede (negative error) or lag after (positive error) the equivalent point; the absolute value of the error is given by: $(i_r/i_1\,(\lambda = 0)) \times 100\%$, where i_r is the residual current and i_1 the limiting current of the initial solution (before the start of the titration).

The following may serve to illustrate this point: a platinized-platinum electrode may serve as an indicating electrode for acid–base titrations[14]. Whenever

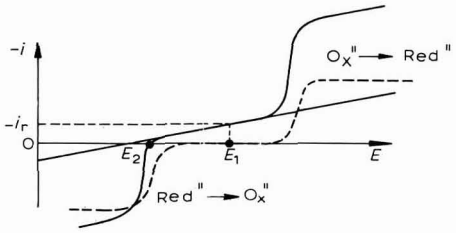

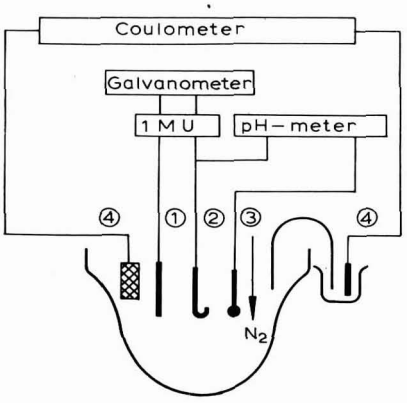

Fig. 3. Current–potential curves for a redox system, at the equivalence point. (—) experimental; (— —) theoretical curve.

Fig. 4. Outline of apparatus employed for determining the pH–potential curve for the mercury electrode. (Metrohm coulometer, Type E-211; IMU, differential electrometer according to YARNITZKY[13]; Shimadzu Polarograph voltmeter, Type RP-2; Beckman Expanded Scale pH meter, Model 76. Electrodes: (1) Hg-coated Ag wire or HMDE[17]; (2) commercial SCE; (3) glass electrode; (4) platinum generating electrode.

$[H^+] < 5 \cdot 10^{-5}$ N, the limiting current due to the reduction of hydrogen ions falls below the value of the residual current; an error of 10% must, therefore, be expected in the titration of a $5 \cdot 10^{-4}$ N solution. At the mercury electrode[2], on the other hand, the residual current is only 0.01% of the limiting current for a $5 \cdot 10^{-4}$ N H^+ solution; as a result, a hundredfold gain in sensitivity is achieved.

The differences in the residual currents at the two electrodes are attributable mainly to the enormous difference in the roughness factor of their surfaces; while a significant part of the residual current stems from slow reactions and is, therefore, proportional to the real surface of the electrode, the limiting current, due to the main reaction, is diffusion-controlled and largely proportional to the geometrical surface (provided the diffusion layer is relatively thick). This reasoning applies equally to classical potentiometry: whenever dilute solutions are titrated, smoothly-polished electrodes are desirable.

SENSITIVITY

In titrations performed with blank recording, the sensitivity of the determination is limited by the reproducibility of the residual current, which, in turn, depends largely on the constancy of the electrode surface throughout the blank and sample determination. Measurements carried out at zero current—as discussed here—minimize surface changes and thus enhance the reproducibility of the residual current. Accuracy may be further improved by following the sample determination by an additional determination, carried out after performing an appropriate standard addition (in addition to performing the usual blank determination).

EXPERIMENTAL

The apparatus employed has been described[1,2].

Recording of pH–potential curves

The schematic outline of the apparatus employed is given in Fig. 4. 10% KNO_3 soln. was introduced into the titration cell and HNO_3 electrogenerated by the passage of a 20 mA current for 30 sec. The polarity of the current was reversed and the acid titrated coulometrically. The titration was interrupted (i.e. the generating current stopped) periodically and two simultaneous measurements were taken: the potential of the mercury electrodes was measured against a commercial calomel electrode and the pH of the solution measured with a pH electrode. The solution was stirred continuously. Before each series of measurements, the following precautions were taken: (i) The mercury-coated silver electrode was conditioned to ensure its proper functioning, and its condition tested by the method previously described[2]; (ii) the platinum electrode dipping into the main cell was rinsed with conc. HNO_3, to ensure the removal of any traces of mercury which might have been deposited on it (due to chemical dissolution, from the mercury electrodes, traces of mercury ions are found in solutions containing dissolved oxygen; this attack is enhanced whenever the electrodes are immersed in alkaline solutions, such as are formed after the equivalence point of the titration of nitric acid. These mercury ions deposit on the generating platinum electrode during its cathodic cycle (acid titration) and redissolve during the anodic cycle (generation of acid). The presence of mercury ions in solution vitiates the proper interpretation of results. Dissolved oxygen was removed from the solution by bubbling purified nitrogen gas through them, for periods of 20 min; during these deaeration periods the mercury electrodes were removed from the cell. Nitrogen was passed over the solution surface throughout the measurements.

Apparatus employed

Beckman Expanded Scale pH meter, Type 76; Shimadzu polarograph, Type RP-2; IMU according to YARNITZKY[13]; Metrohm coulometer, Type E-211.

Recording of current–potential curves

The outline of apparatus employed is shown in Fig. 5. Since the current passing through the mercury electrode during the recording of the current–potential curve affects the state of its surface, the hanging mercury drop electrode described by SHAIN[15] was employed. This allows the electrode to be renewed at will by detaching the used drop and attaching a fresh replicate drop in its place. The SCE was constructed as recommended by LINGANE[16]; its salt bridge was stoppered with a little cylinder of tissue paper, assuring good contact and preventing electrolyte diffusion; its electrical resistance was 500–2000 Ω.

The rate of linear change of the potential, impressed on the mercury electrode, was chosen as a compromise between two extremes: since manual change is too slow, the amount of current passing through the electrode becomes excessive, causing significant changes on its surface; on the other hand, rapid potential changes are accompanied by considerable capacity currents and the resulting distortion of the current–potential curve. 100 mV min^{-1} was found to be the optimum rate of change : capacity currents are negligible and the current–potential curve can be recorded on a single drop (the curve is identical to that obtained with a number of drops, each serving for the recording of another section).

The potential changes were carried out from negative towards more positive

values, since the main changes in the mercury electrodes occur at excessively positive potentials.

The cell, stirring, oxygen removal, precautions against the presence of dissolved mercury and the coulometric titration were carried out as described above. The linear potential scan was provided by a polarograph, which also served as recorder.

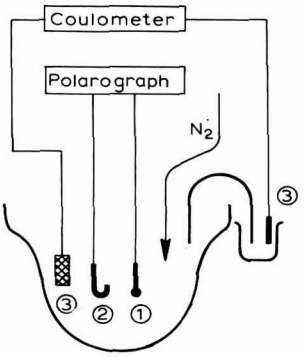

Fig. 5. Outline of apparatus employed for determining the current–potential curves. (1) HMDE according to SHAIN[15]; (2) SCE; (3) platinum generating electrode.

SUMMARY

Factors affecting the functioning of electrodes employed in the "twin-electrode at zero current" indicating system are discussed and the advantages, limitations, accuracy and sensitivity of the method surveyed. A proposed mechanism, explaining the pH response of "clean" metal electrodes to pH changes, or generally, in uncoupled redox reactions, is advanced.

REFERENCES

1 M. ARIEL AND E. KIROWA-EISNER, *J. Electroanal. Chem.*, 10 (1965) 319.
2 M. ARIEL AND E. KIROWA-EISNER, *J. Electroanal. Chem.*, 13 (1967) 90.
3 E. KIROWA-EISNER AND M. ARIEL, *J. Electroanal. Chem.*, 12 (1966) 286.
4 E. KIROWA-EISNER, *D.Sc. Thesis*, Technion—Israel Institute of Technology, 1965.
5 E. KIROWA, *M.Sc. Thesis*, Technion—Israel Institute of Technology, 1960.
6 J. E. B. RANDLES AND K. W. SOMERTON, *Trans. Faraday Soc.*, 48 (1952) 937.
7 S. E. S. EL-WAKKAD AND T. M. SALEM, *J. Phys. Chem.*, 54 (1950) 1371.
8 P. L. ALLEN AND A. HICKLING, *Anal. Chim. Acta*, 11 (1954) 467.
9 S. SIGGIA, D. W. EICHLIN AND R. C. REINHART, *Anal. Chem.*, 27 (1955) 1745.
10 G. CHARLOT, J. BADOZ-LAMBLING AND B. TRÉMILLON, *Electrochemcial Reactions*, Elsevier Amsterdam, 1962.
11 E. KIROWA-EISNER AND M. ARIEL, to be published.
12 C. N. REILLEY AND W. W. PORTERFIELD, *Anal. Chem.*, 28 (1956) 443.
13 CH. YARNITZKY, *J. Electroanal. Chem.*, 12 (1966) 265.
14 Ref. 10., p. 159.
15 I. SHAIN, *Anal. Chem.*, 33 (1966) 1961.
16 J. J. LINGANE. *Electroanalytical Chemistry*, Interscience, New York, 1953, p. 261.
17 W. KEMULA AND Z. KUBLIK, *Anal. Chim. Acta*, 18 (1958) 104.

ELECTROANALYTICAL CHEMISTRY AND INTERFACIAL ELECTROCHEMISTRY
Elsevier Sequoia S.A., Lausanne – Printed in The Netherlands

MEASUREMENT OF CHEMICAL REACTION RATES FOLLOWING ELECTRON TRANSFER. AN EMPIRICAL APPROACH USING RING-DISK ELECTRODES

P. A. MALACHESKY*, K. B. PRATER**, G. PETRIE AND R. N. ADAMS
Department of Chemistry, University of Kansas, Lawrence, Kansas 66044 (U.S.A.)
(Received April 3rd, 1967)

Since the original papers of the Frumkin school[1–3], the rotating ring-disk electrode (RRDE) has been relatively neglected. Except for studies on the reduction of oxygen[4,5], applications of the RRDE to electrode mechanisms are sparse and largely qualitative in nature[6,7]. HEUSLER AND SCHURIG used a double ring electrode to estimate the half-life of oxidized diphenylamine[8].

RRDE's with the narrow spacings between disk and ring necessary for kinetics studies, are indeed difficult to build and this has hampered practical applications. In addition, however, exact solutions for the boundary value problems pertinent to the RRDE have been lacking. The latter problem has been resolved in the recent series of authoritative papers by ALBERY AND BRUCKENSTEIN[9–12].

ALBERY AND BRUCKENSTEIN calculated an exact solution for N, the collection efficiency of a RRDE, in the absence of any chemical complications[10]. N is defined as the amount of material produced at the inner disk that reaches the outer ring. If all this material reaching the ring is electrochemically converted back to its precursor, then:

$$N = I_R/I_D$$

where I_R and I_D are the ring and disk currents, respectively. ALBERY AND BRUCKENSTEIN pointed out in particular, that N is a complex function of the electrode geometry.

The RRDE is ideally suited to the study of EC processes (Electron transfer followed by Chemical reaction) which can be formulated in general as:

$$A \rightleftharpoons B \quad (1)$$

$$B \xrightarrow{k} C \quad (2)$$

BRUCKENSTEIN AND FELDMAN[13] gave an approximate solution for a first-order decomposition of an intermediate (B) formed at the disk, in terms of the "transit time" for species B between disk and ring.

In a later paper, ALBERY AND BRUCKENSTEIN[11] examined this same situation of a first-order reaction of intermediate B. They were able to find exact expressions only for the two limiting cases: (a) where the chimical reaction (with rate constant, k)

* Present address: Tyco Labs., Waltham, Mass.
** Present address: Department of Chemistry, University of Texas, Austin, Texas.

was very fast, and (b) when the chemical kinetic loss of B was very small. No rigorous solution was available in the intermediate range which is characterized by the thickness of the diffusion layer, δ, being comparable to that of the reaction layer, μ.

It was suggested by ALBERY AND BRUCKENSTEIN that if EC processes with known rate constants could be studied at the RRDE, an empirical method for measuring intermediate rates could be developed. Thus, with a given RRDE, a "calibration curve" of N *vs.* δ/μ could be constructed. Since electrochemical systems with equal values of this ratio should give equal N-values, rate constants of unknown systems could be determined using the rotation rate as the experimental variable. An intuitive approach similar to this had been attempted in our laboratory and the studies of the above workers pointed the way for its practical utilization. These results are reported herein.

EXPERIMENTAL

The rotator assembly has already been described[14]. The RRDE had electroactive surfaces of carbon paste. It was constructed in the following manner. An elec-

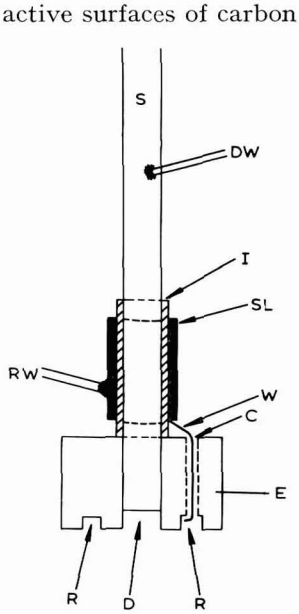

Fig. 1. Rotated ring-disk electrode. (S), brass shaft, top to chuck of rotator motor; (DW), wiper arm for disk electrical contact (typically multi-strand copper wire); (I), insulation layer of electrical tape; (SL), brass sleeve connected *via* wire W to ring electrode; (RW), wiper arm for ring electrical contact (typically multi-strand copper wire); (W), copper wire connecting sleeve to ring; (C), channel to back-surface of ring; (E), plastic body of RRDE; (D), disk cut-out, packed with carbon paste; (R), ring cut-out, packed with carbon paste.

trode "blank" was molded using a self-setting resin (Quick-Mount, Fulton Metallurgical Products Corp.) around an axial 1/4-in. brass rod. After the resin had set, the blank was machined on a lathe into a cylinder. The central disk portion was then drilled out (radius of the disk = 0.22 cm). Electrical contact to the carbon-paste disk was *via* the central brass rod and a wiper contact, DW, as seen in Fig. 1. The ring portion was cut,

with a cutting tool, into the electrode to a depth of *ca.* 1/16 in. A channel, C, was then drilled from the top of the cylinder down through the back-side of the ring. A copper wire contact, W, from the ring, passed through the channel and up to the top of the cylinder. It made contact to a brass sleeve, SL, insulated from the main shaft, S, *via* a simple electrical tape wrapping marked I in Fig. 1. Electrical contact was then made *via* the ring wiper arm, RW, which contacted the brass sleeve. The radius from the center of the disk to the inner boundary of the ring was 0.29 cm. The radius from the center of the disk to the outer circumference of the ring was 0.44 cm. Obviously, the gap between the disk and ring is not particularly narrow but this type of electrode is relatively easy to fabricate. The electroactive surfaces were packed with carbon paste in the usual fashion[15]. Care must be taken that excess paste on the plastic surface does not cause a conducting path between disk and ring. The RRDE of Fig. 1 is immersed to a depth no greater than about $\frac{1}{2}$ the height of the plastic cylinder.

The rate constants for the hydrolysis of the quinoneimines of *p*-aminophenol (PAP) and 3-methyl-*p*-aminophenol (3-MePAP) are easily measured by reverse current chronopotentiometry[16]. These electrode reactions correspond to eqns. (1) and (2) and were used to calibrate the RRDE. The PAP and 3-MePAP were purified by sublimation and recrystallization. Triply-distilled water was used for all solutions.

The disk electrode was held at a constant potential on the limiting current plateau for the oxidation of the aminophenols. A controlled-potential polarograph was used here. A Leeds and Northrup Electrochemograph was used to record the ring current as a function of applied potential at the ring electrode. Since the two reduction processes (of uncharged quinoneimine and hydrolysed quinone) are not well separated in potential, the measurement of current corresponding to quinoneimine reduction was empirical. This difficulty is also inherent in the chronopotentiometry measurements. However aminophenol systems have been examined by a variety of workers and the consistent results obtained make them reliable tests for EC processes.

RESULTS AND DISCUSSION

The calibration of the RRDE was accomplished by plotting I_R/I_D *vs.* $(k/\omega)^{\frac{1}{2}}$ where k is a known hydrolysis rate constant, and ω the rotation rate in rad/sec. The value of $(k/\omega)^{\frac{1}{2}}$ was chosen as an experimental parameter for the plot, since δ/μ is equal to a constant, 1.62 $D^{-\frac{1}{3}}\gamma^{\frac{1}{6}}$, multiplied by $(k/\omega)^{\frac{1}{2}}$. The values for the hydrolysis of the quinoneimines of PAP and 3-MePAP in 0.05 M sulfuric acid were used as known rate constants. These values, from reverse current chronopotentiometry[16], are: PAP, 0.10 sec^{-1} and 3-MePAP, 0.30 sec^{-1}.

The experimental data are given in Table 1 and plotted in Fig. 2 (points for both PAP and 3-MePAP make up the graph of Fig. 2). It can be seen that the intercept I_R/I_D, at $(k/\omega)^{\frac{1}{2}}=0$ should correspond to N, the collection efficiency with no chemical complications. This intercept in Fig. 2 is 0.519, in good agreement with the N-value, determined about a year previously with the same electrode, for the oxidation of *o*-dianisidine in 1M sulfuric acid where no chemical follow-up reaction occurs. The latter value was 0.525 ± 0.010. A least-squares fit of the straight line of Fig. 2 gives the following empirical equation relating I_R/I_D and $(k/\omega)^{\frac{1}{2}}$:

$$I_R/I_D = 0.519 - 1.350(k/\omega)^{\frac{1}{2}} \quad (3)$$

Equation (3) now allows rate constants for similar processes at this RRDE to

be determined. To test its validity, the hydrolysis rates of the quinoneimines were measured under considerably different solution conditions. Table 2 shows the calculated values of k from a variety of ω-values for 3-MePAP (quinoneimine hydrolysis) now in 0.01 M sulfuric acid. The average value is 0.58 ± 0.03 sec^{-1}. This is in good

TABLE 1

CALIBRATION DATA FOR RRDE

R(rev./sec)	ω[a]	k/ω	$(k/\omega)^{\frac{1}{2}}$	I_R/I_D
PAP in 0.05 M H_2SO_4 (k=0.10 sec^{-1})				
1	6.28	0.0161	0.124	0.323
2	12.56	0.0080	0.090	0.384
3	18.84	0.0054	0.073	0.408
4	25.12	0.0040	0.063	0.418
5	31.40	0.0032	0.057	0.433
3-MePAP in 0.05 M H_2SO_4 (k=0.30 sec^{-1})				
1	6.28	0.0481	0.219	0.218
2	12.56	0.0240	0.155	0.294
3	18.84	0.0160	0.126	0.349
4	25.12	0.0120	0.110	0.362
5	31.40	0.0096	0.098	0.405
6	37.68	0.0080	0.090	0.394
8	50.24	0.0060	0.078	0.435

[a]. in rad/sec, $\omega = 2\pi R$ where R = rev./sec.

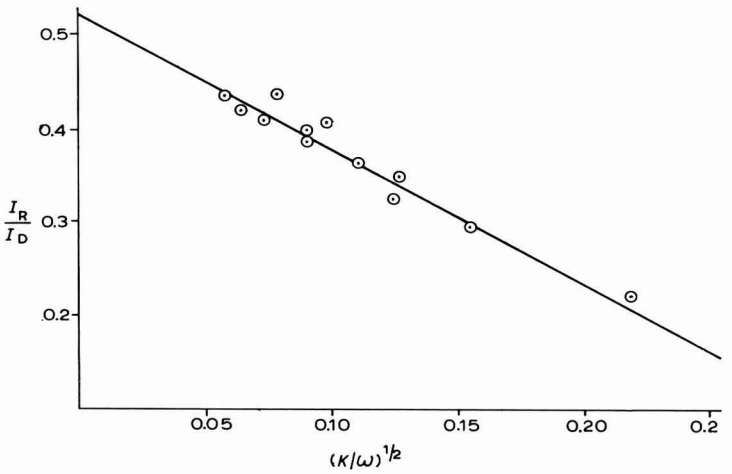

Fig. 2. Calibration plot for RRDE.

agreement with the value 0.50 ± 0.05 sec^{-1} measured at this acidity by reverse-current chronopotentiometry. For a check at a considerably lower value of k, the PAP system in 0.20 M sulfuric acid was chosen. Table 3 shows the RRDE data, and the average value of k is 0.052 ± 0.006 sec^{-1}. This is in excellent agreement with the reverse-current chronopotentiometric value of 0.052 sec^{-1}. The "calibration" technique obviously works quite well with the RRDE. The results also show that much

TABLE 2

DETERMINATION OF HYDROLYSIS RATE OF QUINONEIMINE OF 3-MePAP IN 0.01 *M* SULFURIC ACID

R(rev./sec)	$(1/\omega^{\frac{1}{2}})$*	I_R/I_D	$(k/\omega)^{\frac{1}{2}}$†	$k(sec^{-1})$
1.0	0.398	0.112	0.302	0.58
1.5	0.328	0.196	0.239	0.53
2.0	0.282	0.231	0.213	0.57
3.0	0.230	0.286	0.173	0.57
4.0	0.200	0.304	0.159	0.63
5.0	0.179	0.332	0.139	0.60
6.0	0.163	0.348	0.127	0.61
10.0	0.126	0.387	0.098	0.60
				Av. 0.58 ± 0.03

* in $rad^{-\frac{1}{2}}sec^{\frac{1}{2}}$
† calc. from eqn. (3) using these data.

TABLE 3

DETERMINATION OF HYDROLYSIS RATE OF QUINONEIMINE OF PAP IN 0.20 *M* SULFURIC ACID

R(rev./sec)	$(1/\omega^{\frac{1}{2}})$*	I_R/I_D	$(k/\omega)^{\frac{1}{2}}$†	$k(sec^{-1})$
1.5	0.328	0.424	0.0704	0.046
2.0	0.282	0.431	0.0652	0.053
2.5	0.252	0.437	0.0608	0.058
3.0	0.230	0.442	0.0570	0.062
3.5	0.213	0.458	0.0452	0.045
4.0	0.200	0.460	0.0437	0.048
				Av. 0.052 ± 0.006

* in $rad^{-\frac{1}{2}}sec^{\frac{1}{2}}$
† calcd. from eqn. (3) using these data.

valuable information can be obtained at the RRDE using only moderate rotation rates.

It should be stressed that eqn. (3) is applicable only to the particular electrode geometry described—each RRDE must be calibrated. While differences in diffusion coefficients will not cause major errors in k, this empirical approach is best suited to rate constants for related compounds. Unfortunately, at present data are not available for a wider variety of compounds (many of the systems we would like to study show filming of the electrode surface during oxidation and hence the kinetics data are unreliable).

ACKNOWLEDGEMENTS

This work was supported by the National Science Foundation through Grant GP-5079X. This support is gratefully acknowledged.

SUMMARY

An empirical calibration procedure for the rotated ring-disk electrode has been developed, following a suggestion by ALBERY AND BRUCKENSTEIN. This allows the

precise measurement of the rates of simple EC processes (Electron transfer followed by Chemical reaction) of moderate rates. A rather wide-gap carbon-paste ring-disk electrode, which is not too difficult to construct, is described.

REFERENCES

1 A. N. FRUMKIN AND L. I. NEKRASOV, *Dokl. Akad. Nauk SSRR*, 126 (1959) 115.
2 YU. B. IVANOV AND V. G. LEVICH, *ibid.*, (1959) 1029.
3 A. N. FRUMKIN, L. NEKRASOV, V. G. LEVICH AND YU. B. IVANOV, *J. Electroanal. Chem.*, 1 (1959) 84.
4 L. I. NEKRASOV AND L. MULLER, *Electrochim. Acta*, 9 (1964) 1015.
5 M. GENSHAW, A. DAMJANOVIC AND J. O'M. BOCKRIS, *J. Electroanal. Chem.*, 15 (1967) 163.
6 Z. GALUS AND R. N. ADAMS, *J. Am. Chem. Soc.*, 84 (1962) 2061.
7 C. A. CHAMBERS AND J. Q. CHAMBERS, *ibid.*, 88 (1966) 2922.
8 K. E. HEUSLER AND H. SCHURIG, *Z. Physik. Chem.*, 47 (1965) 117.
9 W. J. ALBERY, *Trans. Faraday Soc.*, 62 (1966) 1915.
10 W. J. ALBERY AND S. BRUCKENSTEIN, *ibid.*, (1966) 1920.
11 W. J. ALBERY AND S. BRUCKENSTEIN, *ibid.*, (1966) 1946.
12 W. J. ALBERY AND S. BRUCKENSTEIN, to be published.
13 S. BRUCKENSTEIN AND J. FELDMAN, *J. Electroanal. Chem.*, 9 (1965) 395.
14 Z. GALUS AND R. N. ADAMS, *J. Phys. Chem.*, 67 (1963) 866.
15 C. OLSEN AND R. N. ADAMS, *Anal. Chim. Acta*, 22 (1960) 582.
16 D. HAWLEY AND R. N. ADAMS, *J. Electroanal. Chem.*, 10 (1965) 376.

ELECTROANALYTICAL CHEMISTRY AND INTERFACIAL ELECTROCHEMISTRY
Elsevier Sequoia S.A., Lausanne – Printed in The Netherlands

REDOX EQUILIBRIA, PART IV*
TITRATION CURVE EQUATIONS FOR HOMOGENEOUS AND SYMMETRICAL REDOX REACTIONS

JAMES A. GOLDMAN
Department of Chemistry, Polytechnic Institute of Brooklyn, Brooklyn, New York (U.S.A.)
(Received April 13th, 1967)

INTRODUCTION

A general equation for the description of titration curves of homogeneous and symmetrical redox reactions has recently been presented[1]. The results of investigations into the properties of this equation have been discussed[1–3]. The general conclusion was that for any practical titration, the differences between the various values of interest (*e.g.*, the potential at 50% titrated) calculated from the rigorous equation and those calculated from the familiar simpler equations, were considerably smaller than any errors incurred in their experimental location.

Only the simplest titration situations have so far been discussed. The solution to be titrated has been considered to contain *only* a single species capable of being oxidized by the titrant. This obviously is never the situation in an actual titration because (even if no oxidized species is already present as a contaminant in the solid reagent used to prepare the solutions) the reduction of hydrogen ion makes it impossible to prepare a *perfectly* pure aqueous solution of any species capable of undergoing oxidation[4]. In other words, the potential at the very start of the titration is not infinitely negative but rather is finite and dependent upon the initial ratio of reductant to oxidant in the solution. It is now demonstrated that the general equation previously presented[1] may be readily modified to take into account the actual composition of the initial solution containing not only the original reductant but also some concentration of oxidant of the same couple.

Because of its significance in coulometric titrations with electrolytically-generated titrant, the situation where the original solution contains not only the reductant but, in addition, a particular concentration of the reduced form of the titrant, is also to be discussed.

Furthermore, reconsideration of some of the previously presented equations[1,2] has shown that in certain circumstances they may be expressed in somewhat more convenient forms than had been recognized and these results are also presented. The restrictions appropriate to the already derived general equation are first reviewed.

* Parts I, II and III, see refs. 1, 2 and 3, respectively.

GENERAL RELATIONSHIPS

Restricting ourselves to homogeneous and symmetrical redox reactions the following two reversible redox couples are considered:

$$Ox_1 + n_1 e \rightleftharpoons Red_1 \tag{1}$$

$$Ox_2 + n_2 e \rightleftharpoons Red_2 \tag{2}$$

for which the respective Nernst expressions are

$$E = E_1^{0\prime} - (RT/n_1F) \ln [Red_1]/[Ox_1] \tag{3}$$

$$E = E_2^{0\prime} - (RT/n_2F) \ln [Red_2]/[Ox_2] \tag{4}$$

where $E^{0\prime}$ represents the formal potential of the indicated couple, R, T, and F have their usual significance, and the concentrations of all species are expressed as molarity.

In the titration of Red_2 *with* Ox_1 as the titrant, the chemical equation representing the titration reaction is:

$$n_2\, Ox_1 + n_1\, Red_2 \rightleftharpoons n_2\, Red_1 + n_1\, Ox_2 \tag{5}$$

The relationship between the equilibrium constant for this reaction and the two formal potentials is

$$\Delta E^{0\prime} = E_1^{0\prime} - E_2^{0\prime} = (RT/n_1n_2F) \ln K \tag{6}$$

The equivalence point is defined in the following manner:

$$C_1^0 q = (n_2/n_1) C_2^0 V^0 \tag{7}$$

where C_2^0 is the initial molar concentration of Red_2, C_1^0 is the molar concentration of Ox_1 in the titrant solution, and q is the volume (ml) of titrant required to reach the equivalence point in the titration of V^0 ml of the original solution. In view of eqn. (7), the progress of the titration is most conveniently expressed in terms of f, defined as:

$$f = n_1C_1^0 V / n_2C_2^0 V^0 \tag{8}$$

where V represents ml of titrant added at any point. At the equivalence point, $V = q$. Because of their frequence occurrence it is also convenient to define the following quantities as follows:

$$\beta = V/(V^0 + V)\,, \quad \beta^0 = V^0/(V^0 + V) \tag{9}$$

Therefore, eqn. (8) may be rewritten as

$$f = n_1C_1^0\beta / n_2C_2^0\beta^0 \tag{8a}$$

THE GENERAL EQUATION WHEN $[Red_1] = 0$, $[Ox_2] = 0$, and $[Red_2] = C_2^0$, at $f = 0$

The application of material balance principles to the species involved in each couple is accomplished by the following expressions:

$$C_1^0\beta = [Ox_1] + [Red_1] \tag{10}$$

$$C_2^0\beta^0 = [Ox_2] + [Red_2] \tag{11}$$

Because at $f=0$, it is assumed that there is *only* Red_2 present in solution, it is evident that

$$[Red_1] = 0, \quad [Ox_2] = 0 \qquad \text{at } f = 0 \tag{12}$$

so that throughout the titration it is required by the stoichiometry of eqn. (5) that

$$[Red_1] = (n_2/n_1)\,[Ox_2] \tag{13}$$

At the equivalence point *only*, does

$$[Ox_1]^* = (n_2/n_1)\,[Red_2]^* \qquad (\text{at } f = 1) \tag{14}$$

It has previously been shown[1] that the combination of eqns. (3) and (4) with eqns. (6)–(14) results in

$$f = \{1 + k\exp(n_1\psi)\}/\{1 + k\exp(-n_2\psi)\} \tag{15}$$

where $\psi = (F/RT)(E - E^*)$, $E^* = (n_1E_1^{0\prime} + n_2E_2^{0\prime})/(n_1 + n_2)$, $\delta = (F/RT)\Delta E^{0\prime}$, $k = \exp(-n\delta)$, and $n = n_1n_2/(n_1 + n_2)$.

At $E = E_2^{0\prime}$, it has also been shown that

$$f = \tfrac{1}{2} + \tfrac{1}{2}\exp(-n_1\delta) \tag{16}$$

and that at $E = E_1^{0\prime}$

$$f = 2/[1 + \exp(-n_2\delta)] \tag{17}$$

From the definitions of δ and k, it is evident that

$$k^{(n_1+n_2)/n_2} = \exp(-n_1\delta) \tag{18}$$

and

$$k^{(n_1+n_2)/n_1} = \exp(-n_2\delta) \tag{19}$$

so that eqns. (16) and (17) may be rewritten respectively as

$$f = \tfrac{1}{2} + \tfrac{1}{2}k^{(n_1+n_2)/n_2} \qquad \text{at } E = E_2^{0\prime} \tag{20}$$

and

$$f = 2/[1 + k^{(n_1+n_2)/n_1}] \qquad \text{at } E = E_1^{0\prime} \tag{21}$$

For symmetrical reactions ($n_1 = n_2 = p$), these equations assume the particularly simple forms

$$f = \tfrac{1}{2} + \tfrac{1}{2}k^2 \qquad \text{at } E = E_2^{0\prime} \tag{22}$$

$$f = 2/(1 + k^2) \qquad \text{at } E = E_1^{0\prime} \tag{23}$$

from which it is obvious that for a given value of k, the values of f at these two points of interest are independent of the value of p, but because under these circumstances $k = \exp(-\frac{1}{2}p\delta)$, the value of p is not entirely unimportant.

Although eqn. (15) is generally valid throughout the titration, it was, nevertheless, convenient to rewrite it in two forms[1], one appropriate to the region prior to equivalence, and the other to the region subsequent to the equivalence point. For $f < 1$

$$E - E_2^{0\prime} = -(RT/n_2F)\ln\{(1-f)/f + (k^{(n_1+n_2)/n_2}/f)\exp(n_1F/RT)(E - E_2^{0\prime})\} \tag{24}$$

and for $f > 1$

$$E - E_1^{0\prime} = (RT/n_1F)\ln\{(f-1) + fk^{(n_1+n_2)/n_1}\exp(-n_2F/RT)(E - E_1^{0\prime})\} \tag{25}$$

where eqns. (18) and (19) have been used. It had been previously stated[1,2] that whereas f is readily calculated as a function of E from an explicit equation (eqn. (15)), the method of successive approximations applied to eqns. (24) and (25) was the only procedure by which E could be calculated as a function of f. In general, this is a valid statement. However, for *symmetrical* reactions it is possible to calculate directly a value of E for any particular value of f, as is now demonstrated.

For symmetrical reactions, eqn. (15) becomes

$$f = \{1 + k \exp(p\psi)\}/\{1 + k \exp(-p\psi)\} \tag{26}$$

or

$$f + fk \exp(-p\psi) = 1 + k \exp(p\psi) \tag{26a}$$

so that after multiplication by $\exp(-p\psi)$ and transposition of appropriate terms,

$$fk \exp(-2p\psi) + (f-1) \exp(-p\psi) - k = 0 \tag{26b}$$

which is a quadratic (in $\exp(-p\psi)$) equation. Therefore

$$p\psi = -\ln \left\{ \frac{(1-f) + [(1-f)^2 + 4fk^2]^{\frac{1}{2}}}{2fk} \right\} \tag{27}$$

or $E - E^* = -(RT/pF) \ln H$ where H represents the quantity enclosed within the braces in eqn. (27). It is apparent that $\psi = 0$ at $f = 1$. The notation $H(f, k)$ may be used to emphasize that the values of $E - E^*$ are dependent only upon the values of f for any particular titration in which the values of k and p are defined by the titration reaction. Equation (27) may be written as

$$E - E^* = (RT/pF) \ln k - (RT/pF) \ln \left\{ \frac{(1-f) + [(1-f)^2 + 4fk^2]^{\frac{1}{2}}}{2f} \right\} \tag{28}$$

so that it is readily confirmed that as $k \to 0$, $E - E^* \to (RT/pF) \ln k - (RT/pF) \cdot \ln \{(1-f)/f\}$ as is to be expected.

Although eqns. (27) and (28)—as eqn. (26)—are actually valid throughout the titration, *i.e.*, for $f > 1$ as well as $f < 1$, it is, nonetheless, appropriate to derive from eqn. (26) another expression for the region subsequent to the equivalence point. To do so, each term in eqn. (26a) is multiplied by $\exp(p\psi)$, and the terms rearranged to yield the quadratic (in $\exp(p\psi)$) equation

$$k \exp(2p\psi) + (1-f) \exp(p\psi) - fk = 0$$

the solution of which may be written as

$$p\psi = \ln \left\{ \frac{(f-1) + [(f-1)^2 + 4fk^2]^{\frac{1}{2}}}{2k} \right\} \tag{27a}$$

or

$$E - E^* = -(RT/pF) \ln k + (RT/pF) \ln \left\{ \frac{(f-1) + [(f-1)^2 + 4fk^2]^{\frac{1}{2}}}{2} \right\} \tag{29}$$

so that as $k \to 0$, $E - E^* \to -(RT/pF) \ln k + (RT/pF) \ln (f-1)$ which is the result predicted from the familiar, less rigorously formulated titration equations.

Two of the points of particular interest on the titration curve are the values of E at $f = \frac{1}{2}$ and 2, respectively. From eqn. (28)

$$E-E^* = (RT/pF)\ln k-(RT/pF)\ln\left\{\frac{1+[1+8k^2]^{\frac{1}{2}}}{2}\right\} \qquad \text{at } f=\tfrac{1}{2} \tag{28a}$$

whereas from eqn. (29)

$$E-E^* = -(RT/pF)\ln k+(RT/pF)\ln\left\{\frac{1+[1+8k^2]^{\frac{1}{2}}}{2}\right\} \qquad \text{at } f=2 \tag{29a}$$

Because for $f<1$ it is convenient to write $E-E^*$ as $E-E_2{}^{0\prime}+(RT/pF)\ln k$ and for $f>1$, $E-E^*$ as $E-E_1{}^{0\prime}-(RT/pF)\ln k$, it is evident that $(E-E_2{}^{0\prime})$, at $f=\frac{1}{2}$, is equal to $-(E-E_1{}^{0\prime})$, at $f=2$, as was previously demonstrated[2]. Therefore, the values listed in Table 2 of ref. 2 are valid not only for $p=1$, as was then assumed, but rather are independent of the value of p. In other words, for $p\Delta E^{0\prime}=200$ mV, at $f=\frac{1}{2}$, $-p(E-E_2{}^{0\prime})=0.0215$ mV which is equal to $p(E-E_1{}^{0\prime})$ at $f=2$.

THE GENERAL EQUATION WHEN $[\mathrm{Red_1}]=0$, $[\mathrm{Ox_2}]\neq 0$, AND $[\mathrm{Red_2}]=C_2{}^0$ AT $f=0$

This is the situation where the original solution initially contains not only $\mathrm{Red_2}$ (with $[\mathrm{Red_2}]=C_2{}^0$) but in addition a finite amount of the oxidized form of $\mathrm{Red_2}$, namely $\mathrm{Ox_2}$. The initial concentration of $\mathrm{Ox_2}$ in the solution to be titrated before any titrant has been added will be designated by $C_{\mathrm{Ox_2}}{}^0$. Equations (1)–(10) are still applicable but eqn. (11) is no longer valid and must now be replaced by

$$C_2{}^0\beta^0+C_{\mathrm{Ox_2}}{}^0\beta^0 = [\mathrm{Red_2}]+[\mathrm{Ox_2}] \tag{30}$$

Because at $f=0$, there is already some finite concentration of $\mathrm{Ox_2}$ present in solution, it is now stoichiometrically required that throughout the titration

$$[\mathrm{Ox_2}]-C_{\mathrm{Ox_2}}{}^0\beta^0 = (n_1/n_2)[\mathrm{Red_1}] \tag{31}$$

(instead of eqn. (13)) where the left-hand side of eqn. (31) represents the concentration of $\mathrm{Ox_2}$ produced *via* the titration reaction. At $f=0$, $\beta^0=1$ and $[\mathrm{Ox_2}]=C_{\mathrm{Ox_2}}{}^0$, so that $[\mathrm{Red_1}]=0$. At the equivalence point, it is still required that

$$[\mathrm{Ox_1}]^* = (n_2/n_1)[\mathrm{Red_2}]^* \qquad (\text{at } f=1) \tag{14}$$

Division of eqn. (30) by eqn. (10) yields

$$\frac{C_2{}^0\beta^0+C_{\mathrm{Ox_2}}{}^0\beta^0}{C_1{}^0\beta} = \frac{[\mathrm{Ox_2}]}{[\mathrm{Red_1}]}\,\frac{1+[\mathrm{Red_2}]/[\mathrm{Ox_2}]}{1+[\mathrm{Ox_1}]/[\mathrm{Red_1}]} \tag{32}$$

or

$$\frac{C_2{}^0\beta^0}{C_1{}^0\beta}+\frac{C_{\mathrm{Ox_2}}{}^0\beta^0}{C_1{}^0\beta} = \frac{[\mathrm{Ox_2}]}{[\mathrm{Red_1}]}\,\frac{1+k\exp(-n_2\psi)}{1+k\exp(n_1\psi)} \tag{32a}$$

where use has been made of $[\mathrm{Red_2}]/[\mathrm{Ox_2}]=\exp[-(n_2F/RT)(E-E_2{}^{0\prime})]=k\exp(-n_2\psi)$ and $[\mathrm{Ox_1}]/[\mathrm{Red_1}]=\exp[(n_1F/RT)(E-E_1{}^{0\prime})]=k\exp(n_1\psi)$. Using eqn. (8a), we may rewrite eqn. (32a) as

$$\frac{n_1}{n_2}\,\frac{1}{f}\,(1+\alpha_2{}^0) = \frac{[\mathrm{Ox_2}]}{[\mathrm{Red_1}]}\,\frac{1+k\exp(-n_2\psi)}{1+k\exp(n_1\psi)} \tag{32b}$$

where $\alpha_2{}^0=C_{\mathrm{Ox_2}}{}^0/C_2{}^0$. It is readily shown by use of eqns. (14), (31) and (32) that at $f=1$: $(C_2{}^0+C_{\mathrm{Ox_2}}{}^0)\beta^0=[\mathrm{Ox_2}]^*+[\mathrm{Red_2}]^*$ whereas in the previous case considered (where $C_{\mathrm{Ox_2}}{}^0=0$) it is evident that $C_2{}^0\beta^0=[\mathrm{Ox_2}]^*+[\mathrm{Red_2}]^*$, β^0 being evaluated at $f=1$.

To obtain a general equation for the titration curve from eqn. (32b) it is now necessary to find an expression for the ratio $[Ox_2]/[Red_1]$ for the entire course of the titration. In the situation previously considered, where $C_{Ox_2}{}^0 = 0$, it was shown that $[Ox_2]/[Red_1] = n_1/n_2$. However, in the present case this is no longer valid because of the requirement of eqn. (31).

To obtain an expression for $[Ox_2]/[Red_1]$, we must explicitly introduce the equilibrium constant for the reaction represented by eqn. (5)

$$K = \frac{[Red_1]^{n_2}[Ox_2]^{n_1}}{[Ox_1]^{n_2}[Red_2]^{n_1}} \tag{33}$$

or

$$K^{1/n_2}/([Ox_2]/[Red_2])^{n_1/n_2} = [Red_1]/[Ox_1] \tag{33a}$$

Now using eqn. (10) and eqn. (31), we can rewrite eqn. (33a) as

$$Q = \frac{(n_2/n_1)\{[Ox_2] - C_{Ox_2}{}^0\beta^0\}}{C_1{}^0\beta - (n_2/n_1)\{[Ox_2] - C_{Ox_2}{}^0\beta^0\}}$$

where Q represents the ratio on the right-hand side of eqn. (33a). Solving for $[Ox_2]$ yields

$$[Ox_2] = (n_1/n_2)[Q/(1+Q)]C_1{}^0\beta + C_{Ox_2}{}^0\beta^0 \tag{34}$$

The first term on the right-hand side of eqn. (34) represents the concentration of Ox_2 that is produced during the titration *via* oxidation of Red_2 according to eqn. (5). The second term represents the initial concentration of Ox_2, corrected for the dilution occurring during the titration. In other words, for the simple case previously considered, where $C_{Ox_2}{}^0 = 0$, the first term of eqn. (34) would express the concentration of $[Ox_2]$ throughout the titration.

Combination of eqns. (34) and (31) yields

$$[Red_1] = [Q/(1+Q)]C_1{}^0\beta \tag{35}$$

which, because it is independent of $C_{Ox_2}{}^0$, is a valid expression even where $C_{Ox_2}{}^0 = 0$. From eqns. (34) and (35)

$$[Ox_2]/[Red_1] = (n_1/n_2) + [(1+Q)/Q](\alpha_2{}^0\beta^0/\alpha^0\beta) \tag{36}$$

where $\alpha^0 = C_1{}^0/C_2{}^0$. Thus, when $\alpha_2{}^0 = 0$, we obtain eqn. (13) again. Whereas for homogeneous and symmetrical reactions in which $C_{Ox_2}{}^0 = 0$, the ratio $[Ox_2]/[Red_1]$ throughout the titration is constant and independent of the initial concentrations and the dilution occurring during the titration, this is not so when $C_{Ox_2}{}^0 \neq 0$. In the latter situation, the ratio depends not only upon the initial concentrations but also upon the dilution occurring during the titration.

Combination of eqns. (8a), (32b) and (36) yields

$$f = \frac{1 + k\exp(n_1\psi)}{1 + k\exp(-n_2\psi)}(1+\alpha_2{}^0) - \alpha_2{}^0(1+Q)/Q$$

Recalling that $[Ox_2]/[Red_2] = k^{-1}\exp(n_2\psi)$ so that $([Ox_2]/[Red_2])^{n_1/n_2} = k^{-n_1/n_2}\exp(n_1\psi)$, and that $K^{1/n_2}k^{n_1/n_2} = k^{-1}$, it may be shown that $(1+Q)/Q = 1 + k\exp(n_1\psi)$. Alternatively, $Q^{-1} = [Ox_1]/[Red_1] = k\exp(n_1\psi)$ so that $1 + Q^{-1} = 1 + k\exp(n_1\psi)$. Therefore the above equation for f may be conveniently written as

$$f = \frac{1 + k \exp(n_1 \psi)}{1 + k \exp(-n_2 \psi)} (1 + \alpha_2{}^0) - \alpha_2{}^0 [1 + k \exp(n_1 \psi)] \tag{37}$$

When $\alpha_2{}^0 = 0$, eqn. (37) yields eqn. (15).

The value of f at which $\psi = 0$, is no longer unity but instead

$$f(\text{at } \psi = 0) = 1 - \alpha_2{}^0 k \tag{38}$$

that is, the potential, *calculated* from $E^* = (n_1 E_1{}^{0\prime} + n_2 E_2{}^{0\prime})/(n_1 + n_2)$, always occurs *before* the equivalence point and the value of f at which it occurs always depends not only upon the magnitude of $C_{Ox_2}{}^0$ but *also* upon the value of k. In other words, f is not simply equal to $1 - \alpha_2{}^0$, as perhaps may have been expected from considerations only of material balance, but is greater than this. This may be better understood by observing that at $\psi = 0$, eqn. (36) becomes $[Ox_2]/[Red_1] = (n_1/n_2) + (1 + k) C_{Ox_2}{}^0 \beta^0 / C_1{}^0 \beta$ so that even at $\psi = 0$, the value of $[Ox_2]/[Red_1]$ is not independent of the value of k. For the simpler case (where $C_{Ox_2}{}^0 = 0$), the oxidant–reductant ratio is, however, independent of k as has always been assumed. From eqn. (38) it is concluded that for any practical titration where $p\Delta E^{0\prime} \geq 300$ mV (and thus $k \leq 2.91 \times 10^{-3}$), the value of $\alpha_2{}^0$ must exceed 0.344 in order for the value of f at $E = E^*$ to differ from unity by 0.1%. In other words, the initial presence of Ox_2 has relatively little effect on the value of f at which $E = E^*$.

Because the value of f is less than unity at $E = E^*$, the value of E at which $f = 1$ will occur at a point where $E - E^* > 0$, that is, with some Ox_2 originally present, the potential at the equivalence point (where $f = 1$) will be at a more positive value than that calculated from the familiar equation using the weighted average of the two formal potentials. This conclusion has been previously stated[5] but no general equation was presented.

Before considering the value of E at $f = 1$, *i.e.*, at the equivalence point, it is of some interest to consider the point, $f = 0$. Whereas from eqn. (15) it is predicted that at $f = 0$ the potential must be infinitely negative, eqn. (37) does not possess this limitation. At $f = 0$, eqn. (37) may be written as:

$$[1 + k \exp(n_1 \psi)][1 + \alpha_2{}^0] = \alpha_2{}^0 [1 + k \exp(n_1 \psi)][1 + k \exp(-n_2 \psi)]$$

which for *symmetrical* reactions may be rearranged to yield

$$\alpha_2{}^0 k \exp(-2p\psi) - (1 - \alpha_2{}^0 k^2) \exp(-p\psi) - k = 0$$

so that

$$p\psi = -\ln \left\{ \frac{(1 - \alpha_2{}^0 k^2) + [(1 - \alpha_2{}^0 k^2)^2 + 4\alpha_2{}^0 k^2]^{\frac{1}{2}}}{2\alpha_2{}^0 k} \right\} \tag{39}$$

and it is only as $\alpha_2{}^0 \to 0$ that $p\psi \to -\infty$. When $k = 10^{-3}$ and $\alpha_2{}^0 = 10^{-1}$, $p(E - E^*) = -236.6$ mV (at 25°) at $f = 0$, whereas for $k = 10^{-3}$ and $\alpha_2{}^0 = 10^{-2}$, $p(E - E^*) = -295.8$ mV. It is therefore the *initial* potential that is strongly dependent upon the concentration of Ox_2 originally present. This is understandable because the solution is then very poorly poised. Indeed, for reasonable values of $\alpha_2{}^0$ and k encountered in redox titrations, eqn. (39) may be approximated by the expression $p\psi \simeq \ln(\alpha_2{}^0 k)$ when $\alpha_2{}^0 k^2 \ll 1$, and therefore it is again evident that $p\psi \to -\infty$ as $\alpha_2{}^0 \to 0$.

Let us now consider the potential at which $f = 1$. Again restricting ourselves to symmetrical redox reactions, eqn. (37) at $f = 1$ may be rearranged to yield

$$\exp(2p\psi) - \alpha_2{}^0 k \exp(p\psi) - (\alpha_2{}^0 + 1) = 0$$

so that

$$p\psi = \ln\left\{\frac{\alpha_2{}^0 k + [(\alpha_2{}^0 k)^2 + 4(\alpha_2{}^0 + 1)]^{\frac{1}{2}}}{2}\right\} \tag{40}$$

It is evident that $p\psi \to 0$ as $\alpha_2{}^0 \to 0$. When $k = 10^{-3}$ and $\alpha_2{}^0 = 10^{-1}$, $p(E - E^*) = +1.224$ mV at $f = 1$ whereas when $k = 10^{-3}$ but $\alpha_2{}^0 = 10^{-2}$, $p(E - E^*) = +0.1278$ mV at $f = 1$. For the values of $\alpha_2{}^0$ and k commonly encountered, eqn. (40) may be approximated by $p\psi \simeq \frac{1}{2} \ln(1 + \alpha_2{}^0)$ when $\alpha_2{}^0 k^2 \ll 1$, and therefore it is obvious that $p\psi \to 0$ as $\alpha_2{}^0 \to 0$.

It is thus seen that the value of the potential at $f = 1$ is dependent almost entirely upon the magnitude of $\alpha_2{}^0$, and is essentially independent of the magnitude of k, whereas at $f = 0$ the value of the potential is dependent upon the values of $\alpha_2{}^0$ *and* of k. The discussion accompanying eqn. (38) may perhaps now be more clearly understood.

We now consider the values of f at which $E = E_2{}^{0\prime}$ and $E = E_1{}^{0\prime}$, respectively. Following an analogous procedure to that used to obtain eqns. (16)–(21), it may be shown that

$$f = \tfrac{1}{2}(1 + k^{(n_1+n_2)/n_2})(1 - \alpha_2{}^0) \qquad \text{at } E = E_2{}^{0\prime} \tag{41}$$

and

$$f = \{2/[1 + k^{(n_1+n_2)/n_1}]\}\{1 - \alpha_2{}^0 k^{(n_1+n_2)/n_1}\} \qquad \text{at } E = E_1{}^{0\prime} \tag{42}$$

which for symmetrical reactions assume the simple forms:

$$f = \tfrac{1}{2}(1 + k^2)(1 - \alpha_2{}^0) \qquad \text{at } E = E_2{}^{0\prime} \tag{43}$$

and

$$f = [2/(1 + k^2)][1 - \alpha_2{}^0 k^2] \qquad \text{at } E = E_1{}^{0\prime} \tag{44}$$

It is evident that when $\alpha_2{}^0 = 0$, eqns. (41)–(44) become identical to eqns. (20)–(23). It is interesting to note that the value of f at which $E = E_2{}^{0\prime}$ is now not always less than $\frac{1}{2}$. The value of f at $E = E_2{}^{0\prime}$ may be exactly equal to $\frac{1}{2}$ only if $\alpha_2{}^0 = k^2/(1 + k^2)$ whereas if $\alpha_2{}^0 > k^2/(1 + k^2)$, then f at $E = E_2{}^{0\prime}$ will be less than $\frac{1}{2}$. It is only when $\alpha_2{}^0 < k^2/(1 + k^2)$ that $f > \frac{1}{2}$. In contradistinction, the value of f at $E = E_1{}^{0\prime}$ is *always less than 2 and* is always less than the value of f at which $E = E_1{}^{0\prime}$ in the situation where there is *no* Ox_2 initially present.

For *symmetrical* redox reactions, eqn. (37) may be written in the following form

$$k(f + \alpha_2{}^0) \exp(-2p\psi) + (f - 1 + \alpha_2{}^0 k^2) \exp(-p\psi) - k = 0$$

so that

$$p\psi = -\ln\left\{\frac{(1 - f - \alpha_2{}^0 k^2) + [(1 - f - \alpha_2{}^0 k^2)^2 + 4k^2(f + \alpha_2{}^0)]^{\frac{1}{2}}}{2k(f + \alpha_2{}^0)}\right\} \tag{45}$$

which becomes identical to eqn. (27) when $\alpha_2{}^0 = 0$. When $f = \frac{1}{2}$, eqn. (45) may be rewritten as

$$p\psi = -\ln\left\{\frac{(1 - 2\alpha_2{}^0 k^2) + [(1 - 2\alpha_2{}^0 k^2)^2 + 8k^2(1 + 2\alpha_2{}^0)]^{\frac{1}{2}}}{2k(1 + 2\alpha_2{}^0)}\right\} \tag{45a}$$

which becomes identical to eqn. (28a) when $\alpha_2{}^0 = 0$. For $p\psi > 0$, it is convenient, for symmetrical reactions, to rewrite eqn. (37) as

$$k\exp(2p\psi)+(1-f-\alpha_2{}^0k^2)\exp(-p\psi)-k(f+\alpha_2{}^0)=0$$

so that

$$p\psi=\ln\left\{\frac{(f-1+\alpha_2{}^0k^2)+[(f-1+\alpha_2{}^0k^2)^2+4k^2(f+\alpha_2{}^0)]^{\frac{1}{2}}}{2k}\right\} \tag{46}$$

which becomes identical to eqn. (27a) when $\alpha_2{}^0=0$. When $f=2$, eqn. (46) may be rewritten as

$$p\psi=\ln\left\{\frac{(1+\alpha_2{}^0k^2)+[(1+\alpha_2{}^0k^2)^2+4k^2(2+\alpha_2{}^0)]^{\frac{1}{2}}}{2k}\right\} \tag{46a}$$

which when $\alpha_2{}^0=0$ corresponds to eqn. (29a). Because the argument of the logarithmic expression in eqn. (45a) possesses a larger magnitude when $\alpha_2{}^0=0$ than when $\alpha_2{}^0\neq 0$, the potential at the half-way point is always more positive for a non-zero value of $\alpha_2{}^0$ than it is for the solution that does not initially contain any Ox_2. Similarly, the potential at which $f=2$, is always more positive when there is Ox_2 initially present than when $C_{Ox_2}{}^0=0$ because the argument of the logarithmic expression in eqn. (46a) possesses a larger value when $\alpha_2{}^0$ is non-zero than when $\alpha_2{}^0=0$. In other words, for a given initial concentration of Red_2 and a given initial concentration of Ox_2, the *potential at any point is always more positive* than when the solution originally contains only Red_2. Equation (45) is a general equation for $p\psi$ at any value of f and it is readily apparent that at $f=0$, it reduces to eqn. (39). Similarly, eqn. (46) when $f=1$, reduces to eqn. (40). For the values of $\alpha_2{}^0$ and k commonly encountered, eqn. (45a) may be written as $p\psi\simeq\ln[k(1+2\alpha_2{}^0)]$ at $f=\frac{1}{2}$, and similarly at $f=2$, eqn. (46a) becomes $p\psi\simeq\ln[(1/k)+k(2+\alpha_2{}^0)]$. That is, at $f=\frac{1}{2}$: $p\psi\simeq(p\psi \text{ for } \alpha_2{}^0=0)+\ln(1+2\alpha_2{}^0)$ whereas at $f=0$: $p\psi\simeq(p\psi \text{ for } \alpha_2{}^0=0)+\ln\{[1+2k^2(1+\alpha_2{}^0)]/(1+2k^2)\}$. Again it is seen that a non-zero value of $\alpha_2{}^0$ has a greater effect on the region prior to the equivalence point than the region subsequent. This was the conclusion when we investigated the effect of a non-zero value of $\alpha_2{}^0$ upon the magnitude of E at $f=0$ as compared with its effect upon E at $f=1$.

THE GENERAL EQUATION WHEN $[Red_1]\neq 0$, $[Ox_2]=0$, AND $[Red_2]=C_2{}^0$, AT $f=0$

This is the situation where the original solution initially contains not only Red_2, to be oxidized during the titration by the Ox_1 in the titrant, but also an excess of the reduced form of the titrant, namely, Red_1. The initial concentration of Red_1 in the solution to be titrated, before any titrant has been added, will be designated by $C_{Red_1}{}^0$. Equations (1)–(9), and eqn. (11), are still applicable but eqn. (10) is no longer valid and must be replaced by

$$C_1{}^0\beta+C_{Red_1}{}^0\beta^0=[Ox_1]+[Red_1] \tag{47}$$

and it is now stoichiometrically required that throughout the titration

$$[Red_1]-C_{Red_1}{}^0\beta^0=(n_2/n_1)[Ox_2] \tag{48}$$

(instead of eqn. (13); also, *cf.* eqn. (31)). The left-hand side of eqn. (48) represents the concentration of Red_1 produced *via* the titration reaction. Equation (14) is still valid, at the equivalence point

$$[Ox_1]^*=(n_2/n_1)[Red_2]^* \tag{14}$$

Division of eqn. (47) by eqn. (11) yields

$$\frac{C_1{}^0\beta + C_{\mathrm{Red}_1}{}^0\beta^0}{C_2{}^0\beta^0} = \frac{[\mathrm{Red}_1]}{[\mathrm{Ox}_2]} \frac{1+[\mathrm{Ox}_1]/[\mathrm{Red}_1]}{1+[\mathrm{Red}_2]/[\mathrm{Ox}_2]} \tag{49}$$

or

$$\alpha_R{}^0 + (n_2/n_1)f = \frac{[\mathrm{Red}_1]}{[\mathrm{Ox}_2]} \frac{1+k\exp(n_1\psi)}{1+k\exp(-n_2\psi)} \tag{50}$$

where the same definitions are used as those in the derivation of eqn. (32) except that $\alpha_R{}^0 = C_{\mathrm{Red}_1}{}^0/C_2{}^0$. It is readily shown by the use of eqns. (14), (48) and (49) that at $f=1$: $C_2{}^0\beta^0 = [\mathrm{Ox}_2]^* + [\mathrm{Red}_2]^*$ where β^0 is to be evaluated at $f=1$.

As in the case just considered where $C_{\mathrm{Ox}_2}{}^0 \neq 0$, it is now necessary to find an expression for the ratio $[\mathrm{Red}_1]/[\mathrm{Ox}_2]$ for the entire course of the titration. The procedure for this follows that used in obtaining eqn. (37). We begin with eqn. (33a)

$$Q = [\mathrm{Red}_1]/[\mathrm{Ox}_1] \tag{33a}$$

Using eqn. (47) and (48), we can rewrite eqn. (33a) as

$$Q = \frac{C_{\mathrm{Red}_1}{}^0\beta^0 + (n_2/n_1)[\mathrm{Ox}_2]}{C_1{}^0\beta - (n_2/n_1)[\mathrm{Ox}_2]}$$

which upon solving for $[\mathrm{Ox}_2]$ yields (*cf.* eqn. (34))

$$[\mathrm{Ox}_2] = (n_1/n_2)[Q/(1+Q)]C_1{}^0\beta - [(n_1/n_2)/(1+Q)]C_{\mathrm{Red}_1}{}^0\beta^0 \tag{51}$$

where the first term on the right-hand side represents the concentration of Ox_2 that is produced during the titration *via* oxidation of Red_2 according to eqn. (5). Combination of eqn. (51) with eqn. (48) yields (*cf.* eqn. (35))

$$[\mathrm{Red}_1] = [Q/(1+Q)][C_1{}^0\beta + C_{\mathrm{Red}_1}{}^0\beta^0] \tag{52}$$

The quantity, $[Q/(1+Q)](C_1{}^0\beta)$, represents the concentration of Red_1 produced by the titration reaction. It is interesting to note that this contribution to the overall concentration of Red_1 is not directly added to the initial concentration—corrected for dilution occurring during the titration—of Red_1, *viz.*, $C_{\mathrm{Red}_1}{}^0\beta^0$, but only to a fraction of it.

Using eqns. (52) and (51), it is evident that

$$[\mathrm{Red}_1]/[\mathrm{Ox}_2] = (n_2/n_1)Q \frac{(n_2/n_1)f + \alpha_R{}^0}{Q(n_2/n_1)f + \alpha_R{}^0}$$

which may be substituted into eqn. (50) to obtain

$$f = \frac{1+k\exp(n_1\psi)}{1+k\exp(-n_2\psi)} + (n_1/n_2)(\alpha_R{}^0/Q)$$

or

$$f = \frac{1+k\exp(n_1\psi)}{1+k\exp(-n_2\psi)} + \alpha_R{}^0(n_1/n_2)k\exp(n_1\psi) \tag{53}$$

When $\alpha_R{}^0 = 0$, eqn. (53) yields eqn. (15).

The value of f at which $\psi = 0$, is no longer unity but

$$f(\text{at } \psi = 0) = 1 + \alpha_R{}^0(n_1/n_2)k$$

so that the potential calculated from $E^* = (n_1E_1{}^{0\prime} + n_2E_2{}^{0\prime})/(n_1+n_2)$ always occurs

after the equivalence point and the value of f at which it occurs depends not only on the value of $C_{\mathrm{Red_1}}{}^0$ but also on the value of k. Therefore, for any practical titration where $p\Delta E^{0\prime} \geq 300$ mV (and thus $k \leq 2.91 \times 10^{-3}$), the value of $\alpha_{\mathrm{R}}{}^0$ must exceed 0.344 (for $n_1 = n_2 = p$) in order for the value of f at $E = E^*$ to differ from unity by more than 0.1%.

Restricting our considerations to *symmetrical* redox reactions, eqn. (53) may be rearranged to

$$(\alpha_{\mathrm{R}}{}^0 + 1)k \exp(2p\psi) + (1 - f + \alpha_{\mathrm{R}}{}^0 k^2) \exp(p\psi) - fk = 0 \tag{54}$$

so that

$$p\psi = \ln \left\{ \frac{-(1 - f + \alpha_{\mathrm{R}}{}^0 k^2) + [(1 - f + \alpha_{\mathrm{R}}{}^0 k^2)^2 + 4fk^2(1 + \alpha_{\mathrm{R}}{}^0)]^{\frac{1}{2}}}{2k(1 + \alpha_{\mathrm{R}}{}^0)} \right\} \tag{55}$$

and at $f = 1$ (*cf.* eqn. (40))

$$p\psi = \ln \left\{ \frac{-\alpha_{\mathrm{R}}{}^0 k + [(\alpha_{\mathrm{R}}{}^0 k)^2 + 4(1 + \alpha_{\mathrm{R}}{}^0)]^{\frac{1}{2}}}{2(1 + \alpha_{\mathrm{R}}{}^0)} \right\}$$

Therefore, whenever $\alpha_{\mathrm{R}}{}^0 k \ll 1$, it is sufficiently accurate to use

$$p\psi = -\tfrac{1}{2} \ln(1 + \alpha_{\mathrm{R}}{}^0) \qquad \text{at } f = 1$$

which is analogous to the approximate equation derived from eqn. (40). For example, when $k = 10^{-3}$ and $\alpha_{\mathrm{R}}{}^0 = 10^{-1}$, $p(E - E^*) = -1.222$ mV at $f = 1$. In the previous case considered where $\alpha_2{}^0 \neq 0$, it was found that $p\psi \simeq \frac{1}{2} \ln(1 + \alpha_2{}^0)$ at $f = 1$ so that the modifications in the two cases are essentially of the same nature.

At $f = 2$, eqn. (55) becomes

$$p\psi = \ln \left\{ \frac{(1 - \alpha^0 k^2) + [(1 - \alpha^0 k^2)^2 + 8k^2(1 + \alpha_{\mathrm{R}}{}^0)]^{\frac{1}{2}}}{2k(1 + \alpha_{\mathrm{R}}{}^0)} \right\}$$

which reduces to eqn. (29a) when $\alpha_{\mathrm{R}}{}^0 = 0$. For values of $\alpha_{\mathrm{R}}{}^0 k^2$ usually encountered, it is possible to approximate this expression by $p\psi \simeq \ln[1/k(1 + \alpha_{\mathrm{R}}{}^0) + 2k]$ or further by $-\ln[k(1 + \alpha_{\mathrm{R}}{}^0)]$.

Alternatively, eqn. (54) may be written as

$$fk \exp(-2p\psi) + (f - 1 - \alpha^0 k^2) \exp(-p\psi) - k(\alpha_{\mathrm{R}}{}^0 + 1) = 0$$

so that

$$p\psi = -\ln \left\{ \frac{-(f - 1 - \alpha_{\mathrm{R}}{}^0 k^2) + [(f - 1 - \alpha^0 k^2)^2 + 4fk^2(\alpha_{\mathrm{R}}{}^0 + 1)]^{\frac{1}{2}}}{2fk} \right\} \tag{56}$$

and thus at $f = \frac{1}{2}$

$$p\psi = -\ln \left\{ \frac{(1 + 2\alpha_{\mathrm{R}}{}^0 k^2) + [(1 + 2\alpha_{\mathrm{R}}{}^0 k^2)^2 + 8k^2(\alpha_{\mathrm{R}}{}^0 + 1)]^{\frac{1}{2}}}{2k} \right\}$$

which reduces to eqn. (28a) when $\alpha_{\mathrm{R}}{}^0 = 0$. For values of $\alpha_{\mathrm{R}}{}^0 k^2$ usually encountered, it is possible to approximate this expression by $p\psi \simeq -\ln[(1/k) + 2k(1 + \alpha_{\mathrm{R}}{}^0)]$.

Comparison of these equations for $p\psi$ at various locations of interest (*e.g.*, $f = \frac{1}{2}$, 1, and 2) with the corresponding equations derived for $\alpha_{\mathrm{R}}{}^0 = 0$, demonstrates that the potential is always more negative when there is some $\mathrm{Red_1}$ initially present and moreover, consideration of eqn. (56) indicates that throughout the titration curve, the *potential at any point is always more negative* than when the solution

originally contains only Red_2. Recognition of this characteristic is not entirely new[5,6] but no general equations have previously been presented to describe quantitatively the titration curve for the *entire* course of the titration.

We now consider the values of f at which $E=E_2{}^{0\prime}$ and $E=E_1{}^{0\prime}$, respectively. Following an analogous procedure to that used to obtain eqns. (16)–(21), it may be shown from eqn. (53) that

$$f=\tfrac{1}{2}(1+k^{(n_1+n_2)/n_2})+(n_1/n_2)\alpha_R{}^0 k^{(n_1+n_2)/n_2} \qquad \text{at } E=E_2{}^{0\prime} \tag{57}$$

and

$$f=\{2/[1+k^{(n_1+n_2)/n_1}]\}+(n_1/n_2)\alpha_R{}^0 \qquad \text{at } E=E_1{}^{0\prime} \tag{58}$$

which for *symmetrical* reactions assume the simple forms

$$f=\tfrac{1}{2}(1+k^2)+\alpha_R{}^0 k^2 \qquad \text{at } E=E_2{}^{0\prime} \tag{59}$$

and

$$f=[2/(1+k^2)]+\alpha_R{}^0 \qquad \text{at } E=E_1{}^{0\prime} \tag{60}$$

It is evident that when $\alpha_R{}^0=0$, eqns. (57)–(60) become identical to eqns. (20)–(23). Whereas the value of f at $E=E_2{}^{0\prime}$ is always greater than $\frac{1}{2}$, and greater than it would be if $\alpha_R{}^0=0$, it is interesting to note that the value of f at $E=E_1{}^{0\prime}$ may be exactly equal to 2 only if $\alpha_R{}^0=2k^2/(1+k^2)$ which therefore restricts the magnitude of $\alpha_R{}^0$ to values less than unity. For f at $E=E_1{}^{0\prime}$ to be greater than 2, it is necessary that $\alpha_R{}^0>2k^2/(1+k^2)$, and for f to be less than 2, the requirement is that $\alpha_R{}^0<2k^2/(1+k^2)$. However, because the value of $\alpha_R{}^0$ cannot be negative, it is evident that $E=E_1{}^{0\prime}$ can never occur at $f=1$ nor even at $f=1.5$. Indeed, the value of f will always be within the region: $2>f>2/(1+k^2)$ whenever $\alpha_R{}^0<2k^2/(1+k^2)$.

SUMMARY

The earlier parts of this series have presented some results of investigations into the characteristic properties of potentiometric titration curves for symmetrical and homogeneous redox reactions. It was always assumed that only one redox form (*e.g.*, the oxidized form, in the particular situation investigated) of the titrant couple was in the titrant and that the solution to be titrated contained initially only one redox form (*e.g.*, the reduced form) of the other couple. For this *idealized* situation, a rigorously derived equation was obtained which readily permitted the calculation of the progress of the titration, f, as an explicit function of the potential, E. It has now been shown that for *symmetrical* redox reactions it is possible to solve this equation analytically so as to express E *directly* as a function of f.

Furthermore, the theoretical treatment of redox titration curves has been extended beyond the idealized situation where initially only one form of each couple is present in each solution. The results for two cases of analytical interest have been presented.

The solution to be titrated often contains some Ox_2 as well as some Red_2, which latter is to be oxidized by the Ox_1 in the titrant. The effect of this initial amount of Ox_2 on the nature of the titration curve is to cause the potential to be always *more positive* throughout the titration than it would be at corresponding locations, *i.e.*, values of f, in the absence of some initially present Ox_2. An immediate result of this is that now the theoretically derived equation indicates that at $f=0$,

E is not negatively infinite but rather possesses a finite value. The value of f at which $E=E^*=(n_1E_1^{0\prime}+n_2E_2^{0\prime})/(n_1+n_2)$ occurs at a value of f *less* than unity and depends upon $\Delta E^{0\prime}$ as well as upon the concentration of Ox_2 initially present. Whereas in the idealized case the value of f at $E=E_2^{0\prime}$ was always greater than $\frac{1}{2}$ and the value of f at $E=E_1^{0\prime}$ always less than 2, it is now possible at $E=E_2^{0\prime}$ for f to be exactly equal to, or less than, $\frac{1}{2}$ when $\alpha_2^0(=C_{Ox_2}^0/C_{Red_2}^0)$ is less than k^2, where $k=\exp[-(0.5\,pF/RT)\Delta E^{0\prime}]$.

The other case for which results are presented is that which occurs often in coulometric titrations, where the original solution to be titrated contains not only the reductant, Red_2, but also a particular concentration of the reduced form of the titrant. The effect of this is to cause the potential to be always *more negative* throughout the titration than it would be at corresponding locations in the absence of some initially present Red_1. At $E=E^*$, the value of f is greater than unity, and is dependent upon n_1/n_2 and k as well as upon the value of $\alpha_R^0(=C_{Red_1}^0/C_{Red_2}^0)$. For symmetrical reactions, the value of f at which $E=E_2^{0\prime}$, is always greater than $\frac{1}{2}$ whereas at $E=E_1^{0\prime}$, the value of f may be equal to, or less than, 2 whenever α_R^0 is less than $2k^2$.

In the course of the derivations, equations were obtained which explicitly express the variation in concentration of the various species during the titration. Each concentration may be written as the sum of two individual contributions: one arising from that which is produced during the titration, and the other arising from the initially present constituent of the appropriate redox couple.

REFERENCES

1 J. A. GOLDMAN, *J. Electroanal. Chem.*, 11 (1966) 255.
2 J. A. GOLDMAN, *J. Electroanal. Chem.*, 11 (1966) 416.
3 J. A. GOLDMAN, *J. Electroanal. Chem.*, 14 (1967) 373.
4 J. J. LINGANE, *Electroanalytical Chemistry*, Interscience Publishers, Inc., New York, 2nd ed., 1958, p. 137.
5 *ibid.*, p. 139.
6 L. MEITES AND H. C. THOMAS, *Advanced Analytical Chemistry*, McGraw-Hill Book Company, Inc., New York, 1958, pp. 64–65.

ELECTROANALYTICAL CHEMISTRY AND INTERFACIAL ELECTROCHEMISTRY
Elsevier Sequoia S.A., Lausanne – Printed in The Netherlands

POLAROGRAPHIC REDUCTION OF OXYGEN IN FORMAMIDE

FRANCESCO RALLO AND LILIANA RAMPAZZO
Istituto di Chimica, Facoltà di Ingegneria dell'Università di Roma (Italy)
(Received April 7th, 1967)

The polarographic reduction of oxygen in non-aqueous organic solvents has recently been the subject of several publications[1–5]; aprotic solvents or solvents with weakly labile protons, such as acetonitrile, dimethylformamide, dimethylsulfoxide, pyridine, acetone have mainly been used. In these solvents, the first reduction wave corresponds to a reversible one-electron process giving superoxide ion which is stable in the absence of protonating agents. In aqueous solutions, on the contrary, the first reduction wave is always a two-electron process at all pH-values, regardless of the reversibility.

This paper reports on the reduction of oxygen in formamide (FMM) at the dropping mercury electrode. FMM is frequently a good solvent for electrolytes ($\varepsilon^{25°} = 111.3$) and, unlike the non-aqueous solvents mentioned above, shows some autoprotolytic behaviour ($pK^{20°} \cong 17$)[6].

EXPERIMENTAL

Polarographic current–potential curves were recorded using a d.c. two-electrode instrument (Amel model 461). The water content of the solvent was measured by Karl Fisher titration, using a potentiometric titrator (Radiometer model TTT 1c/KF) with an automatic microburette which could titrate a minimum water content of 0.1 p.p.m. on a 5-ml aliquot of solvents.

Electrolyte solutions were 0.1 *F* KCl in FMM; the non-polarizable reference electrode was the mercury pool which was found to have a sufficiently stable potential under our experimental conditions. All potential values reported in this paper are referred to this reference electrode. The capillary used had the following characteristics: drop time, 4.08 sec; m, 1.81 mg sec^{-1}; h_{Hg}, 92 cm and an applied potential of −0.30 V in aerated FMM solution.

Formamide (Merck, chromatographic grade), was dried over BDH molecular sieves Type 4A (1/16 in. pellets) and then distilled three times ($p = 6$ mm Hg, $t =$ 88–89°) discarding the initial 20% and the final 10%. The water content of the purified solvent varied from batch to batch (40–80 p.p.m.; $2.5–5 \cdot 10^{-3}$ M).

The gases used (oxygen, nitrogen and various mixtures of the two) were obtained from the S.I.O. as very pure products; they were dried by passing them through tubes containing Drierite and P_2O_5 on glass-wool. The dried gases were checked for water content by bubbling them into a cell containing FMM of known water content. No detectable water was introduced after 8 h bubbling at a rate of 36 ml/min.

Mercury was triply-distilled; KCl (Merck p.a.) was oven-dried.

The H_2O_2 used, was an aqueous 30% w/v solution (Carlo Erba RS) appropriately diluted with FMM and titrated with $KMnO_4$; the water introduced into the FMM solution by the addition of H_2O_2 corresponded to 10–100% of the original water content of the solvent.

The solubility of oxygen in 0.1 *F* KCl–FMM solutions was determined by a modification of the Winkler method[7] using the following procedure:

A ground-glass-stoppered flask of exactly 47.0 ml volume was filled with aerated distilled water and the total oxygen content determined. The same flask was refilled with the water from the same sample and 10 ml of FMM added expelling the equivalent amount of water. The total oxygen content of the mixed solution was determined. The difference between the two determinations (*i.e.*, the difference between the quantity of oxygen dissolved in 10 ml of water and in 10 ml of FMM solution) was used to calculate the oxygen concentration in the FMM solution.

It was checked, by using deaerated FMM, that FMM itself did not interfere with the Winkler reactions or with the final iodometric titration.

The solubility of oxygen in 0.1 *F* KCl–FMM solution was found by this method to be 2.9×10^{-4} *M* at 19.0° and $P_{O_2} = 153$ mm Hg.

Also, a linear relationship between concentration of dissolved oxygen and its pressure in the gas phase was verified for pressure values between 38 and 767 mm Hg.

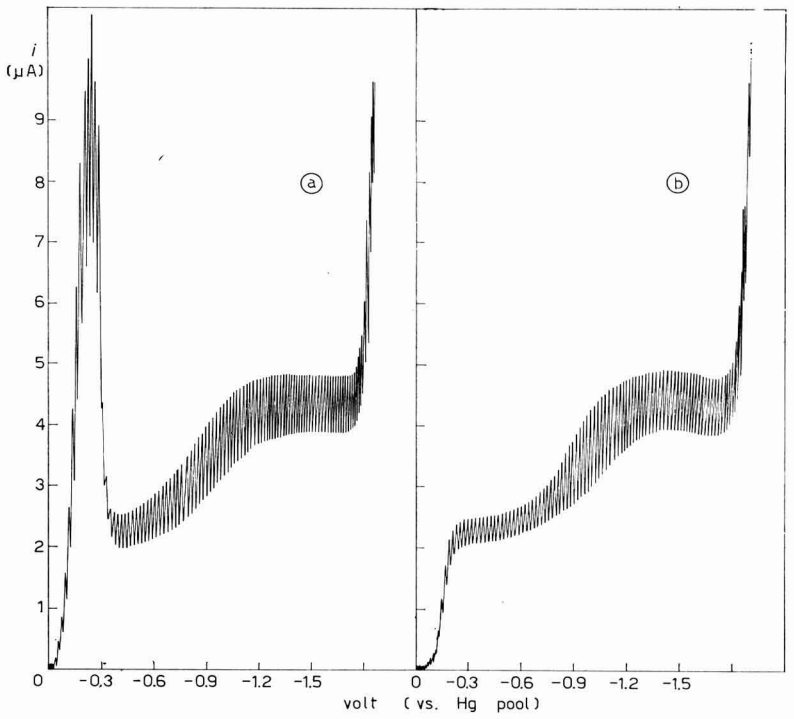

Fig. 1. (a), Polarographic waves of O_2 in 0.1 *F* KCl–FMM; (b), plus $1 \cdot 10^{-5}$ *M* eosin. O_2 concn.: 2.95×10^{-4} *M*; $t = 19 \pm 0.5°$.

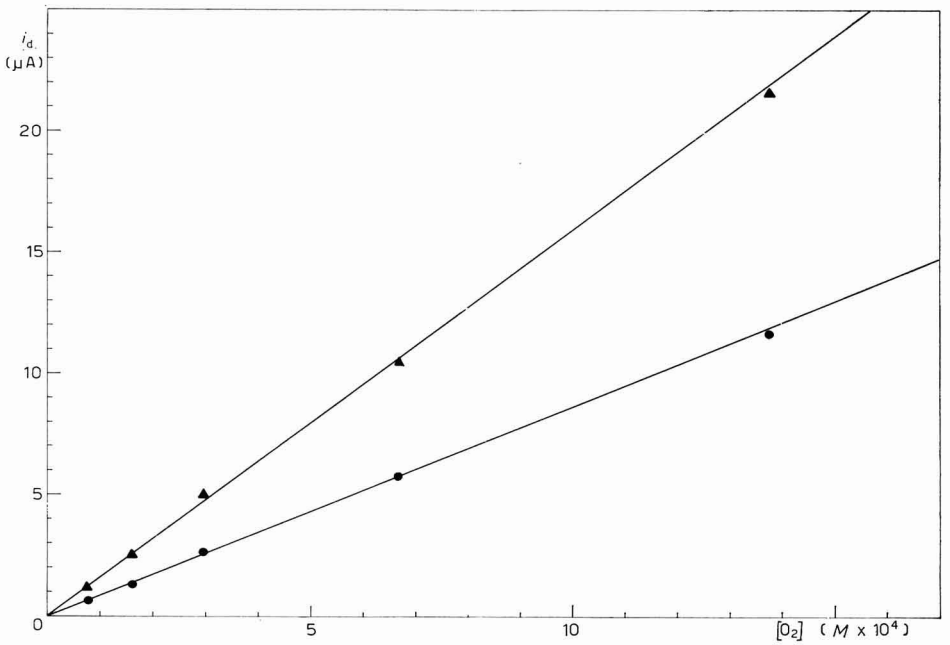

Fig. 2. Diffusion currents of O_2 reduction in 0.1 F KCl–FMM solns. at various O_2 concns. (●), Height of the first wave; (▲), total height of the two waves.

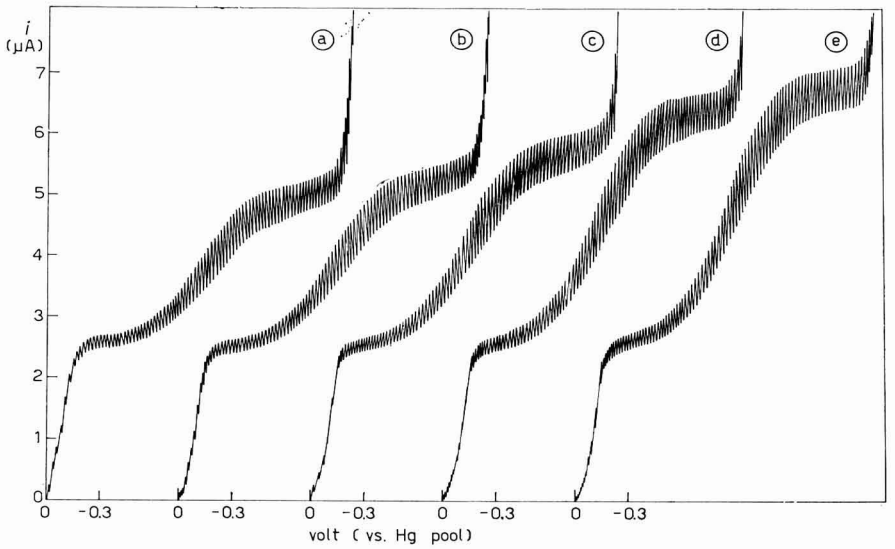

Fig. 3. Reduction waves of $3 \cdot 10^{-4}$ M O_2 in 0.1 F KCl–FMM, $1 \cdot 10^{-5}$ M eosin solns., with the following H_2O_2 concns.: (a), 0; (b), 5.6×10^{-5}; (c), 1.42×10^{-4}; (d), 2.74×10^{-4}; (e), 3.36×10^{-4} M.

The results obtained with this method have been confirmed by MASCINI, who used the stripping method recently proposed[8].

RESULTS AND DISCUSSION

The polarographic reduction of oxygen in 0.1 *F* KCl–FMM solution gives two waves of equal height, the first showing a strong maximum of the first kind, easily suppressed with eosin $\sim 10^{-5}$ *M* (Fig. 1, a and b).

Both waves are diffusion-controlled, as indicated by the proportionality of i_d to the square root of mercury column height; the diffusion currents are also proportional to oxygen concentration (Fig. 2). The half-wave potential values are $E_{\frac{1}{2}}^1 = -0.14$ V and $E_{\frac{1}{2}}^2 = -0.92$ V without noticeable changes at different oxygen concentration. On the addition of increasing amounts of H_2O_2, the height of the second wave increases, whereas the first remains unchanged (Fig. 3). The increase of the second wave is strictly proportional to the H_2O_2 concentration.

The addition of water below 2 *M*, does not lead to any detectable change in half-wave potential values or wave heights.

The experimental data suggest that an equal number of electrons is involved in the two oxygen reduction steps; furthermore, the effect of H_2O_2 additions indicates that the first wave reduction product is H_2O_2, which is further reduced at the potential of the second wave, two electrons being involved in each process. On this basis, the calculated polarographic diffusion coefficient (from the Ilkovič equation) for oxygen in 0.1 *F* KCl–FMM is $D = 1.4 \times 10^{-5}$ cm^{2}sec^{-1} at 19.0° (viscosity of FMM, $\eta^{20°} = 3.31$ cpoise).

The logarithmic plot for the first oxygen reduction wave (Fig. 4) is a straight line with slope equal to 63 mV; if $n = 2$ on the basis of the previous considerations, the first wave should correspond to an irreversible electrode reaction, with $\alpha_{app.} \cong 0.5$.

The addition of eosin to suppress the maximum, does not appreciably affect

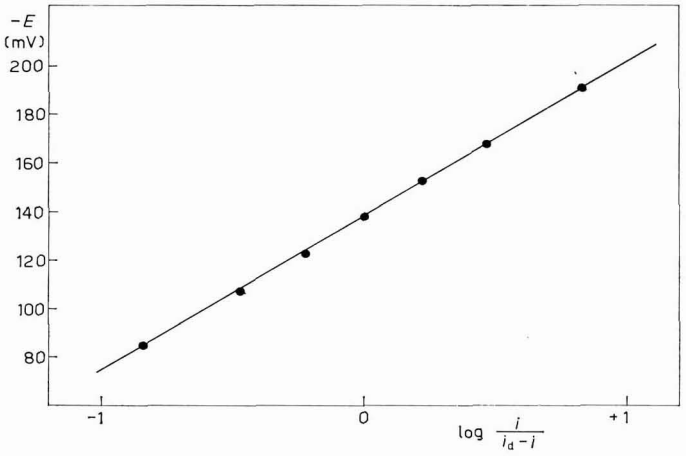

Fig. 4. Plot of $-E$ *vs.* log $[i/(i_d - i)]$ for the first reduction wave of O_2 in 0.1 *F* KCl–FMM, $1 \cdot 10^{-5}$ *M* eosin soln.

the electrode kinetics at the concentration used since the half-wave potential value is the same for eosin concentrations over the range $1–3 \cdot 10^{-5}$ *M*. This is therefore similar to the well known mechanism for oxygen reduction in aqueous KCl.

It does not seem that the amount of water contained in the solvent under the conditions used can affect the reduction process which is mainly dependent on the structure and composition of the electrode–solution interphase. Recent measurements of double-layer capacitance at the dropping mercury electrode in FMM solutions[9] were not affected by the addition of large amounts of water, showing that the adsorbed layer at the electrode is composed of FMM molecules even when the water concentration is as high as 10 *M*.

The reduction process for the first wave may therefore be written as:

$$O_2 + 2\ FMM + 2\ e \rightarrow H_2O_2 + 2\ FMM^- \qquad (1)$$

One of the possible mechanisms leading to the overall reaction expressed by eqn. (1) is:

$$2\ O_2 + 2\ e \rightarrow 2\ O_2^- \qquad (a)$$
$$2\ O_2^- + 2\ FMM \rightarrow 2\ HO_2 + 2\ FMM^- \qquad (b)$$
$$2\ HO_2 \rightarrow H_2O_2 + O_2 \qquad (c)$$

assuming the steps (b) and (c) to be fast with respect to step (a).

This mechanism is consistent with other proposals[4] for oxygen reduction in the presence of protic solvents.

The second reduction wave, highly irreversible (see Fig. 1b), could correspond to one of the two processes:

$$H_2O_2 + 2\ e \rightarrow 2\ OH^- \qquad (2a)$$
$$H_2O_2 + 2\ FMM + 2\ e \rightarrow 2\ H_2O + 2\ FMM^- \qquad (2b)$$

Equations (2a) and (2b) can be considered as equivalent because of the protic nature of the solvent.

ACKNOWLEDGEMENT

The authors wish to thank Professor PAOLO SILVESTRONI for helpful discussions.

SUMMARY

The polarographic reduction of oxygen in 0.1 *F* KCl–formamide solutions shows two irreversible waves of equal height, with half-wave potentials of −0.14 V and −0.92 V (*vs.* internal Hg pool), respectively.

The first reduction process leads to H_2O_2; the polarographic diffusion coefficient for oxygen in formamide solutions has been evaluated.

Experimental results suggest that oxygen reduction in KCl–formamide solution is similar to that in aqueous KCl solution.

REFERENCES

1 I. M. KOLTHOFF AND T. B. REDDY, *J. Electrochem. Soc.*, 108 (1961) 980.
2 M. E. PEOVER AND B. S. WHITE, *Chem. Commun. (London)*, 10 (1965) 183.

3 D. L. MARICLE AND W. G. HODGSON, *Anal. Chem.*, 37 (1965) 1562.
4 D. T. SAWYER AND J. L. ROBERTS, *J. Electroanal. Chem.*, 12 (1966) 90.
5 E. L. JOHNSON, R. H. POOL AND R. E. HAMM, *Anal. Chem.*, 38 (1966) 183.
6 F. M. VERHOEK, *J. Am. Chem. Soc.*, 58 (1936) 2577.
7 J. BARGH, *Chem. Ind. London*, (1959) 1307.
8 E. SCARANO AND M. MASCINI, *Ric. Sci.*, 36 (1966) 498.
9 R. PAYNE, *J. Chem. Phys.*, 42 (1965) 3371.

ELECTROANALYTICAL CHEMISTRY AND INTERFACIAL ELECTROCHEMISTRY
Elsevier Sequoia S.A., Lausanne – Printed in The Netherlands

ÜBER DIE REDUKTION VON JODAT IN SAUREN LÖSUNGEN AN AKTIVEN, GLATTEN Pt-ELEKTRODEN

L. MÜLLER
Physikalisch-Chemisches Institut der Humboldt Universität zu Berlin, 108 Berlin, DDR
(Eingegangen am 6. Dezember, 1966)

Bei der Reduktion von Jodat zu Jodid, die nach der summarischen Reaktionsgleichung

$$IO_3^- + 6\,H^+ + 6\,e^- \rightarrow I^- + 3\,H_2O \qquad (1)$$

verläuft, werden 6 Elektronen ausgetauscht. Diese Reaktion, die ohnehin nicht zu den einfachen zählt, wird jedoch noch kompliziert durch die Möglichkeit des gleichzeitigen Ablaufes der Dushman-Reaktion, bei der nach

$$IO_3^- + 5\,I^- + 6\,H^+ \rightarrow 3\,I_2 + 3\,H_2O \qquad (2)$$

gebildetes Jodid mit Jodat unter Bildung von Jod reagiert, das in einer elektrochemischen Reaktion wieder zu I^- reduziert wird. Auf diese Weise überlagert sich der eigentlichen elektrochemischen Reduktionsreaktion nach (1) noch eine nachgelagerte Reaktion (2). VETTER[1] und DESIDERI[2], die in ihren Arbeiten zeigten, dass Spuren von I_2 in der Lösung die Reaktion wesentlich beschleunigen, nehmen an, dass die Reduktion von IO_3^- im wesentlichen in der Reduktion von I_2 besteht, das nach Reaktion (2) nachgebildet wird. Beide Autoren schenken dem stark ausgeprägten Einfluss von Pt-Oberflächenoxiden auf die Geschwindigkeit des Reduktionsprozesses von IO_3^-, der bereits von ANSON[3] beschrieben wurde, keine Beachtung. ANSON UND KING[3] sind der Meinung, dass der beschleunigende Einfluss von Oberflächenoxiden des Pt auf die Geschwindigkeit des kathodischen Reduktionsprozesses von Jodat ein indirekter ist und auf die hemmende Wirkung von an der Pt-Oberfläche adsorbiertem Jodid, das nach Reaktion (2) entsteht, zurückzuführen ist. Bekanntlich ist die adsorbierte Jodidmenge an oxidfreier Pt-Oberfläche grösser als an oxidbedeckter, so dass Reduktion der Pt-Oxide zu einem Ansteigen der Jodadsorption führt, was verbunden ist mit einem Anwachsen der Hemmung der elektrochemischen Reaktion.

Es steht ausser Zweifel, dass die Adsorption von Jodidionen Einfluss auf die Geschwindigkeit der kathodischen Reduktion hat. Die in der vorliegenden Arbeit angeführten Versuchsergebnisse über die beschleunigende Wirkung von Pt-Oberflächenoxiden lassen sich jedoch in ihrer Gesamtheit nicht ohne weiteres durch den Mechanismus von ANSON UND KING erklären. Die Tatsache, dass die beschleunigende Wirkung von Pt-Oberflächenoxiden von uns auch in Systemen beobachtet wurde (Reduktion von H_2O_2, $S_2O_8^{2-}$ und ClO^- in KOH und HNO_2 und NH_3^+–OH in H_2SO_4), in denen Hemmung der Reduktionsreaktion infolge Adsorption der Reduktions- bzw. Ausgangsprodukte äusserst unwahrscheinlich ist, bewog uns, die Frage

der beschleunigenden Wirkung von Pt-Oberflächenoxiden auf die Jodatreduktion in saurer Lösung von einem anderen Gesichtspunkt aus zu betrachten.

Die Versuche wurden mit Hilfe einer rotierenden Scheibenelektrode in 0.1 *N* H_2SO_4 durchgeführt. Die Versuchslösungen wurden aus bidestilliertem Wasser und bidestillierter Schwefelsäure hergestellt und anschliessend einer 12-stündigen kathodischen Vorelektrolyse an einer Pt-Drahtelektrode unterworfen. Um eine gute Durchmischung der Lösung bei der Vorelektrolyse zu erzielen und gleichzeitig die Lösung von Sauerstoff zu befreien, wurde gereinigter Stickstoff durch die Lösung geleitet. Die mit Hilfe der rotierenden Scheibenelektrode erhaltenen Strom–Spannungs-Kurven (Abb. 1) durchlaufen bei einem Potential $\varphi \sim 0.75$ V* ein Maximum,

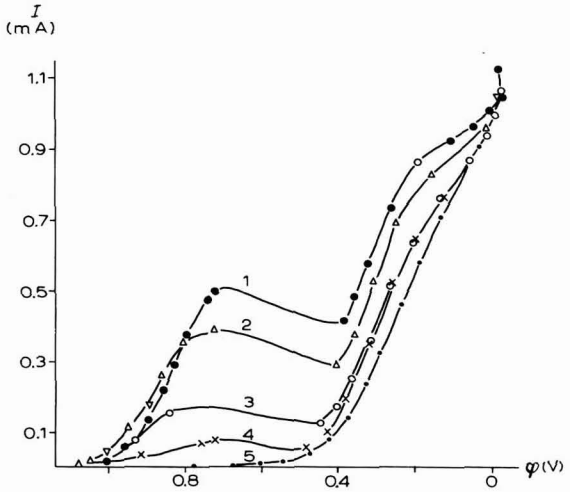

Abb. 1. Reduktion von Jodat in 0.1 *N* H_2SO_4 in Abhängigkeit von φ_{AE}; $m = 27$ U/sec. φ_{AE}: (●), +2.0; (△), 1.6; (○), 1.4; (+), +1.2; (·), +1.0 V.

wonach ein Abfall des Stromes bis zu einem Potential von $\varphi \sim +0.4$ V beobachtet wird. Bei $\varphi \sim 0.4$ V bleibt der Strom und das Potential eine gewisse Zeit konstant und erst danach bemerkt man einen weiteren Abfall bis zum Potential der Wasserstoffentwicklung. Die Kurven in Abb. 1 wurden erhalten, indem man nach Erreichen des Haltepunktes bei $\varphi \sim +0.4$ V sofort die Polarisation erhöhte.

Der Stromabfall im Potentialbereich $\varphi = 0.75$–0.4 V ist, wie der Vergleich mit Ladekurven zeigt (4), durch Reduktion der Pt-Oberflächenoxide bedingt. Der Haltepunkt bei $\varphi \sim 0.4$ V entspricht hiernach der weitestgehenden Reduktion der Pt-Sauerstoffverbindungen.

Die Höhe des Strommaximums bei $\varphi \sim 0.75$ V hängt stark vom Potential der anodischen Endaktivierung (φ_{AE}) ab (Abb. 1) und fällt mit sinkender anodischer Endaktivierung ab, um bei $\varphi_{AE} = +1.0$ V Null zu werden. Die Elektrode wurde vor jedem Versuch im Verlaufe von 2 min wechselseitig je 15 sec anodisch bei +1.9 V und kathodisch bei −0.2 V polarisiert. Nach der letzten kathodischen Polarisation wurde die Elektrode 3 min bei dem gewünschten Potential der anodischen Endaktivierung φ_{AE} gehalten und danach sofort die Polarisationskurve aufgenommen.

* Alle Potentiale beziehen sich auf die reversible Wasserstoffelektrode in der gleichen Lösung.

Auf diese Weise konnten Pt-Elektroden mit verschiedenem Oxidationsgrad, d.h. Pt-Oberflächen mit verschieden grossem Sauerstoffbedeckungsgrad und verschiedener Festigkeit der Pt-Sauerstoffbindung erhalten werden. Da für $\varphi_{AE} < 1.2$ V das Maximum bei $\varphi \sim 0.75$ V verschwindet, folgt die wichtige Schlussfolgerung, dass Pt-Oberflächenoxide den Initialschritt der elektrochemischen Reduktion von Jodat in 0.1 N H_2SO_4 beschleunigen.

Die Untersuchung der Rührabhängigkeit der Polarisationskurven (I–φ-Kurven) zeigte, dass die Ströme der Reduktion von IO_3^- im Potentialbereich $\varphi = 1.1$–0.75 V rein kinetischer Natur sind, da sie bei $m \geqslant 13$ U/sec unabhängig von der Rührgeschwindigkeit der Elektrode sind (Abb. 2).

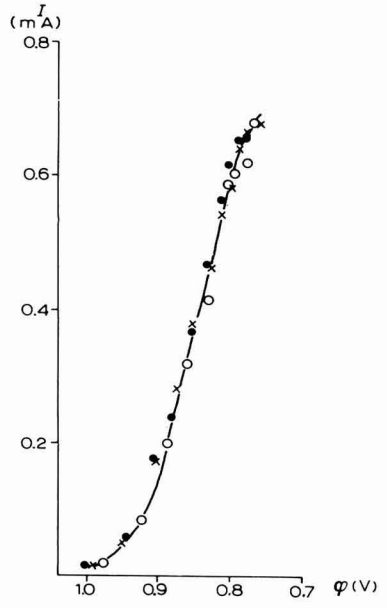

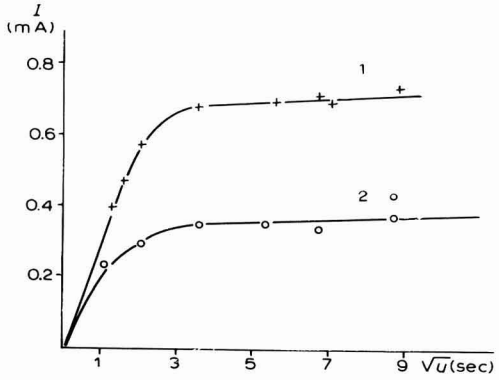

Abb. 2. Strom–Spannungs-Kurve der Reduktion von Jodat in 0.1 N H_2SO_4 in Abhängigkeit von der Umdrehungsgeschwindigkeit der Elektrode. m: (●), 79; (○), 49; (×), 13 U/sec.

Abb. 3. Abhängigkeit der Höhe des Strommaximums bei $\varphi \sim 0.75$ V von der Umdrehungsgeschwindigkeit der Elektrode für verschiedene φ_{AE}. (1), $\varphi_{AE} = +1.9$ V; (2), $\varphi_{AE} = +1.5$ V.

An Abb. 3 ist die Abhängigkeit der Höhe des Strommaximums bei $\varphi \sim 0.75$ V von der Umdrehungsgeschwindigkeit der Pt-Elektrode (m) dargestellt. Diese Abbildung zeigt, dass bei konstanter Endaktivierung der Strom des Maximums bei $\varphi \sim 0.75$ V für $m > 13$ U/sec ebenfalls nicht von der Rührgeschwindigkeit abhängig ist.

Von grossem Interesse ist die Frage nach dem durch Pt-oxide beschleunigten Prozess, bei dem es sich nur um einen an der Pt-Oberfläche ablaufenden heterogenen Teilschritt handeln kann. Da Pt-Oxide die Geschwindigkeit des Initialschrittes der Jodatreduktion beschleunigen, gibt es nur zwei Möglichkeiten, dass entweder die Geschwindigkeit der elektrochemischen Durchtrittsreaktion durch Pt-Oxide beschleunigt wird oder die Geschwindigkeit eines heterogenen Prozesses, der der elektrochemischen Durchtrittsreaktion vorgelagert ist und in dessen Verlauf Produkte

entstehen, die sich leichter elektrochemisch reduzieren lassen als das Ausgangsprodukt selbst.

Die Untersuchung der Abhängigkeit der Reduktionsgeschwindigkeit des Jodates vom Oxidationsgrad der Pt-Elektrode ergab, dass einerseits mit steigendem φ_{AE} das Strommaximum bei $\varphi \sim 0.75$ V ansteigt, andererseits sich aber die Polarisationskurve im Potentialbereich 1.1–0.8 V nach negativen Potentialen verschiebt, d.h. die Geschwindigkeit des elektrochemischen Prozesses im genannten Potentialbereich absinkt (vgl. Kurve 1 und Kurve 2 in Abb. 1). Dieses Verhalten weist darauf hin, dass die Geschwindigkeiten zweier verschiedener Prozesse durch Oberflächenoxide beeinflusst werden, wobei der eine von ihnen durch Pt-Oberflächenoxide beschleunigt, während der andere gehemmt wird.

Die Auftragung von log I gegen φ für die Kurven 1 und 2 in Abb. 1 gibt im Anfangsgebiet der Strom–Spannungs-Kurve gute Tafel-Geraden (Abb. 4), was zeigt, dass in diesem Potentialbereich der geschwindigkeitsbestimmende Schritt der Jodatreduktion die elektrochemische Durchtrittsreaktion ist. Dabei ergeben sich für beide Polarisationskurven verschiedene Werte für den Faktor "b" der Tafelgleichung. Bei $\varphi_{AE} = +2.0$ V erhält man für $b = 0.151$ V und bei $\varphi_{AE} = +1.6$ V ist $b = 0.112$ V, was Werten für den Durchtrittsfaktor α von $\alpha = 0.39$ und $\alpha = 0.52$ entspricht.

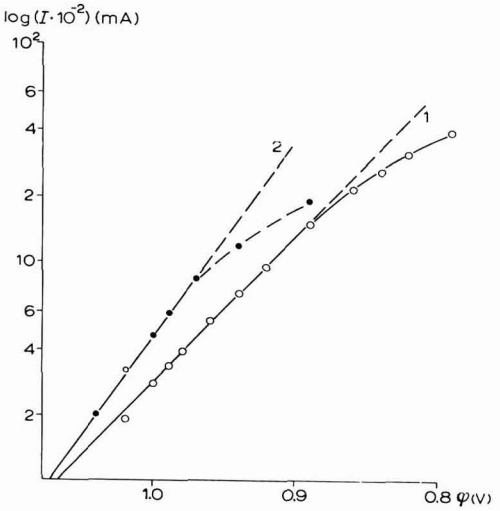

Abb. 4. Logarithmische Abhängigkeit des Stromes vom Potential der Elektrode im Anfangsgebiet der Strom–Spannungs-Kurve; $m = 27$ U/sec. (1), $\varphi_{AE} = +2.0$ V; (2), $\varphi_{AE} = +1.6$ V.

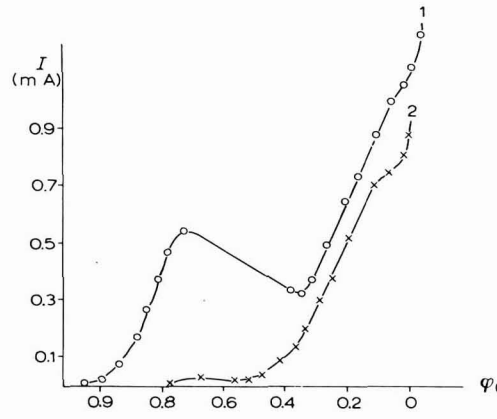

Abb. 5. Strom–Spannungs-Kurven der Reduktion von: (1), IO_3^-; (2), BrO_3^-. $m = 27$ U/sec; $\varphi_{AE} = +2.0$ V.

Die Verringerung des Zahlenwertes des Durchtrittsfaktors α mit Erhöhung von φ_{AE}, die auf eine Hemmung der elektrochemischen Durchtrittsreaktion mit steigendem Oxidationsgrad der Elektrode zurückzuführen ist, bestätigt die bereits in einer früheren Arbeit[5] gemachte Aussage, dass Pt-Oberflächenoxide die elektrochemische Durchtrittsreaktion hemmen. Die gleiche Schlussfolgerung ergibt sich auch

aus der Verschiebung der Tafelgeraden im Potentialbereich $\varphi = 1.1$–0.8 V bei Erhöhung von φ_{AE} nach negativen Potentialen (Abb. 4).

Da Pt-Oberflächenoxide den Initialschritt der Jodatreduktion beschleunigen, folgt, dass der geschwindigkeitsbestimmenden elektrochemischen Durchtrittsreaktion eine durch Pt-Oberflächenoxide beschleunigte heterogen-katalytische Reaktion vorgelagert sein muss.

So ist die Erhöhung des Strommaximums bei $\varphi \sim 0.75$ V mit wachsendem φ_{AE} auf die Erhöhung der katalytischen Aktivität der Pt-elektrode gegenüber der dem elektrochemischen Ladungsdurchtritt vorgelagerten heterogen-katalytischen Reaktion zurückzuführen, während die parallel hierzu auftretende Verschiebung der I–φ-Kurve nach negativen Potentialen durch die Verlangsamung der Geschwindigkeit des Ladungsdurchtrittes durch Pt-Oberflächenoxide bedingt ist.

Zur Klärung der Frage welcher Art die durch Pt-oxide beschleunigte katalytische Reaktion ist, verglichen wir die elektrochemische Reduzierbarkeit der Anionen IO_3^-, BrO_3^- und ClO_3^-. Die vergleichende Aufnahme von Strom–Spannungs-Kurven der IO_3^-, BrO_3^- und Chloratreduktion an einer glatten, aktiven Pt-Elektrode in 0.1 N-H_2SO_4 (Abb. 5) zeigt, dass sich BrO_3^- erst bei wesentlich negativeren Potentialen merklich reduziert als IO_3^-, während ClO_3^- unter diesen Bedingungen überhaupt nicht reduziert werden kann. Abb. 5 zeigt ganz deutlich, dass die beschleunigende Wirkung von Pt-Oberflächenoxiden auf die Geschwindigkeit des heterogen-katalytische Initialprozesses im Fall von BrO_3^- wesentlich schwächer ausgeprägt ist als bei IO_3^- (im Falle der BrO_3^--Reduktion beobachtet man selbst bei $\varphi_{AE} = +2.0$ V nur ein sehr schwach ausgeprägtes Strommaximum bei $\varphi \sim 0.75$ V). Diese Abstufung der katalytischen Wirkung von Pt-Sauerstoffverbindungen auf den der Durchtrittsreaktion vorgelagerten heterogen-katalytischen Prozess ($IO_3^- > BrO_3^- > ClO_3^-$) ist die gleiche wie sie für die Halbwellenpotentiale und Überspannung der elektrochemischen Reduktion dieser Anionen an einer Hg-Tropfelektrode beobachtet wurde[6]. NIGHTINGALE[6] gibt für die Reduktion von IO_3^- und BrO_3^- bei pH = 0 an Hg folgende Überspannungswerte an:

$$\eta_{IO_3^-} = 0.7 \text{ V}; \quad \eta_{BrO_3^-} = 1.3 \text{ V}$$

Dies lässt vermuten, dass für die Verringerung der Geschwindigkeit der katalytischen Reaktion an oxidbedeckter Pt-Oberfläche in der Reihenfolge $IO_3^- > BrO_3^- > ClO_3^-$ die gleichen Ursachen geltend gemacht werden können wie für die Vergrösserung der Überspannung bei der kathodischen Reduktion an Hg[6] und das Absinken der Reaktionsfähigkeit der Halogenoxyanionen in homogenen Reaktionen[7]. Experimentell wurde beobachtet[6], dass die Abnahme der chemischen Reaktivität von $IO_3^- > BrO_3^- > ClO_3^-$ in homogenen Reaktionen bzw. die Vergrösserung der kathodischen Überspannung parallel geht mit der Verkürzung des Bindungsabstandes der kovalenten Einfachbindung Hal–O, der im Falle von $IO_3^- = 1.83$ Å, $BrO_3^- = 1.68$ Å und $ClO_3^- = 1.48$ Å[6] beträgt. Parallel mit der Verkürzung der kovalenten Einfachbindung steigt der Doppelbindungscharakter der Hal–O-Bindung[6], was zur Folge hat, dass die Reaktionsfähigkeit der Hal–O-Bindung in der Reihenfolge $IO_3^- > BrO_3^- > ClO_3^-$ abnimmt.

Röntgenstrahlbeugungsuntersuchungen an Jodsäurekristallen zeigten[8], dass eine der drei I–O-Bindungen sich in ihrem Charakter von den anderen zwei unterscheidet. Während zwei I–O-Bindungen einen Bindungsabstand von 1.80 bzw. 1.81 Å

haben, ist der Abstand der dritten I-O-Bindung mit 1.89 Å merklich grosser. Auf Grund dieser und anderer spektroskopischer Daten schliessen DASENT UND WADDINGTONs, dass das Jodation teilweise in Jodatform IO_2-OH vorliegt, als das es auch mit grosser Wahrscheinlichkeit elektrochemisch reduziert bzw. katalytisch zersetzt wird.

Die elektrochemische Durchtrittsreaktion wie sie an Hg bzw. an der oxidfreien Pt-Oberflache ablauft, wäre dann folgendermassen zu formulieren:

$$IO_2\text{–}OH + e \rightarrow IO_2^- + OH^\cdot$$

wahrend die durch Pt-Oberflachenoxide beschleunigte katalytische Reaktion, in deren Verlauf Produkte entstehen mussen, die sich mit geringerer Uberspannung reduzieren lassen als das IO_2-OH mit aller Wahrscheinlichkeit in der dissoziativen Chemisorption von IO_2-OH nach

$$IO_2\text{–}OH \rightleftarrows IO_2'\,chem + OH'\,chem$$

besteht.

Die Ruhrunabhangigkeit der Polarisationskurve der Jodatreduktion im Potentialbereich 1.I- o.75 V gestattete es, aus der Konzentrationsabhangigkeit des Stromes bei gegebenem konstanten Potential die Reaktionsordnung n der Reduktion von Jodat zu bestimmen. Die Ergebnisse zeigen, dass die Strome der Jodatreduktion der Quadratwurzel aus der Jodatkonzentration proportional sind (Abb. 6). Das gilt unabhangig von der anodischen Endaktivierung der Elektrode (Abb. 7). Die Reaktionsordnung n hat demnach unabhangig vom Oxidationsgrad der Elektrode im

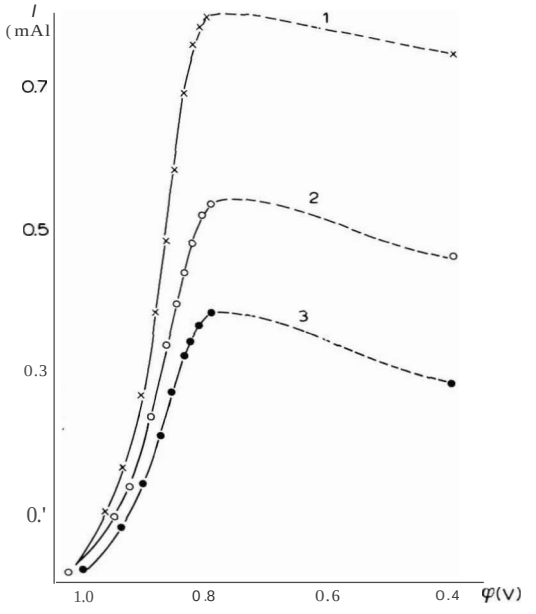

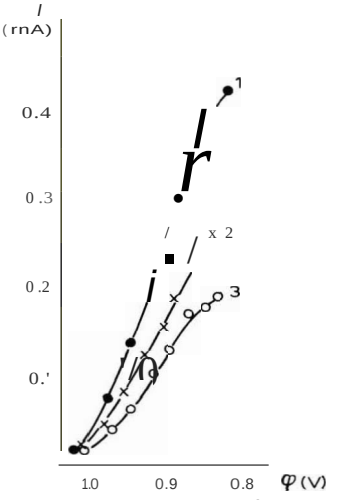

Abb. 6. I(onzentrationsabhangigkeit der Strome cler Recluktion von Joclat. φ_{AE} = +1.9 V; m=79U/sec. (I), 4'IO-3M; (Z), Z'IC-3M; (3), I·Io-3M.

Abb. 7. Konzentrationsabhangigkeit der Strome der Reduktion von Joclat. φ_{AE} = +1.6 V; m = 79U/sec. (I), 4'Io-3M; (z), Z'IO-3M; (3), I·IO-3M.

Potentialbereich $\varphi = 1.1$–0.75 V den Wert $n = 0.5$. Im Minimum der Polarisationskurve bei $\varphi \sim 0.4$ V (bei diesem Potential ist die Oberfläche im wesentlichen frei von chemisorbiertem Sauerstoff und Pt-Oxiden, und man beobachtet hier einen Haltepunkt, bei dem für eine gewisse Zeit Potential und Strom sich nicht verändern) errechnet man aus der Konzentrationsabhängigkeit der Ströme einen Wert von $n \sim 0.71$.

Die ermittelten Reaktionsordnungen ermöglichen es, Aussagen über den Reduktionsmechanismus von Jodat zu machen.

Die Reaktionsordnung $n = 0.5$ für den Prozess des elektrochemischen Ladungsdurchtrittes weist darauf hin, dass sich der chemisorptiven Dissoziation nach (4) eine schnelle Folgereaktion anschliessen muss, wenn nicht angenommen werden soll, dass die Geschwindigkeit der beiden möglichen nachfolgenden Durchtrittsreaktionen

$$IO_2^{\cdot}{}_{Chem} + e \rightarrow IO_2^-$$

$$OH^{\cdot}{}_{Chem} + e \rightarrow OH^-$$

gleich ist, was uns wenig wahrscheinlich erscheint. Die Reaktionsordnung $n = 0.5$ lässt sich erklären, wenn man annimmt, dass die Folgereaktion in der Reaktion des gebildeten $IO_2^{\cdot}{}_{Chem}$-Radikals mit Wasser nach

$$IO_2^{\cdot}{}_{Chem} + H_2O \rightleftarrows IO_2^- + H^+ + OH^{\cdot} \tag{5}$$

besteht.

Unter der Annahme, dass Reaktion (5) sehr schnell verläuft, erhält man für den vorgelagerten katalytischen Prozess nachstehende Reaktionsfolge:

$$IO_2\text{–}OH \rightleftarrows IO_2^{\cdot}{}_{Chem} + OH^{\cdot}{}_{Chem}$$

$$IO_2^{\cdot}{}_{Chem} + H_2O \rightleftarrows IO_2^- + OH^{\cdot}{}_{Chem} + H^+ \quad \text{(schnell)}$$

$$IO_2\text{–}OH + H_2O \rightleftarrows IO_2^- + 2\,OH^{\cdot}{}_{Chem} + H^+ \tag{6}$$

d.h. bei Ablauf der vorgelagerten katalytischen Reaktion (6) bilden sich zwei $OH^{\cdot}{}_{Chem}$-Radikale, die in der anschliessenden elektrochemischen Durchtrittsreaktion reduziert werden.

Das gleichzeitig gebildete IO_2^--Ion ist äusserst instabil[9] und disproportioniert sofort nach

$$3\,IO_2^- \rightarrow 2\,IO_3^- + I^-$$

in die für die kathodische Durchtrittsreaktion im untersuchten Potentialgebiet (1.1–0.75 V) inaktiven Jodat- und Jodidionen.

Für die Geschwindigkeit der Durchtrittsreaktion

$$OH^{\cdot}{}_{Chem} + e^- \rightarrow OH^- \tag{7}$$

gilt der Ausdruck:

$$I = K\,[OH^{\cdot}]_{Chem} \exp[(-\alpha F/RT)] \tag{8}$$

bzw. da aus einem IO_2–OH zwei OH·-Radikale entstehen (Gl. 6)

$$I = K\,[IO_2\text{–}OH]^{0.5} \exp[(-\alpha F/RT)] \tag{9}$$

d.h. wir erhalten für die Geschwindigkeit der elektrochemischen Durchtrittsreaktion eine Konzentrationsabhängigkeit bezüglich Jodat von $(IO_2\text{–}OH)^{0.5}$.

Bei $\varphi \sim 0.4$ V ist die Pt-Oberfläche im wesentlichen frei von Pt-Sauerstoffverbindungen, so dass Reaktion (4) stark gehemmt ist, und somit auch die Geschwindigkeit der elektrochemischen Reduktion von Jodat wesentlich geringer ist als bei $\varphi \sim +0.75$ V. Die starke Verschiebung des Potentials um 0.35 V nach negativen Potentialen führt jedoch dazu, dass hier bereits Reaktion (3), d.h. die direkte elektrochemische Reduktion des Jodations im stärkeren Masse möglich ist. Dieser Prozess ist eine Reaktion 1. Ordnung bezüglich der Jodatkonzentration, so dass bei Überlagerung der beiden Reaktionsfolgen (3) und [(4)+(6)+(7)] eine Reaktionsordnung zwischen 0.5 und 1 gefunden werden sollte. Aus dem Experiment lässt sich bei $\varphi \sim 0.4$ V ein Wert von $n \sim 0.71$ berechnen.

Die Abweichung der Abhängigkeit log I–φ von der Geradlinigkeit bei höheren kathodischen Potentialen (Abb. 4) unter Berücksichtigung, dass in diesem Potentialbereich (1.1–0.75 V) n konstant 0.5 ist, ist dadurch bedingt, dass Reaktion (4) nur an den Stellen der Oberfläche schnell verläuft, die mit Oxid bedeckt sind. Die Einstellung des Chemisorptionsgleichgewichtes (6) verläuft an den oxidbedeckten Stellen schnell gegenüber der elektrochemischen Durchtrittsreaktion (Rk 7), so dass letztere die Geschwindigkeit des Gesamtprozesses bestimmt. Die Geschwindigkeit der direkten elektrochemischen Reduktion von IO_3^- nach (3) ist in diesem Potentialbereich vernachlässigbar klein.

Für die in Gleichung (8) enthaltene stationäre $[OH^{\cdot}]_{Chem}$-Radikalkonzentration gilt deshalb die Beziehung

$$[OH^{\cdot}]_{Chem} = f(\theta_{oxid})$$

wobei mit θ_{oxid} der Bedeckungsgrad der Pt-Oberfläche mit Oxid bezeichnet wird, für den wiederum die Beziehung gilt:

$$\theta_{oxid} = f(\varphi)$$

Daraus ergibt sich, dass in dem Masse wie sich die Pt-Oberflächenoxide beim Übergang zu negativeren Potentialen reduzieren auch die stationäre Konzentration von $[OH^{\cdot}]_{Chem}$ ständig kleiner wird. Die Verringerung der stationären Konzentration von $[OH^{\cdot}]_{Chem}$ beim Übergang zu negativeren Potentialen bewirkt die beobachtete Verringerung der elektrochemischen Reaktionsgeschwindigkeit (Abb. 4) bei gleichzeitiger Konstanz der Reaktionsordnung $n = 0.5$. Zusammenfassend lassen sich in Abhängigkeit vom Oberflächenzustand und Potential der Pt-Elektrode die zwei folgenden möglichen Reaktionswege formulieren:

I. Oxidbedeckte Oberfläche

$$3\ IO_3^- + 3\ H^+ \rightarrow 3\ IO_2\text{–}OH$$

$$3\ IO_2\text{–}OH \rightleftarrows 3\ IO_2^{\cdot}{}_{Chem} + 3\ OH^{\cdot}{}_{Chem}$$

$$\underline{3\ IO_2^{\cdot}{}_{Chem} + 3\ H_2O \rightleftarrows 3\ IO_2^- + 3\ OH^{\cdot}{}_{Chem} + 3\ H^+}$$

$$3\ IO_2\text{–}OH + 3\ H_2O \rightleftarrows 3\ IO_2^- + 6\ OH^{\cdot}{}_{Chem} + 3\ H^+$$

$$3\ IO_2^- \rightarrow 2\ IO_3^- + I^-$$

$$\underline{6\ OH^{\cdot}{}_{Chem} + 6\ H^+ + 6\ e^- \rightarrow 6\ H_2O}$$

$$IO_3^- + 6\ e^- + 6\ H^+ \rightarrow I^- + 3\ H_2O$$

II. Reduzierte Oberfläche

$$3\ IO_2\text{–}OH + 3\ e^- \rightarrow 3\ IO_2^- + 3\ OH^\cdot$$

$$3\ IO_2^- \rightarrow 2\ IO_3^- + I^-$$

$$2\ IO_3^- + 2\ H^+ \rightarrow 2\ IO_2\text{–}OH$$

$$\underline{3\ OH^\cdot + 3\ e^- + 3\ H^+ \rightarrow 3\ H_2O}$$

$$IO_2\text{–}OH + 6\ e^- + 5\ H^+ \rightarrow HI + 3\ H_2O$$

Herrn Prof. R. LANDSBERG möchte ich für die kritische Durchsicht des Manuskripts recht herzlich danken.

ZUSAMMENFASSUNG

Bei der Reduktion von Jodat in 0.1 *N* H_2SO_4 an einer Pt-Elektrode zeigte sich, dass Pt-Oberflächenoxide den Initialschritt der elektrochemischen Reduktion von Jodat beschleunigen. Die durch Pt-Oxide beschleunigte Reaktion besteht in der dissoziativen Chemisorption von Jodat nach

$$IO_2\text{–}OH \rightleftarrows IO_2^{\cdot}{}_{\text{Chem}} + OH^{\cdot}{}_{\text{Chem}}$$

Für den im Potentialbereich $\varphi = 1.1$–0.75 V geschwindigkeitsbestimmenden Durchtrittsprozess wurde eine Reaktionsordnung von $n = 0.5$ ermittelt, was so gedeutet wird, dass das entstandene $IO_2^{\cdot}$-Radikal schnell mit Wasser reagiert unter Bildung eines $OH^{\cdot}$-Radikals nach

$$IO_2^{\cdot} + H_2O \rightleftarrows IO_2^- + H^+ + OH^{\cdot}$$

so dass aus einem IO_2–OH-Molekül zwei $OH^{\cdot}$-Radikale entstehen, die elektrochemisch reduziert werden. Das gebildete IO_2^- ist instabil und disproportioniert mit grosser Geschwindigkeit nach

$$3\ IO_2^- \rightarrow 2\ IO_3^- + I^-$$

SUMMARY

In the reduction of iodate in 0.1 *N* H_2SO_4 at a Pt electrode it is shown that the Pt surface oxide accelerates the initial step of the electrochemical reduction of iodate. The reaction accelerated by Pt oxide consists of the dissociative chemisorption of iodate according to

$$IO_2\text{–}OH \rightleftharpoons IO_2^{\cdot}{}_{\text{chem}} + OH^{\cdot}{}_{\text{chem}}.$$

In the potential region $\phi = 1.1$–0.75 V the rate-determining transfer process yields a reaction order of $n = 0.5$; this was interpreted as due to the rapid reaction of the $IO_2^{\cdot}$ radical with water forming an $OH^{\cdot}$ radical according to

$$IO_2^{\cdot} + H_2O \rightleftharpoons IO_2^- + H^+ + OH^{\cdot},$$

so that from one IO_2–OH molecule, two $OH^{\cdot}$ radicals are produced, which are then

reduced electrochemically. The IO_2^- formed is unstable and disproportionates with a high velocity according to

$$3\ IO_2^- \rightarrow 2\ IO_3^+ + I^- .$$

LITERATUR

1 K. J. VETTER, *Elektrochemische Kinetik*, Springer-Verlag, Berlin, 1961, S. 374.
2 P. G. DESIDERI, *J. Electroanal. Chem.*, 9 (1965) 218.
3 F. C. ANSON, *J. Am. Chem. Soc.*, 81 (1959) 1554; F. C. ANSON UND D. M. KING, *Anal. Chem.*, 34 (1962) 362.
4 W. VIELSTICH, *Z. Instrumentenk.*, 71 (1963) 29.
5 L. MÜLLER, *Elektrochim. Acta*, 12 (1967) 557.
6 E. R. NIGHTINGALE, JR., *J. Phys. Chem.*, 64 (1960) 162.
7 J. HALPERN UND H. TAUBE, *J. Am. Chem. Soc.*, 74 (1952) 375.
8 W. E. DASENT UND T. C. WADDINGTON, *J. Chem. Soc. (London)*, (1960) 2429.
9 *Gmelin's Handbuch der Chemie*, Bd. Jod, 1926, S. 464.

ELECTROANALYTICAL CHEMISTRY AND INTERFACIAL ELECTROCHEMISTRY
Elsevier Sequoia S.A., Lausanne – Printed in The Netherlands

POLAROGRAPHIC BEHAVIOUR OF Th(IV) IN DIMETHYL SULFOXIDE*

J. SANCHO, J. ALMAGRO AND A. PUJANTE
Department of Physical Chemistry, University of Murcia, Institute "A. de G. Rocasolano" of the C.S.I.C. (Spain)
(Received October 10th, 1966; in revised form, April 20th, 1967)

INTRODUCTION

The polarographic behaviour of Th(IV) has been the subject of contradictory literature reports. It was first investigated by LAUBENGAYER AND EATON[1] and COZZI[2], who found that the wave-height in hydrochloric acid is almost directly related to the total thorium concentration. MASEK[3] studied the depolarising effects of Th(IV) in water and ethanol–water, and found a certain reduction of the hydrogen ion in the aqueous solution, which he verified by experiments with buffer solutions of Th(IV) in water–alcohol solutions.

KAPOOR AND AGRAWAL[4] studied the polarographic behaviour of $Th(NO_3)_4$ in Li_2SO_4 and KNO_3, and found that the limiting current was not entirely reproducible.

In a previous paper[5], we reported that thorium tetrachloride in aqueous and water–alcohol media, with LiCl as supporting electrolyte, gave one irreversible, usually diffusion-controlled wave.

Other work on the polarographic behaviour of thorium has been carried out by SARMA AND RAGHAVA RAO[6], FARAONE AND TROZZI[7], FARAONE AND D'AMORE[8], KOMAREK[9], GRAHAM AND LARRABEE[10], and ZHDANOV *et al.*[11].

GUTMANN AND SCHOEBER[12] studied several ions, among them hafnium and titanium, in dimethyl sulfoxide, with tetraethylammonium nitrate as supporting electrolyte; they found one reduction wave for titanium and two for hafnium. DEHU *et al.*[13] studied aluminum in 90% and 10% dimethyl sulfoxide–acetylacetone mixtures and observed proportionality between concentration and diffusion current. Later, they described the behaviour of beryllium in the same solvent[14].

In this paper, we have investigated the behaviour of thorium in dimethyl sulfoxide (DMSO), using both normal and derivative polarography, in order to obtain data to explain the reduction mechanism in the dropping electrode.

EXPERIMENTAL

The polarogram recording (and derivative polarography) was carried out with a direct reading Radiometer polarograph, model PO4.

An automatically heated Berenguer thermostat with continuous stirring was used for temperature control; this maintained the temperature constant to within $\pm 0.5°$.

* Communication to the IVth International Congress of Polarography, Prague, 1966.

The Radiometer capillary was 10 cm long and 96 μ in diameter. Its characteristics were: drop time, 2.72 sec and mercury flow, 1.7836 mg/sec.

The polarographic cell used was the conventional polarographical type and work was carried out in a nitrogen atmosphere. Commercial cylinder nitrogen was purified by bubbling it through ammoniacal solutions of copper, and concentrated sulfuric acid; it was dried by passage through a calcium oxide tower and passed finally into a wash-bottle containing the dimethyl sulfoxide test solution.

These solutions were prepared by diluting 1 M LiCl and 10^{-2} M $Th(NO_3)_4$ with dimethyl sulfoxide solution. Lithium chloride was obtained from British Drug Houses Ltd. (and was vacuum dried before use), and $Th(NO_3)_4$ from Schuchardt. The DMSO used was the pure quality from Fluka AG. Buchs SG. and in order to find out whether it could be used as supplied, the water content was determined by titration with Karl Fischer reagent (Merck). The same determination was carried out with the LiCl solution in DMSO. No water was detected in either case.

10 ml of the test solution were placed in the cell, and nitrogen bubbled through for 20 min. The temperature was kept constant at 25°, except when the effect of temperature was being investigated. The height of the mercury column was 40 cm.

The half-wave potentials were calculated from the curve E *vs.* log. $\{i/(i_d - i)\}$, and the peak potentials of the derivative waves obtained graphically from the polarograms. The diffusion current was measured on the polarographic curves by the tangent method.

RESULTS AND DISCUSSION

The use of dimethyl sulfoxide as a solvent in polarography has been studied by SCHWABE[15], and GUTMANN AND SCHOEBER[12,16]. KOLTHOFF AND REDDY[17] carried out an exploratory volumetric study of several acids, some ions and benzoquinones. The study of the characteristics of this solvent has also been dealt with in other general papers on non-aqueous solvents[18,19]. Usually, one wave is obtained for the alkaline

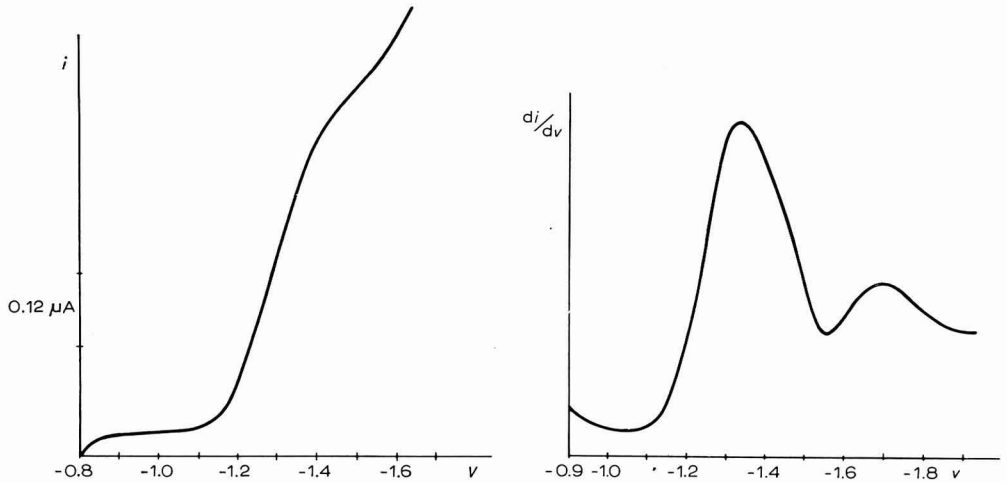

Figs. 1–2. Polarograms of (1) $3 \cdot 10^{-3}$ M Th(IV) and (2) $4 \cdot 10^{-3}$ M Th(IV) in anhydrous dimethyl sulfoxide and 0.1 M LiCl.

and alkaline-earth metals (as well as for some transition metals) and two or three waves for the others. Reduction is reversible in the case of alkaline elements, but irreversible with the transition elements, indicating strong solvation.

We have found that $Th(NO_3)_4$ in dimethyl sulfoxide, with LiCl as supporting electrolyte, produces one, usually well defined, polarographic wave, see the polarograms obtained in normal and derivative polarography in Figs. 1 and 2.

In the concentration range studied, $1 \cdot 10^{-3}$–$5 \cdot 10^{-3}$ M, the variation of diffusion current with concentration is perfectly linear (Fig. 3).

The effect of temperature on the diffusion current is 1.1%/degree centigrade,

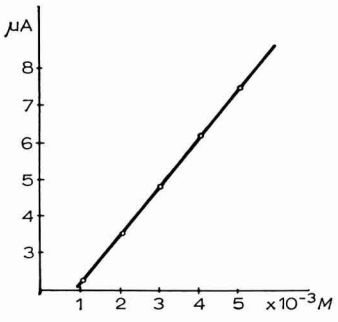

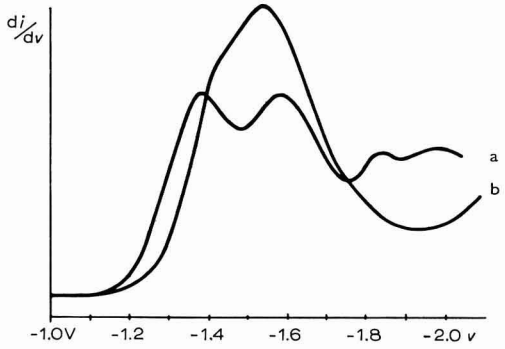

Fig. 3. Variation of wave height with Th(IV) concn.

Fig. 4. Polarograms of $3 \cdot 10^{-3}$ *M* Th(IV) in dimethyl sulfoxide–water mixtures and 0.1 *M* LiCl: (a), 10% H_2O; (b), 20% H_2O.

TABLE 1

$Th(NO_3)_4$ IN ANHYDROUS DIMETHYL SULFOXIDE AND 0.1 *M* LiCl

Conc. Th(IV) *($M \cdot 10^3$)*	*Diff. current* *(μA)*	*Slope* *E vs.* *log $i/(i_d - i)$*	*$E_{\frac{1}{2}}$ (V)* *vs. Hg pool*	*i_d/C*	*I*	*E_p (V)* *vs. Hg pool*
1	2.28	0.123	−1.290	2.280	1.312	−1.350
2	3.57	0.115	−1.286	1.785	1.027	−1.340
3	4.86	0.120	−1.280	1.630	0.938	−1.330
4	6.30	0.130	−1.288	1.575	0.900	−1.330
5	7.56	0.123	−1.292	1.512	0.870	−1.340
		Mean value	−1.287 ±0.006			−1.338±0.008

TABLE 2

$3 \cdot 10^{-3}$ *M* Th(IV), SUPPORT SOLUTION 0.1 *M* LiCl IN ANHYDROUS DIMETHYL SULFOXIDE

T *(°C)*	*Diff. current* *(μA)*	*Slope* *E vs. log. $i/(i_d - i)$*	*$E_{\frac{1}{2}}$ (V)* *vs. Hg pool*
25	4.86	0.120	−1.280
30	5.34	0.113	−1.242
35	5.52	0.108	−1.260
40	5.76	0.110	−1.244

and the half-wave potentials vary several millivolts/degree centigrade, showing that the process is governed by diffusion and is irreversible (Table 2). The irreversibility is confirmed by the steep slopes of the curve E *vs.* log $\{i/(i_d - i)\}$ and the variation of half-wave potential with concentration (Table 1).

With increase of water concentration in the water–dimethyl sulfoxide mixtures (Table 3), the value of the slope of the graph E *vs.* log $\{i/(i_d - i)\}$ moves away from irreversibility and half-wave potentials move towards more negative values until the water concentration is 30%, above which they shift again towards more positive potentials. The diffusion current values gradually increase. These facts may be explained by an increase of water complexes at the expense of Th(IV) ions solvated by dimethyl sulfoxide.

TABLE 3

$3 \cdot 10^{-3}$ M Th(IV), SUPPORT SOLUTION 0.1 M LiCl; SOLVENT: WATER–DIMETHYL SULFOXIDE IN DIFFERENT PROPORTIONS

H_2O conc. (%)	*Diff. current (μA)*	*Slope E vs. log $i/(i_d - i)$*	*$E_{\frac{1}{2}}$ (V) vs. Hg pool*	*E_p (V) vs. Hg pool*
—	4.86	0.120	−1.280	−1.330
10	4.08	0.099	−1.299	−1.410
20	10.92	0.273	−1.462	−1.540
30	10.92	0.139	−1.476	−1.480
40	12.60	0.119	−1.462	−1.500
50	14.40	0.097	−1.460	−1.460
60	15.85	0.093	−1.419	−1.470
70	18.24	0.067	−1.385	−1.440

Finally, it has been observed that Th(IV) gives only *one* wave, except at a water concentration in dimethyl sulfoxide of 10%, when *two* waves, of almost the same height, appear at potentials of −1.299 and −1.520V, possibly due to the fact that the thorium ion can exist in two different solvation states (Fig. 4).

In order to prove that the polarographic wave is due to Th(IV) reduction, and not to hydrolysis, we have repeated all the measurements of Table 3 using 0.001–0.01 M solutions of HCl with the same results as in the absence of this acid. This indicates that the polarographic wave is not due to any hydrolysis phenomenon.

SUMMARY

A study of Th(IV) in anhydrous dimethyl sulfoxide has been carried out using 0.1 M, 0.5 M and 1 M LiCl as supporting electrolyte. One well-defined wave has been observed, its height being linearly proportional to the Th(IV) concentration.

The half-wave potentials have been measured, using a mercury pool as reference electrode.

Waves have been obtained under different conditions of temperature and water concentration, in order to study the effect on the polarograms of these variations. The concentration range studied was $1 \cdot 10^{-3}$–$5 \cdot 10^{-3}$ M.

The values for the diffusion current constant, and the peak potentials obtained in derivative polarography are presented.

REFERENCES

1 A. W. LAUBENGAYER AND R. B. EATON, *J. Am. Chem. Soc.*, 62 (1940) 2704.
2 D. COZZI, *Proc. Intern. Congr. Pure Appl. Chem. 11th, (London), 1947*, pp. 57–58.
3 J. MASEK, *Chem. Listy*, 52 (1958) 7; *Z. Physik. Chem. (Leipzig)*, (1958) 108; *Collection Czech. Chem. Commun.*, 24 (1959) 159.
4 R. C. KAPOOR AND O. P. AGRAWAL, *Proc. Nat. Acad. Sci., India, Sect.* A, 29 (1960) 273–6; *Vijnana Parishad Anusandhan Patrika*, 3 (1960) 185–7.
5 J. SANCHO, J. ALMAGRO, A. PUJANTE AND A. RODRIGUEZ, *Anales Real Soc. Espan. Fis. Quim. (Madrid)* (in press).
6 T. P. SARMA AND S. V. RAGHAVA RAO, *Current Sci. India*, 27 (1958) 167–68.
7 G. FARAONE AND M. TROZZI, *Atti Soc. Peloritana Sci. Fis. Mat. Nat.*, 7 (1961) 233–44.
8 G. FARAONE AND G. D'AMORE, *Ann. Chim. Rome*, 46 (1956) 508–16.
9 K. KOMAREK, *Proc. Intern. Polarog. Cong. I, Prague*, (1951) 605.
10 R. P. C. GRAHAM AND G. B. LARRABEE, *Analyst*, 82 (1957) 415–22.
11 S. I. ZHANOV, V. I. ZYCOV AND T. V. KALISH, *Trudy Chetvertogo Soveshchamiyapo po Elektrokhim. Moscow, 1956*, pp. 164–9.
12 V. GUTMANN AND G. SCHOEBER, *Z. Anal. Chem.*, (1959) 339–43.
13 H. DEHU, V. GUTMANN AND G. SCHOEBER, *Nikrochim. Acta*, (1962) 959–62.
14 H. DEHU, V. GUTMANN AND G. SCHOEBER, *Monatsh. Chem.*, 93 (1962) 877–80.
15 K. SCHWABE, *Z. Elektrochem.*, 61 (1957) 484–9.
16 V. GUTMANN AND G. SCHOEBER, *Angew. Chem.*, 70 (1958) 98–104.
17 I. M. KOLTHOFF AND T. B. REDDY, *J. Electrochem. Soc.*, 108 (1961) 980–5.
18 I. M. KOLTHOFF, *J. Polarog. Soc.*, 10 (2) (1964) 22–36.
19 R. TILDEN BURNES, Univ. Microfilms (Ann Arbor, Mich.), Order No. 63–4101, 161 pp.

ELECTROANALYTICAL CHEMISTRY AND INTERFACIAL ELECTROCHEMISTRY
Elsevier Sequoia S.A., Lausanne – Printed in The Netherlands

DOUBLE-LAYER EFFECT ON TRICHLOROACETIC ACID REDUCTION AT THE DROPPING MERCURY ELECTRODE. II*

GIANCARLO TORSI AND PAOLO PAPOFF
Istituto di Chimica Analitica dell'Universita di Bari (Italy)
(Received August 8th, 1966; in revised form, May 14th, 1967)

In a previous paper[1] the behaviour of trichloroacetate ion at the dropping mercury electrode was studied in NaF, KCl and KI. The Frumkin relation was verified over a wide range of potentials and concentrations above pH 4. In fact, at pH >4 the slope and the position of the wave depend only on the ionic strength and the type of supporting electrolyte[2]. The present paper reports on the effect of a number of anions and cations on the reduction of trichloroacetate ion.

Owing to the lack of diffusion coefficient data, the Koutecký parameter[3], χ, is used instead of the rate constant, k. The two quantities are related, for a totally irreversible process, by the equation $\chi = k\sqrt{(12D/7t)}$ where D is the diffusion coefficient and t the drop time. When the diffusion current was not clearly defined, the diffusion current of iodoacetate under the same conditions was used, since it had been verified that the diffusion current in 2 M $MgSO_4$, where well developed polarographic waves can be obtained for both, is the same. Moreover, since i/i_d ratios higher than 0.85 have not been used, an error in i_d of $\pm 10\%$ shifts the corrected Tafel lines (with $\alpha = 0.20$) by approximately only ± 10 mV.

The temperature was $25 \pm 0.1°$. All potentials are referred to the SCE. No correction was made for the liquid junction potential. The drop time was 3 sec and the concentration of trichloroacetate 10^{-4} M except for 0.1 F solutions of I^- where, in order to have good i-values in the potential range 500–900 mV, (where the current is very low) $3 \cdot 10^{-3}$ M trichloroacetate was used, assuming i_d/c to be constant.

ANION EFFECT

The effect of anions was studied at a concentration of the supporting electrolyte of 0.1 F and a constant cation (K^+) concentration. The anions studied were: F^-, Cl^-, I^-, OH^-, SO_4^{2-}, CO_3^{2-}, CH_3COO^- and NO_3^-.

Figure 1 shows the log χ *vs.* E curves for F^-, Cl^- and I^-, the curves for other anions being mostly coincident with the Cl^- curve.

In Fig. 2 the same systems are plotted using the Frumkin equation

$$\log \chi = \log \chi_0 - \frac{\alpha nf}{2.3}(E - \psi_0) - \frac{zf}{2.3}\psi_0$$

in order to obtain the corrected Tafel lines.

* Presented at the IVth International Congress on Polarography, Praha, 1966.

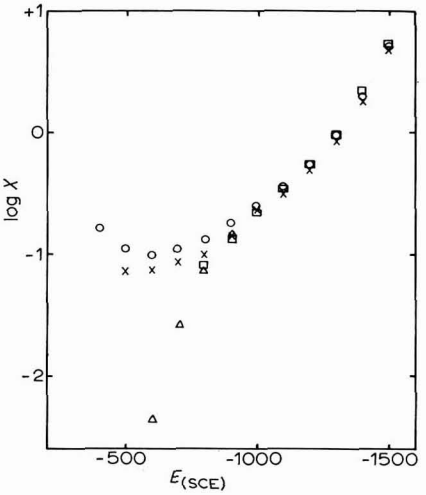

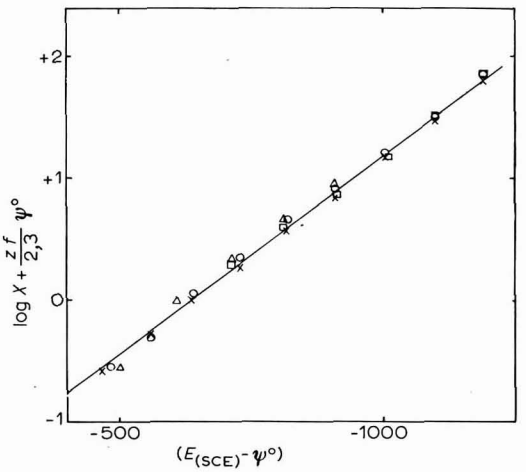

Fig. 1. Effect of different anions (0.1 F) on the reduction of trichloroacetate. log χ *vs.* E for: (○) KF, 10^{-4} M Cl_3CCOO^-; (□) KI, 10^{-4} M Cl_3CCOO^-; (×) KCl, 10^{-4} M Cl_3CCOO^-; (△) KI, $3 \cdot 10^{-3}$ M Cl_3CCOO^-.

Fig. 2. Corrected Tafel lines for the same systems as in Fig. 1. The symbols are the same.

Using ψ_0-values which take into account the specific anion adsorption[4-6], the corrected Tafel lines appear to be, within the limits of experimental error, independent of the anion type. They are also independent of the concentration of different supporting electrolytes: (NaF, KCl, KI[1], KF and CsF 10^{-3}–1 F, LiF $2 \cdot 10^{-2}$ and $3 \cdot 10^{-3}$ F). The independence of concentration of the supporting electrolyte has already been verified for many other systems[7a].

CATION EFFECT

Figure 3 shows the plot of log χ *vs.* E for chlorides of different cations. If it is first assumed with GRAHAME[7] that inorganic cations are not specifically adsorbed, the corrected Tafel lines shown in Fig. 4, are obtained. The ψ_0-values used were taken from GRAHAME's work whenever possible. In the case of CsCl and LiCl (0.1 F), ψ_0 was calculated for potentials more negative than −900 mV from the Gouy–Chapman theory, using GRAHAME's data[8]: throughout this potential region the ratios ψ_{0Cs^+}/ψ_{0K^+} and ψ_{0Li^+}/ψ_{0K^+} remain constant. Since with F^- the ratio ψ_{0Cs^+}/ψ_{0K^+} is constant also in the range −500 to −900 mV it was assumed that reasonable values of ψ_0 for CsCl and LiCl could be calculated in this potential range using the ψ_0-data of GRAHAME for KCl and the corresponding ψ_0 ratios. These values give corrected Tafel lines for CsCl coincident with those obtained for CsF using ψ_0-data from GRAHAME[7]. Assuming that the application of the Frumkin equation is correct for this system, we find, from Fig. 4, that:

(a) α depends on the type of cation and there is a linear relation between α and the ionic radius of the cation.

(b) The corrected Tafel lines of different alkaline cations converge approximately at $(E-\psi_0)=-435$, regardless of the type of anion or cation. This means that, excluding an unlikely compensation between α and $\log \chi_0$, $(E-\psi_0)$ is zero in the neighbourhood of -435 mV*.

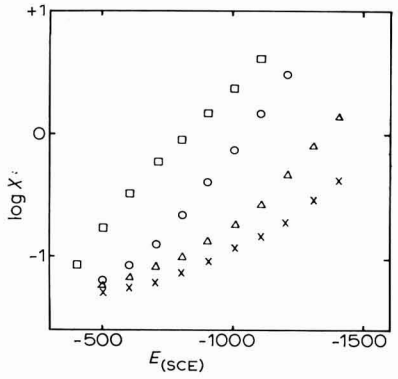

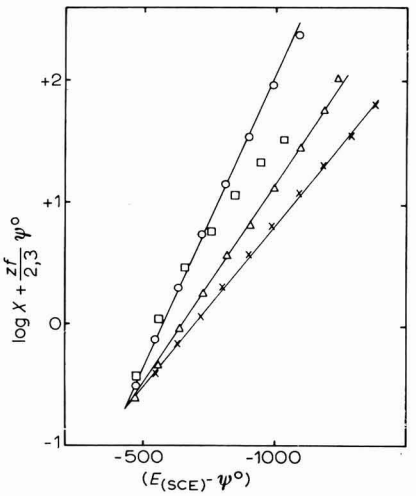

Fig. 3. Effect of different cations (0.1 N salts) on the reduction of trichloroacetate (10^{-4} M). $\log \chi$ *vs.* E for: (×) LiCl; (△) KCl; (○) CsCl; (□) $BaCl_2$.

Fig. 4. Corrected Tafel lines for the same systems as in Fig. 3. The symbols are the same.

This is the rational potential of GRAHAME where it is assumed, apart from water dipoles orientation[9], that the difference of potential between the metal and the outer Helmholtz plane is zero.

On the other hand, the cation effect is generally explained precisely in terms of specific adsorption of cations which in turn affects the double-layer structure. GIERST *et al.*[10], on the basis of cation specific adsorption and using a large number of reactions, have calculated average ψ_0-values and quantities of Cs^+ specifically adsorbed in the absence of anion specific adsorption, taking NaF as reference.

In Table 1 the results of the same calculations are reported for the case of trichloroacetate. The calculated quantity of specifically adsorbed Cs^+ appears consistently high so that it should be evident even in the case of non-kinetic measurements. GRAHAME[7], however, has found no evidence of Cs^+ specific adsorption in 10^{-3}–1 F CsF from capacity measurements, while from surface tension measurements[11] evidence of Cs^+ specific adsorption in CsCl has been found only above 1 F.

Other explanations of the effect of cations on the reduction of anions (such as different distances between the outer Helmholtz plane and the plane where the particle in equilibrium with the activated complex is localized) are difficult to prove owing to

* In the presence of specific adsorption, the value of E at which there is zero difference of potential between the metal and the outer Helmholtz plane is not -435 mV (*vs.* SCE) since the value of ψ_0 is not zero[5–6].

the lack of precise information about the double-layer structure. In order to explain the experimental results one has to assume that $d_{Cs^+} < d_{Li^+}$ where d is the distance between the metal and the outer Helmholtz plane. In the case of bivalent cations (in Figs. 3 and 4 only 0.1 F $BaCl_2$ is shown) the situation is more complex because the

TABLE 1

Cs^+ QUANTITIES SPECIFICALLY ADSORBED FOR DIFFERENT CONCNS. OF Cs^+ SALTS AT DIFFERENT POTENTIALS
NaF as reference; $\alpha = 0.18$.

Concn. Cs^+ (M)	*E (mV)*	*q_{Cs^+} ($\mu C\ cm^{-2}$)*
1	1.000	11
	1.300	18
0.1	1.000	7
	1.300	11
0.01	1.000	4
	1.300	8

corrected Tafel lines, obtained using the ψ_0-data of GRAHAME[4], are not linear. They bend toward the x-axis as in the reduction[12] of $[Fe(CN)_6]^{3-}$. The order of the accelerating effect is normal (Ba > Sr > Ca > Mg). In this case, the difference in log χ, taking NaF as reference, canot be explained in terms of specific adsorption since it is difficult to accept that the quantity specifically adsorbed decreases with increasing negative potential.

One cannot rule out, with bivalent cations, the possibility of ion pairs[13], which should have a greater effect near the point of zero charge[14].

The investigation of many other systems is therefore desirable and might afford a better interpretation of the double-layer effect on kinetic data.

ACKNOWLEDGEMENT

This work has been partly supported by the C.N.R., Rome.

SUMMARY

The effect of a number of anions and cations on the reduction of trichloroacetate ion at the dropping mercury electrode has been studied. The experimental results can be explained by taking into account the specific adsorption of anions and cations.

In the case of Cs salts as supporting electrolyte, since the calculated quantity of Cs^+ specifically adsorbed seems to be consistently high, it should be evident even in the case of non-kinetic measurements.

REFERENCES

1 G. TORSI AND P. PAPOFF, *Z. Anal. Chem.*, 224 (1967) 129.
2 P. J. ELVING AND C.-S. TANG, *J. Am. Chem. Soc.*, 72 (1950) 3244.
3 J. KOUTECKÝ, *Chem. Listy*, 47 (1953) 323.

4 D. C. GRAHAME AND B. A. SODERBERG, *J. Chem. Phys.*, 22 (1954) 449.
5 D. C. GRAHAME AND R. PARSONS, *J. Am. Chem. Soc.*, 83 (1961) 1291.
6 D. C. GRAHAME, *J. Am. Chem. Soc.*, 80 (1958) 4201.
7 D. C. GRAHAME, A. E. HIGINBOTHAM AND F. R. M. DEANE, *Transactions of the Symposium on Electrode Processes*, edited by E. YEAGER, John Wiley and Sons, New York, 1961.
7a P. DELAHAY, *Double-layer and Electrode Kinetics*, Interscience Publishers, Inc., New York, 1965, ch. 9.
8 D. C. GRAHAME, *J. Electrochem. Soc.*, 98 (1951) 343.
9 J. O.'M. BOCKRIS, M. A. V. DEVANATHAN AND K. MULLER, *Proceedings of the First Australian Conference on Electrochemistry*, Pergamon Press, Oxford, 1965, p. 832.
10 L. GIERST, L. VANDENBERGHEN, E. NICOLAS AND A. FRABONI, *J. Electrochem. Soc.*, 113 (1966) 1025.
11 H. WROBLOWA, Z. KOVAC AND J. O.'M. BOCKRIS, *Trans. Faraday Soc.*, 61 (1965) 1523.
12 A. N. FRUMKIN, O. A. PETRY AND N. V. NIKOLAEVA-FEDOROVICH, *Electrochim. Acta*, 8 (1963) 177.
13 K. M. JOSHI AND R. PARSONS, *Electrochim. Acta*, 4 (1961) 129.
14 V. G. LEVICH, *Advan. Electrochem. Electrochem. Eng.*, Vol. 4, edited by P. DELAHAY AND C. W. TOBIAS, Interscience Publishers Inc., New York, 1966, p. 249.

ELECTROANALYTICAL CHEMISTRY AND INTERFACIAL ELECTROCHEMISTRY
Elsevier Sequoia S.A., Lausanne – Printed in The Netherlands

POLAROGRAPHIC REDUCTION OF 8-HYDROXYQUINOLINE IN DIMETHYLFORMAMIDE*

TAITIRO FUJINAGA, KOSUKE IZUTSU AND KAZUNORI TAKAOKA**
Chemical Institute, Faculty of Science, Kyoto University, Kyoto (Japan)
(Received August 9th, 1966)

Polarographic studies of 8-hydroxyquinoline in aqueous medium have been carried out by many investigators[1]. STOCK[2] has made a fundamental investigation of this substance in aqueous solutions: in acidic solutions, 8-hydroxyquinoline produces a single main wave corresponding to a two-electron reduction to a dihydro-derivative; in alkaline solutions of pH 9.2–10.5, a reversible one-electron reduction wave is observed. One author[3] has obtained a similar result to that of STOCK and applied it to the amperometric titration of several metal ions.

In this paper, the study of 8-hydroxyquinoline in dimethylformamide was undertaken as a part of the polarographic investigation of quinolines in non-aqueous solvents[4–6].

EXPERIMENTAL

8-Hydroxyquinoline was purified by recrystallisation from aqueous alcohol. 8-Methoxyquinoline was prepared from 8-hydroxyquinoline by methylation with dimethyl sulfate[7]. Dimethylformamide (DMF) used as a solvent, and tetraethylammonium perchlorate (NEt_4ClO_4) used as a supporting electrolyte, were as previously described[4]. Tetraethylammonium hydroxide (NEt_4OH) in 10% aqueous solution (Tokyokasei Co.) was used as a proton acceptor, and G.R.-grade perchloric acid and phenol as proton donors. All polarographic measurements were carried out in DMF solutions containing 0.1 *M* NEt_4ClO_4, known concentrations of the depolariser and other agents, and 0–90% v/v of water.

Apparatus and techniques were usually the same as described previously. The capillary used was as described in ref. 4 except in the experiments for Figs. 4 and 7 where a capillary as described in ref. 5 was used. All potentials are referred to the aqueous saturated calomel electrode fitted with a DMF–agar salt bridge[8]. After the recording of a polarogram, the bridge potential[8] and the resistance were measured to correct for the applied voltage and the i–R drop, respectively. All polarographic measurements were made at $25 \pm 0.5°$.

Spectrophotometric measurements were carried out using a Hitachi EPU-2A manual spectrophotometer.

RESULTS

Some typical polarograms of 8-hydroxyquinoline (8-quinolinol) in DMF–water

* Presented at the 12th Meeting of the Polarographic Society of Japan, Kyoto, November, 1965.
** Present address: Department of Industrial Chemistry, Fukui Technical College, Sabae (Japan).

media are shown in Fig. 1. In 100% DMF solution, 8-quinolinol gives two waves of equal height (curves a and b in Fig. 1). The first wave, (H), involves a maximum in its limiting current when the quinolinol concentration exceeds 0.6 mM. The maximum becomes more pronounced as the quinolinol concentration is increased. The addition

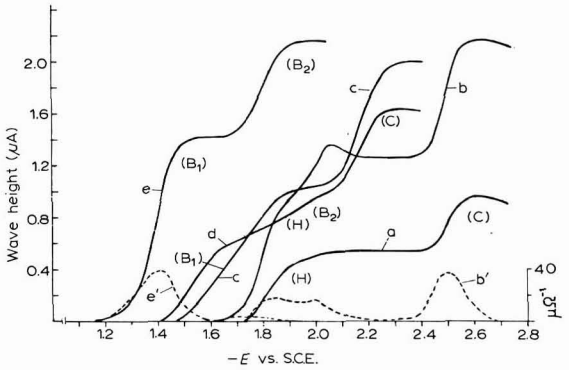

Fig. 1. Polarograms of 8-quinolinol in DMF–water media (corrected for residual current). Concn. quinolinol, 0.8 mM (except curve a, concn., 0.4 mM). Water content: (a, b and b'), 0; (c), 10; (d), 20; (e, e'), 90%.

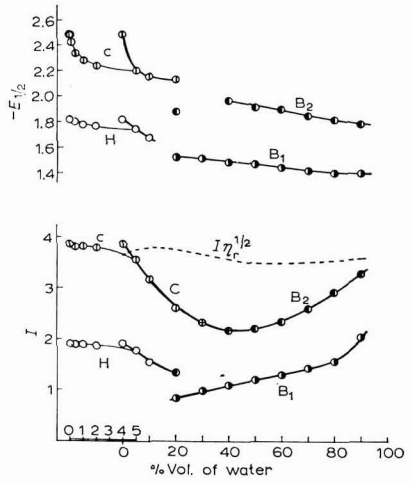

Fig. 2. Effect of water on 8-quinolinol wave in DMF. Curves are extended 5 times between 0 and 5% of water on the abscissa.

of water causes the maximum to decrease and its position to shift to more positive potentials; finally, it disappears, coalescing in the ascending part of the first wave at water contents over 1%. At the potential of the second wave, (C), the a.c. peak (higher than for the first wave (H)) appears (curve b'). As the water content rises to 10%, the second wave, (C), shifts to more positive potentials and the first wave, (H), becomes drawn out, suggesting the presence of a small wave at the foot (curve c). Such a wave, (B_1), preceding wave (H), grows at the expense of wave (H) with increasing water content (curve d). Parallel to this, a new wave, (B_2), appears overlapping wave (H),

and growing at the expense of wave (C). The well-defined wave (C) persists up to approximately 40% water content, where it merges into the ill-defined wave (B_2). At water contents greater than 40%, only two waves, (B_1) and (B_2), of equal height remain; the former is well defined showing a relatively high peak in the a.c. polarogram, and the latter a very small a.c. peak (curves e and e').

The effect of water on the half-wave potential and on the wave height of 8-quinolinol in DMF is shown quantitatively in Fig. 2. The heights and half-wave potentials of wave (B_1) in the region of water content of about 5–10% and of waves (H) and (B_2) in the region 20–40%, could not be determined accurately. The total wave heights (curve C–B_2 in Fig. 2) varies markedly with increasing water content, showing a minimum at about 40% of water. However, the diffusion current constants corrected for the viscosity effect (curve $I\eta_r^{\frac{1}{2}}$, where η_r is the viscosity relative to water[4,6]) show an almost constant value of 3.7 over the entire DMF–water range. It is concluded that the total number of electrons transferred is two[4–6] throughout this concentration range.

The effect of phenol on the quinolinol wave in DMF is shown in Fig. 3. When phenol is added to an 0.6 mM solution of quinolinol, a new wave, (A_1), appears at the potential of the maximum for a quinolinol concentration exceeding 0.6 mM (*cf.* curve b in Fig. 1). Wave (A_1) increases at the expense of wave (C) with increasing phenol concentration. The addition of phenol at concentrations above 1.2 mM for 0.6 mM quinolinol, causes wave (C) to be replaced completely by wave (A_1) (curve d in Fig. 3), the total wave heights remaining nearly constant. A solution of 20% water–DMF behaves similarly, as shown in Fig. 4, in which the height around wave (B_2) increases at the expense of wave (C), while wave (B_1) remains constant.

The effect of perchloric acid on the quinolinol wave in 90% water content is shown in Fig. 5. A new wave, (A), is seen at a potential more positive than that of wave (B_1) (curve b in Fig. 5). With increasing acid concentration, wave (A) grows at the

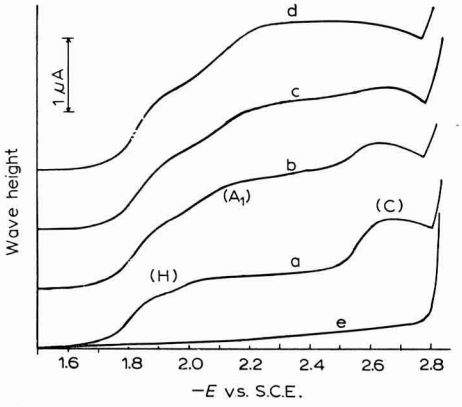

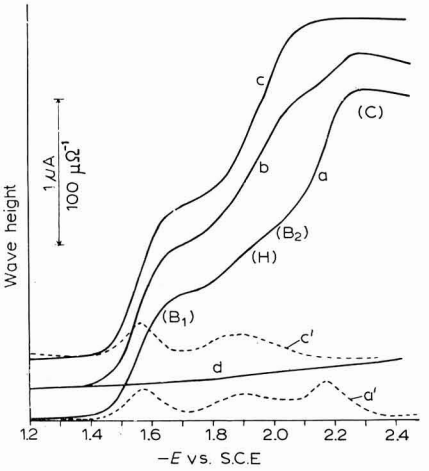

Fig. 3. Polarograms of 8-quinolinol with phenol in DMF. Concn. quinolinol, 0.6 mM. Concn. phenol: (a), 0; (b), 0.3; (c), 0.6; (d), 1.2 mM; (e), residual current.

Fig. 4. Polarograms of 8-quinolinol with phenol in 20% water–DMF. Concn. quinolinol, 1.1 mM. Concn. phenol: (a, a'), 0; (b), 1.0; (c, c'), 2.0 mM; (d), residual current.

expense of wave (B_1) and, after the complete consumption of (B_1) at the expense of wave (B_2). Only wave (A) remains in the presence of excess perchloric acid (curve f). A solution of 50% water–DMF behaves similarly, as shown in Fig. 6. The effect of tetraethylammonium hydroxide (NEt_4OH) on the quinolinol wave in 1% water medium is shown in Fig. 7. The addition of NEt_4OH causes wave (H) to decrease, while the

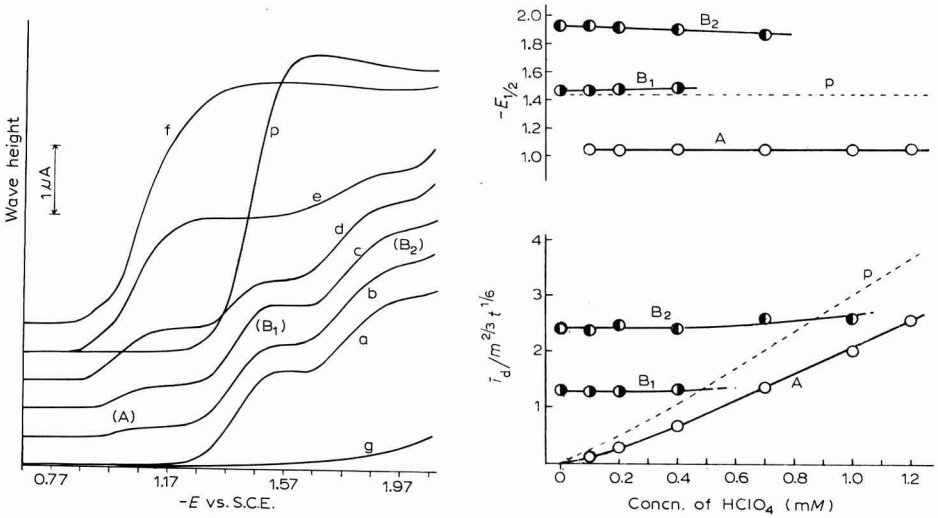

Fig. 5. Polarograms of 8-quinolinol with $HClO_4$ in 90% water–DMF. Concn. quinolinol, 0.8 mM. Concn. $HClO_4$: (a), 0; (b), 0.1; (c), 0.2; (d), 0.4; (e), 0.8; (f), 1.2 mM; (p), 0.8 mM $HClO_4$ only; (g), residual current.

Fig. 6. Effect of $HClO_4$ on 8-quinolinol wave in 50% water–DMF. Concn. quinolinol, 1.0 mM. (p), in the absence of quinolinol.

total wave height at wave (C) and the half-wave potential of wave (C) remain constant. Only wave (C) remains in the presence of excess NEt_4OH (curves d and e in Fig. 7). It can be seen in Fig. 7, that a new wave appears in NEt_4OH solution at a much more positive potential (*ca.*, -1 V *vs.* S.C.E.) with a small d.c. height and a small a.c. peak.*

The C–$i_d/m^{\frac{2}{3}}t^{\frac{1}{6}}$ and C–$E_{\frac{1}{2}}$ relations of various waves of 8-quinolinol in DMF, 50% water, and 90% water media are shown in Fig. 8, in which it can be seen that all wave heights are linearly proportional to the quinolinol concentration. The effect of the mercury height on the limiting currents of the various waves is also shown in Table 1, from which is seen that all waves are diffusion-controlled.

The absorption spectra of 8-quinolinol in DMF–water media are shown in Fig. 9. On the addition of water to the quinolinol solution in DMF, a new absorption

* This wave was observed when the electrolysis solution was allowed to stand for a long time after preparation, and its height was very sensitive to the effect of light, in the visible range, on the solution. Similar behaviour was observed for 5-quinolinol in 1% water medium. The $E_{\frac{1}{2}}$ of the products from both 5- and 8-quinolilol in a 2 mM solution of NEt_4OH was equal to -1.16 V. This means that the product corresponds to quinoline-5,8-quinone, produced from quinolinol by oxidation with oxygen, which is present in a basic solution such as DMF before deaeration.

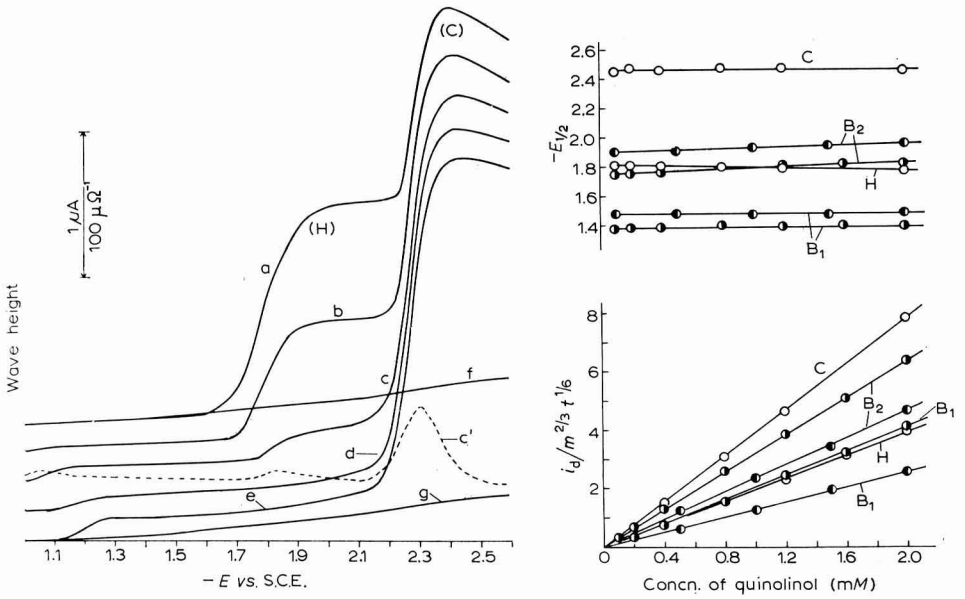

Fig. 7. Polarograms of 8-quinolinol with NEt_4OH in 1% water–DMF. Concn. quinolinol, 1.0 mM. Concn. NEt_4OH: (a, f), 0; (b), 0.5; (c, c'), 1.0; (d), 2.0; (e, g), 5.0 mM; (f, g), residual current.

Fig. 8. Relations between $i_d/m^{\frac{2}{3}}t^{\frac{1}{6}}$, $E_{\frac{1}{2}}$ and 8-quinolinol concn. Water content: (○), 0; (◐), 50; (◑), 90%.

TABLE 1

EFFECT OF THE MERCURY HEIGHT ON THE LIMITING CURRENT

Expt. No.*	*Wave*	i			$ih^{-\frac{1}{2}}$		
		h = 45	*60*	*75*	*45*	*60*	*75 cm*
	(H) at 2.0 V	0.80	0.95	1.03	0.119	0.121	0.119
1	(H) at 2.3 V	0.994	1.16	1.31	0.148	0.150	0.152
	(C)	1.71	1.97	2.20	0.25	0.25	0.254
	(B_1)	0.66	0.80	0.88	0.0985	0.103	0.102
2	(H,B_2) at 2.0 V	0.96	1.14	1.24	0.143	0.147	0.143
	(C)	1.72	2.00	2.18	0.257	0.258	0.252
	(A)	0.548	0.62	0.708	0.0818	0.0802	0.0818
3	(B_1)	1.00	1.16	1.32	0.149	0.150	0.153
	(B_2)	1.60	1.89	2.12	0.239	0.245	0.245
	(B_1)	1.01	1.21	1.36	0.151	0.156	0.157
4	(B_2)	1.70	1.95	2.17	0.254	0.252	0.251

* 1. 0.8 mM 8-quinolinol in DMF.
2. 1 mM quinolinol in 20% water content.
3. 1 mM quinolinol + 0.4 mM $HClO_4$ in 50% water content.
4. 0.8 mM quinolinol in 90% water content.

band appears at 435 mμ (molecular extinction coefficient $\varepsilon = 27.2$ in 90% water medium). The new species absorbing at wave length 435 mμ increases rapidly with increasing water content above 60%. In 90% water content, it is confirmed that the extinction–concentration plot gives a straight line in the quinolinol concentration range,

0–25 mM. Bathochromic shifts in both acid and basic solutions relative to neutral solution were also observed. The results are shown in Fig. 10, and agree well with the results obtained in ethanol by EWING AND STECK[9]. It is clear from Figs. 9 and 10 that the new species at 435 mμ is quite different from those of the quinolinolate anion at 355 mμ (curve d in Fig. 10, $\varepsilon = 2.74 \times 10^3$) or the hydroxyquinolinium cation at 360 mμ (curve c in Fig. 10, $\varepsilon = 1.73 \times 10^3$).

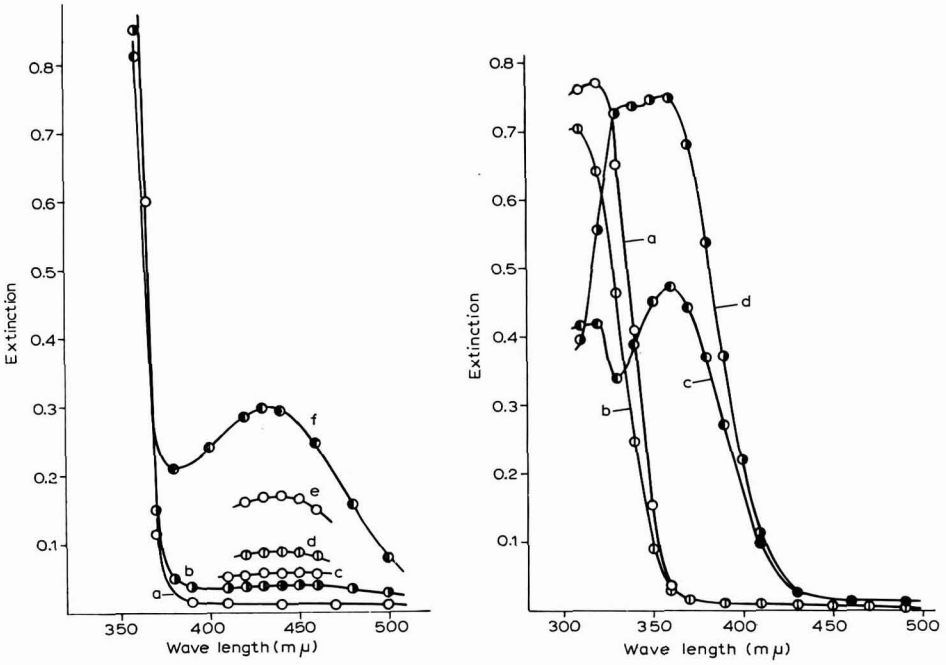

Fig. 9. Water effect in absorption spectra of 8-quinolinol in DMF. Concn. quinolinol, 11.0 mM. Water content: (a), 0; (b), 50; (c), 60; (d), 70; (e), 80; (f), 90%.

Fig. 10. Bathochromic shifts of 8-quinolinol in acid and basic solns. Concn. quinolinol, 0.27 mM. Water content: (a), 0; (b, c and d), 90%; (a, b), neutral soln.; (c), 10 mM $HClO_4$ soln.; (d), 10 mM NaOH soln.

DISCUSSION

I. Reduction mechanism in DMF

Experimental results for quinolines such as quinoline[4], 6-chloroquinoline[5] and 5-hydroxyquinoline[6] have already been reported. Quinoline gives two one-electron reduction waves corresponding to the successive reductions of the pyridine ring ($-E_{\frac{1}{2}}$: 2.13 and 2.6 V *vs.* S.C.E., respectively). 6-Chloroquinoline gives three steps, the first two-electron wave corresponds to the de-chlorination reaction (1.85 V) and the succeeding two one-electron waves, the reductions of the pyridine ring (2.13 and 2.55 V, respectively). 5-Hydroxyquinoline gives two main one-electron waves corresponding to the hydrogen discharge (1.85 V) and to the reduction of the quinolinolate (2.6 V). The reversibility of the waves and the effect of water on the half-wave potentials and on the heights of the waves were very different depending on the re-

spective reduction mechanisms. In the present work, 8-hydroxyquinoline produced two one-electron waves in DMF (1.82 and 2.5 V, respectively). The water effect on the 8-quinolinol wave in DMF was identical with that on 5-quinolinol; two independent one-electron waves remain up to almost a 10% addition of water. Moreover, the addition of the proton acceptor to 8-quinolinol solution in 1% water content causes the first wave to decrease to zero (Fig. 7). It is proposed, therefore, that the reduction mechanism of 8-quinolinol in DMF at the dropping mercury electrode, is the same as in the case of 5-quinolinol[6]:

For wave (H),

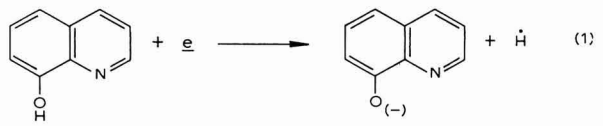

For wave (C),

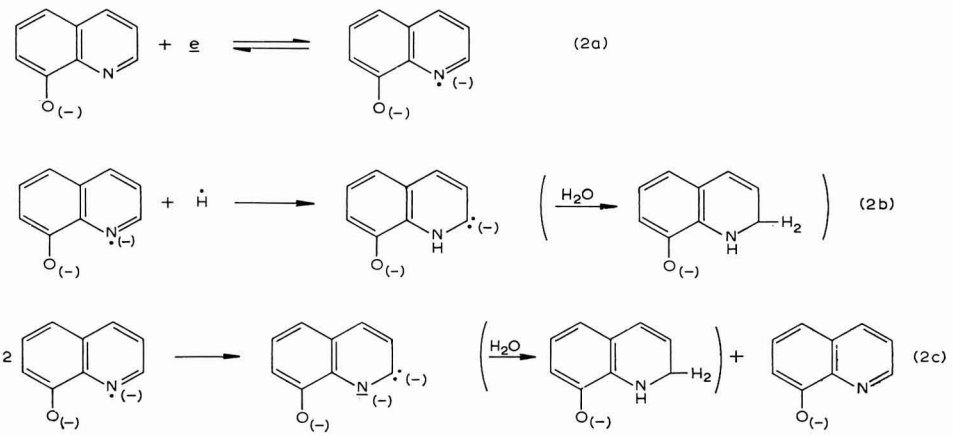

The first wave, (H), corresponds to the hydrogen discharge of the hydroxy group in quinolinol (eqn. (1)). The second wave, (C), corresponds to the one-electron reduction of the pyridine ring in the quinolinolate anion (eqn. (2a)). The quinolinolate anion radical, denoted as $^{-}O\dot{R}^{-}$, thus formed, reacts immediately with the hydrogen atom to form, finally, 1,2(or 1,4)-dihydroquinolinolate anion, $^{-}ORH_2$ (eqn. (2b)). The radical $^{-}O\dot{R}^{-}$ might also disproportionate rapidly as in eqn. (2c) but more slowly than the rate of reaction of (2b). The disproportionation product is the same, $^{-}ORH_2$, as in eqn. (2b). In neutral solution, the electrode reaction proceeds according to eqns. (1), (2a) and (2b), but in basic solution it follows eqns. (2a) and (2c). The final products in both media are the same, $^{-}ORH_2$: always a two-electron transfer with regard to the pyridine ring. Consequently, the experimental results (*i.e.*, the total height at wave (C) and $E_{\frac{1}{2}}$ of wave (C) remain constant in solutions in the presence or absence of the proton acceptor (Fig. 7)) can be fully interpreted by the above schemes.

The effect of phenol addition to the quinolinol solution in DMF can also be explained as in the case of 5-quinolinol. The hydrogen of the OH-group in phenol is not so easily released as that in the quinolinol. Therefore, the protonation or the acid

complex-formation with phenol HA prefers the quinolinolate anion, $^-$OR, to the original quinolinol, HOR. The quinolinolate N-acid complex, $^-$ORHA, will be more easily reduced than the $^-$OR, hence wave (C) (reduction of $^-$OR) shifts to a more positive potential (wave (A_1), probably the reduction of $^-$ORHA).

II. Reduction mechanism in DMF–water

The fact that the new species that absorbs light at 435 mμ, increases with increasing water content (Fig. 9), indicates that the new species corresponding to the formation of wave (B_1) is the hydrate of the quinolinol, $HORH_2O$, which is in equilibrium with the quinolinol, HOR. On the basis of the experimental results, the electrode reaction proposed for 8-quinolinol in solutions containing more than 40% of water is as follows:

For wave (B_1),

$$HORH_2O + e \rightarrow HO\dot{R}H + OH^- \quad (3a)$$

$$HO\dot{R}H + e \rightleftharpoons HORH^- \quad (3b)$$

$$HORH^- + HORH_2O \rightarrow \text{active-dimer} \quad (3c)$$

For wave (B_2),

$$\text{active-dimer} + 2e + H_2O \rightarrow 2\,HORH_2\,(^-ORH_2) \quad (4)$$

Here, $HORH_2$ denotes 1,2(or 1,4)-dihydro-8-quinolinol. The above schemes for waves (B_1) and (B_2) shown by eqns. (3) and (4) are similar to those of quinoline[4], 6-chloroquinoline[5] and 5-hydroxyquinoline[6] in water-rich medium.

The addition of NEt_4OH caused wave (B_1) to shift to a somewhat negative potential. The electrode reaction in basic media takes place according to the following:

$$^-ORH_2O + e \rightarrow {}^-O\dot{R}H + OH^- \quad (3a')$$

$$^-O\dot{R}H + e \rightleftharpoons {}^-ORH^- \quad (3b')$$

$$^-ORH^- + {}^-ORH_2O \rightarrow \text{active-dimer} \quad (3c')$$

In acidic medium, $HClO_4$ reacts with $HORH_2O$ to form the hydroxyquinolinium cation, $HORH^+$, which is much more easily reduced than the hydrated 8-quinolinol, $HORH_2O$. The new wave (A) appears at a potential about 0.4 V more positive than that of wave (B_1), and the mechanism would be,

$$HORH^+ + 2\,e \rightarrow HORH^- \quad (5a)$$

$$HORH^- + HORH_2O \rightarrow \text{active-dimer} \quad (5b)$$

The hydroxyquinolinium anion, $HORH^-$, thus formed, reacts immediately with $HORH_2O$ to form the electro-active dimer (eqn. (5b)), which behaves identically to that in eqn. (3c). Hence, the fact that wave (A) consumes both waves (B_1) and (B_2), successively (Figs. 5 and 6), can be fully interpreted by the above schemes.

For the intermediate solutions containing about 5–40% of water, the polarogram, and hence the electrode reaction, are complicated by the presence of many waves; *i.e.*, waves (B_1), (H), (B_2) and (C) in order of half-wave potential. With increasing water content, waves (H) and (B_2) begin to overlap, waves (H) and (C) decrease to zero, and waves (B_1) and (B_2) increase from zero to the height equivalent to a one-electron reduction.

Equation (3) shows that the half-wave potential of wave (B_1) would shift -0.059 V/unit pH; the experimental results given by STOCK[2] agree well with this

value. STOCK also examined wave (A) and found that the wave corresponds to a two-electron reduction.

III. 8-Methoxyquinoline

The polarography of 8-methoxyquinoline was quite different from that of 8-hydroxyquinoline, and rather similar to that of quinoline, except in water-rich media, where the clear separation of waves (B_1) and (B_2) was not observed.

ACKNOWLEDGEMENT

This work was partially supported by a grant from the Scientific Research Expenditure Department of the Ministry of Education for which the authors are grateful.

SUMMARY

The investigations of the polarographic and spectroscopic behaviour of 8-hydroxyquinoline in DMF solutions containing 0–90% water indicate the following mechanism for the reduction of 8-hydroxyquinoline at the dropping mercury electrode (the reactions are arranged in order of half-wave potential).

In the presence of less than 5% of water:

Wave (H), $HOR + e \rightarrow {}^{-}OR + \dot{H}$;

Wave (C), ${}^{-}OR + e \rightleftharpoons {}^{-}O\dot{R}^{-} + \dot{H} \rightarrow {}^{-}ORH^{-}(\rightarrow {}^{-}ORH_2)$,

$2\,{}^{-}O\dot{R}^{-} \rightarrow {}^{-}OR^{2-}(\rightarrow {}^{-}ORH_2) + {}^{-}OR.$

In the presence of more than 40% of water:

Wave (A), when $HClO_4$ is added,

$HORH^{+} + 2\,e \rightarrow HORH^{-} + HORH_2O \rightarrow$ active-dimer;

Wave (B_1), $HORH_2O + 2e \rightarrow HORH^{-} + HORH_2O \rightarrow$ active-dimer,

and when NEt_4OH is added,

${}^{-}ORH_2O + 2\,e \rightarrow {}^{-}ORH^{-} + {}^{-}ORH_2O \rightarrow$ active-dimer;

Wave (B_2), active dimer $+ 2\,e + H_2O \rightarrow 2\,HORH_2({}^{-}ORH_2)$.

At intermediate concentrations of water, waves (B_1), (H), (B_2) and (C) are involved.

Here, HOR, ${}^{-}ORH_2$, $HORH^{+}$, $HORH_2O$ and $HORH_2$ denote 8-quinolinol, dihydroquinolinolate ion, hydroxyquinolinium ion, hydrated quinolinol and dihydroquinolinol, respectively.

REFERENCES

1 I. M. KOLTHOFF AND J. J. LINGANE, *Polarography*, Interscience Publishers Inc., New York, 1952, p. 819.
2 J. T. STOCK, *J. Chem. Soc.*, (1949) 586.
3 M. ISHIBASHI AND T. FUJINAGA, *Bull. Chem. Soc. Japan*, 23 (1950) 25, 27.
4 T. FUJINAGA, K. IZUTSU AND K. TAKAOKA, *J. Electroanal. Chem.*, 12 (1966) 203.
5 T. FUJINAGA AND K. TAKAOKA, *J. Electroanal. Chem.*, 16 (1968) 99.
6 K. TAKAOKA, *Review of Polarography*, 15 (1967) to be published.
7 B. VARGOLICI AND E. ROTHLIN, *Ber.*, 49 (1916) 581.
8 K. TAKAOKA, *Review of Polarography*, 14 (1966) 63.
9 G. W. EWING AND E. R. STECK, *J. Am. Chem. Soc.*, 68 (1946) 2185.

ELECTROANALYTICAL CHEMISTRY AND INTERFACIAL ELECTROCHEMISTRY
Elsevier Sequoia S.A., Lausanne – Printed in The Netherlands

POLAROGRAPHIC REDUCTION OF 6-CHLOROQUINOLINE IN DIMETHYLFORMAMIDE*

TAITIRO FUJINAGA AND KAZUNORI TAKAOKA**
Chemical Institute, Faculty of Science, Kyoto University, Kyoto (Japan)
(Received November 11th, 1966)

The polarographic behaviour and electrode reaction mechanisms of quinoline and its derivatives at the dropping mercury electrode in non-aqueous solvents have been investigated in this laboratory. This paper deals with the polarographic study of 6-chloroquinoline in dimethylformamide as solvent.

The polarographic behaviour and electrode reaction mechanisms of 6-chloroquinoline were found to be similar to those of quinoline[1], except for the presence of the dehalogenation process of the former. 8-Hydroxyquinoline and 5-hydroxyquinoline, however, behave differently owing to the presence of acidic hydrogen; the details will be reported in further communications[5].

EXPERIMENTAL

6-Chloroquinoline (Nakarai Chemicals) was purified by recrystallisation from petroleum ether (m.p. 41°). Dimethylformamide (DMF) and tetraethylammonium perchlorate (NEt_4ClO_4) were as described previously[1]. The supporting electrolyte in all electrolysis solutions was 0.1 *N* NEt_4ClO_4.

A polarograph (Yanagimoto Model PA-102), an H-type cell and the bridged S.C.E. have already been described[1,2]. The bridge potential and the resistance were measured after recording the polarograms, to correct for the applied voltage and the *i*–*R* drop.

The characteristics of the dropping mercury electrode are shown in Fig. 1. The drop time, t, in various solvents, was plotted in the upper curve (t) and the average mercury flow rate, $\overline{m}=0.5166$ mg/sec (0.5194 in DMF and 0.5138 in H_2O), was used in plotting the lower curve ($m^{\frac{2}{3}}t^{\frac{1}{6}}$). Since t becomes extremely small on increasing the applied voltage, the wave heights were corrected for $m^{\frac{2}{3}}t^{\frac{1}{6}}$, unless otherwise stated.

All measurements were made at $25\pm0.5°$.

RESULTS

Some typical polarograms of 6-chloroquinoline in DMF and DMF–water solutions are shown in Fig. 2. In 100% DMF solution, 6-chloroquinoline gives three well-defined waves, (D_1), (B) and (C), as shown in curve b ((D) is the dehalogenation process, (B) and (C) the reduction processes of the pyridine ring). Wave (D_1) is independent of added water up to 5%, whereas waves (B) and (C) are much affected by the addition

* Presented at the 19th Annual Meeting of the Chemical Society of Japan, April, 1966.
** Present address: Department of Industrial Chemistry, Fukui Technical College, Sabae (Japan).

of a small amount of water. With increase of water content, wave (B) increases at the expense of wave (C), which disappears completely in the presence of above 1% of water. With increasing water content above 1%, wave (B) decreases in height and shifts to more positive potentials, finally coalescing with wave (D_1) (curves d, e).

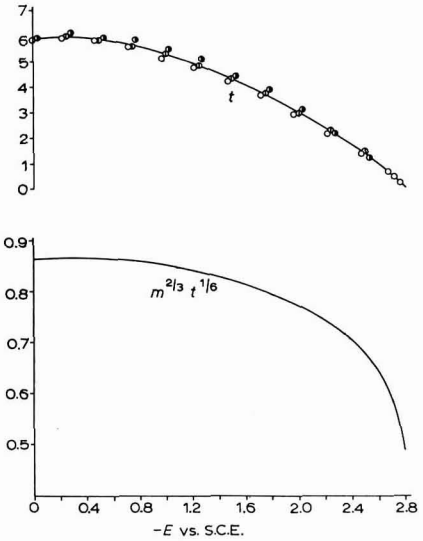

Fig. 1. Drop-time curve in DMF-water, ($\bar{m}$), 0.5166; h, 60 cm. Water content: (○), 0; (◑), 30; (◑), 90%.

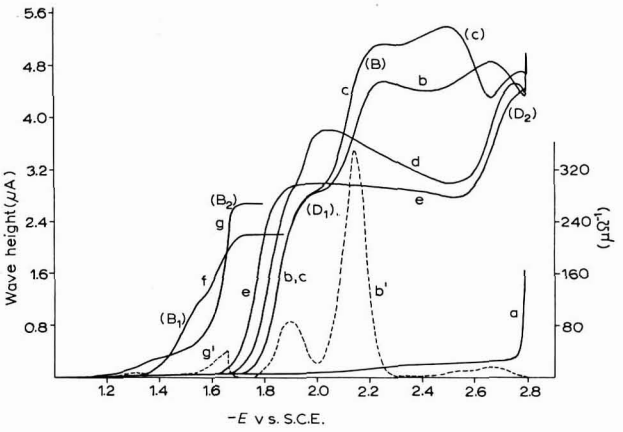

Fig. 2. Polarograms of 6-chloroquinoline in DMF–water media. Concn. 6-chloroquinoline, 1 mM. Water content: (b, b'), 0; (c), 0.4; (d), 5; (e), 10; (f), 60; (g, g'), 90%; (a), residual current in DMF.

Parallel to this, an unusual minimum appears on waves (C) (curve c), and (B) (curve d), after which a new wave, (D_2), becomes visible at about −2.7 V. Wave (D_2) increases in height with decrease of wave (B) and finally merges into the discharge current in solutions containing over 20% of water.

When the water content exceeds about 20%, wave (B) is spread out, and above

50% water content splits clearly into two waves, (B_1) and (B_2), of equal height (curve f). With further increase of water content above 80%, wave (B_1) is abnormally depressed (curve g).

The a.c. polarographic observations show that in 100% DMF solution, wave (B) corresponds to a large a.c. peak which decreases in height with increasing water content; waves (D_1) and (C) correspond to small a.c. peaks (curve b'). The peaks corresponding to waves (B_1) and (B_2) are also very small (curve g').

The effect of water addition on the half-wave potentials and wave heights are shown quantitatively in Fig. 3. The total height of waves (B) and (C) decreases with

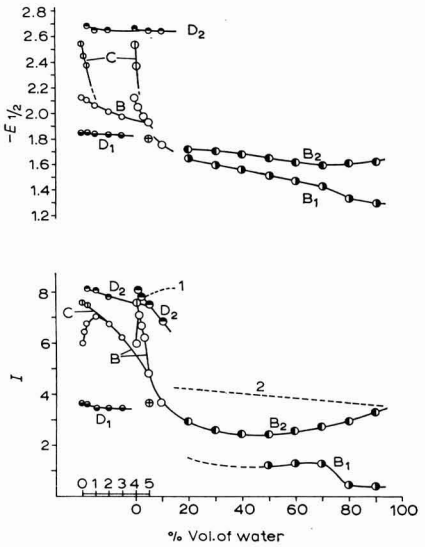

Fig. 3. Effect of water on 6-chloroquinoline wave in DMF. Dotted lines 1 and 2: heights of total wave corrected for viscosity ($I\eta_r^{\frac{1}{2}}$). Curves are extended 5 times between 0 and 5% of water on the abscissa.

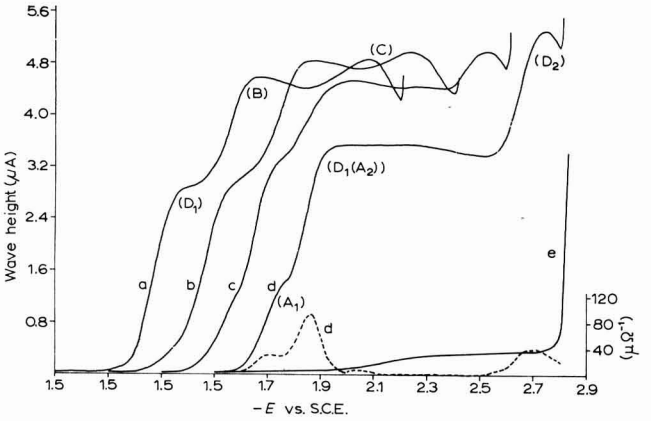

Fig. 4. Polarograms of 6-chloroquinoline with phenol in DMF. Concn. 6-chloroquinoline, 1 mM. Concn. phenol: (a), 0; (b), 1; (c), 3; (d,d'), 6 mM; (e), residual current in DMF containing 6 mM phenol.

increasing water content; the decrease is more than that expected from the viscosity increase of the solvent. On the other hand, the wave height of (D_2) is almost constant after correcting for viscosity, independent of the water content (see dotted line 1). The total number of electrons involved at wave (D_2) was calculated from its diffusion current constant (*ca.*, 8 μA mM^{-1} $m^{-\frac{2}{3}}$ $t^{-\frac{1}{6}}$) to be 4.

Above 20% water, the wave height of (B_1) plus (B_2) was almost constant after the viscosity correction (see dotted line 2). The total number of electrons for the reaction at wave (B_2) was found to be 2.

The effect of phenol on the 6-chloroquinoline wave in DMF is shown in Figs. 4 and 5. The addition of phenol up to a concentration of 1 mM to a solution of 1 mM 6-chloroquinoline had no visible effect (curve b in Fig. 4). At a phenol concentration above 1 mM, wave (D_1) splits into two waves (curve c in Fig. 4); a new wave, (A_1) ((A) is the reduction of the acid complex), appears at a little more positive potential than that of (D_1) and another wave (A_2) at the same potential as that of (D_1). In phenol solutions more concentrated than 2 mM, a new wave, (D_2), appears at a more negative potential than that of wave (C) (curves c, d in Fig. 4). The waves (A_1), (A_2) and (D_2) increase at the expense of waves (D_1), (B) and (C) with increasing phenol concentration. In the presence of phenol concentrations more than five times the equivalent of the substrate, waves (D_1), (B) and (C) are entirely replaced by waves (A_1), (A_2) and (D_2), (ratio of heights is 1:1:2, see Fig. 5).

In Fig. 6 is shown the effect of perchloric acid on the chloroquinoline wave in a solution of 60% water. On the addition of the acid, an irreversible wave, (A), appears at a potential more positive than that for wave (B_1) (curve b). The height of wave (A) increases at the expense of wave (B_1) and, after the disappearance of wave (B_1)

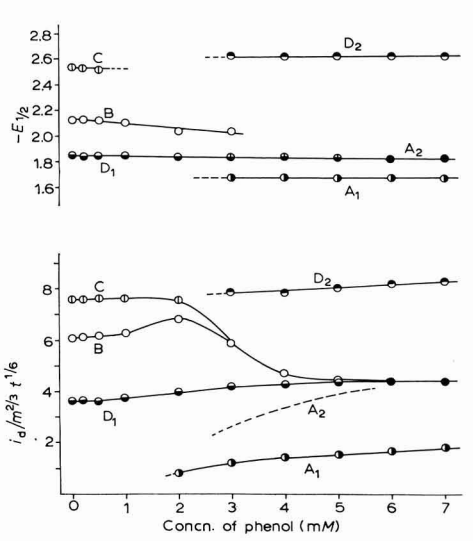

Fig. 5. Effect of phenol on 6-chloroquinoline wave in DMF. Concn. chloroquinoline, 1 mM.

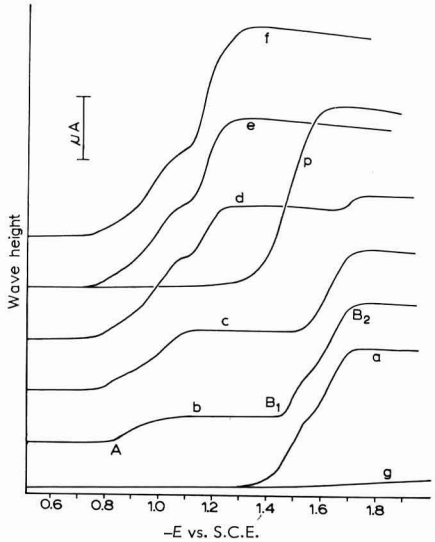

Fig. 6. Polarograms of 6-chloroquinoline with $HClO_4$ in 60% water content. Concn. chloroquinoline, 1 mM. Concn. $HClO_4$: (a), 0; (b), 0.21; (c), 0.42; (d), 0.84; (e), 1.06; (f), 1.27 mM; (g), residual current; (p), 1 mM $HClO_4$ only.

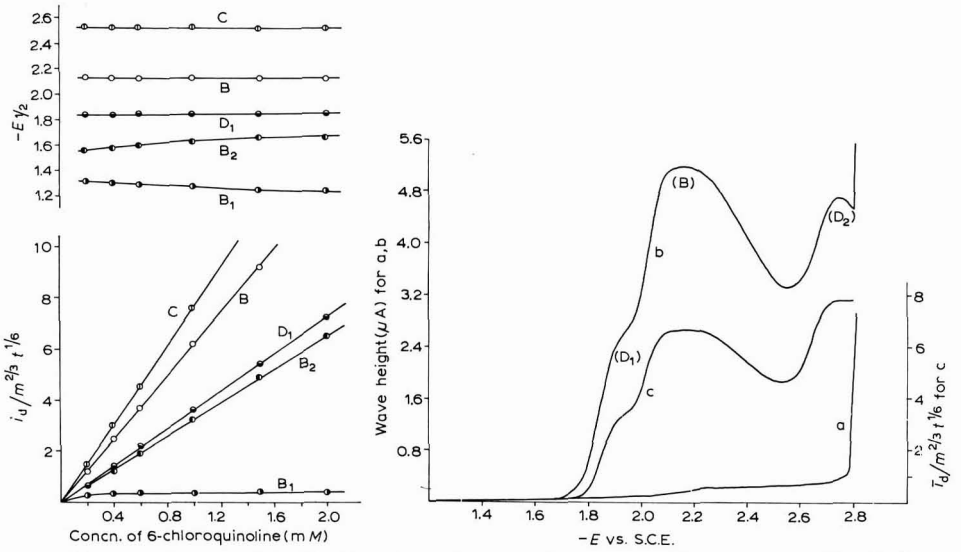

Fig. 7. Relations between $i_d/m^{\frac{2}{3}}t^{\frac{1}{6}}$, $E_{\frac{1}{2}}$ and 6-chloroquinoline concn. Water content: (D_1, B, C), 0; (B_1, B_2), 90%.

Fig. 8. Unusual drop in the limiting current in 2% water content. (a), residual current; (b), polarogram of 1 mM chloroquinoline; (c), corrected for the residual current and $m^{\frac{2}{3}}t^{\frac{1}{6}}$.

TABLE 2

EFFECT OF THE MERCURY HEIGHT ON THE LIMITING CURRENT

Expt. No.*	*Waves*	i			$i\eta^{-\frac{1}{2}}$		
		h = 45	60	75	45	60	75 *cm*
1	(D_1)	1.42	1.62	1.80	0.212	0.209	0.208
	(B)	2.28	2.64	2.94	0.340	0.340	0.340
	(C)	2.36	2.76	3.10	0.352	0.356	0.358
2	(A_1)	1.16	1.24	1.42	0.173	0.160	0.164
	(A_2)	2.94	3.38	3.78	0.439	0.436	0.437
	(D_2)	3.96	4.56	5.08	0.590	0.588	0.588
3	(D_1)	2.30	2.68	2.96	0.343	0.346	0.342
	(B) at 2.15 V	4.40	5.04	5.60	0.657	0.651	0.648
	(B) at 2.45	2.98	3.44	3.86	0.444	0.444	0.446
	(B) at 2.55	2.68	3.08	3.40	0.400	0.397	0.393
	(D_2)	3.78	4.36	4.86	0.564	0.562	0.562
4	(A)	0.36	0.39	0.42	0.054	0.052	0.049
	(B_1)	0.90	1.02	1.10	0.134	0.131	0.127
	(B_2)	1.82	2.12	2.36	0.272	0.274	0.273
5	(B_1)	0.24	0.31	0.38	0.036	0.040	0.044
	(B_2)	4.52	5.20	5.82	0.673	0.672	0.673

* 1. 0.6 mM 6-chloroquinoline in 100% DMF.
2. 1 mM 6-chloroquinoline in 100% DMF containing 5 mM phenol.
3. In a solution of water content 2%.
4. 1 mM 6-chloroquinoline and 0.21 mM $HClO_4$ in 60% water content.
5. 2 mM 6-chloroquinoline in 90% water content.

(above a concentration of 0.5 mM of acid to 1 mM of 6-chloroquinoline) at the expense of wave (B_2). Finally, only wave (A) is present when excess perchloric acid is present (curve e). When the addition of perchloric acid exceeds 0.5 mM, wave (A) is divided into two waves, and the height of the former wave is constant and independent of any further addition of perchloric acid.

The relationship between the wave heights, and $E_{\frac{1}{2}}$ and the concentration of 6-chloroquinoline are shown in Fig. 7, in the absence of water, and at a water concentration of 90%. Wave heights of (D_1), (B) and (C) in 100% DMF solution and the total wave height in 90% water are all directly proportional to the concentration, whereas the plot of the wave height of (B_1) in 90% water was in the shape of an adsorption isotherm. The effect of the mercury pressure, h, on the wave height of (B_1) was examined and tabulated in Table 1. As the $ih^{-\frac{1}{2}}$-values increase with increase of mercury pressure, wave (B_1) in 90% water includes some adsorption phenomena (Expt. No. 5 of the Table). On the contrary, for wave (A), the fact that the $ih^{-\frac{1}{2}}$-values decrease with increasing mecury pressure (Expt. No. 4) indicates that the electrode reaction is of a kinetic nature. The behaviour of waves (A) and (B_1) can be interpreted as for the case of quinoline discussed previously[1].

The data in the Table indicate that the limiting current of other waves is controlled by diffusion.

DISCUSSION

I. Electrolytic reduction of 6-chloroquinoline in DMF

The polarogram of a solution of 6-chloroquinoline in 100% DMF consists of three well-defined waves, the overall wave height corresponding to a four-electron transfer. This is very different from the behaviour of quinoline and 8-hydroxyquinoline. Quinoline[1] gave a polarogram consisting of two waves; the reversible first wave increased at the expence of the irreversible second wave with increase of water content, and, in solutions containing more than 1% of water, only the first wave remained. 8-Hydroxyquinoline[5], also, is reduced in two one-electron steps independent of the water content.

From the results obtained with quinoline and 6-chloroquinoline, the electrolytic reduction of 6-chloroquinoline in DMF at the dropping mercury electrode was assumed to take place according to the following mechanisms:

For wave (D_1):

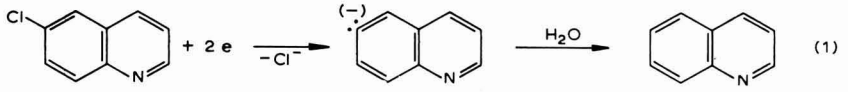

For wave (B):

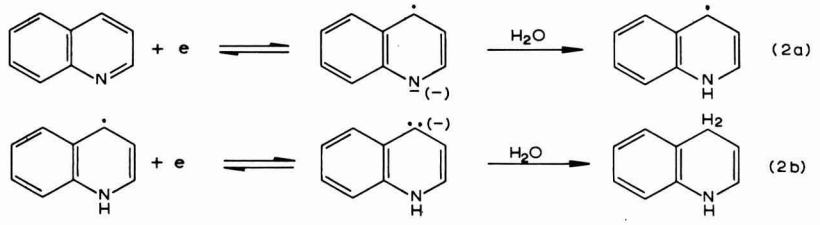

For wave (C):

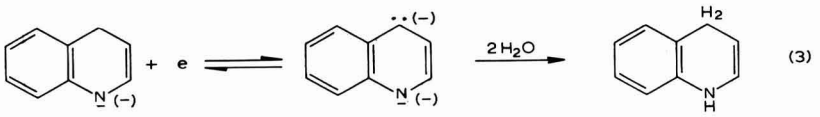

The half-wave potential of wave (B) is perfectly consistent with that of the first wave of quinoline (both 2.13 V *vs.* S.C.E.) and that of wave (C) also coincides with the half-wave potential of the second wave of quinoline (2.55 and 2.60 V). The fact that, with increasing water, wave (B) increases in height at the expense of wave (C) and only wave (B) remains in solutions containing more than 1% of water, suggests strongly that the electrode reactions of waves (B) and (C) correspond to those of quinoline[1] (eqns. (2a), (2b) and (3)). Since the dehalogenation reaction in a non-aqueous solvent is usually much easier than in an aqueous solvent[3], it can be concluded that the first wave (D_1) (eqn. (1)) appearing at -1.8 V, corresponds to the dechlorination of 6-chloroquinoline (*cf.* Ref. 1.)

It may be expected, on the basis of the above scheme, that the ratio of the wave heights of (D_1), (B) and (C) is 2:1:1, respectively. It can be seen from Figs. 2 and 3, however, that wave (B) is a little higher than wave (C) in 100% DMF solution. This extra height can be attributed to the occurrence of reaction (2b) in the presence of trace amounts of water (about 20 mM) that could hardly be eliminated even by the most careful preparations.

The quantitative effect of water on waves (B) and (C) has been discussed in a previous paper[1].

II. Effect of phenol

When phenol is added to a solution of 6-chloroquinoline in DMF, a new wave (A_1) appears at a potential 0.35 V more positive than that of wave (B). Wave (A_1) increases at the expense of waves (D_1), (B) and (C) with increase in phenol concentration, and its height corresponds finally to approximately a one-electron transfer in the presence of concentrations of phenol greater than 5 mM (Figs. 4 and 5).

In the case of quinoline[1], two waves, (A_1) and (A_2), appear at potentials 0.36 V and 0.13 V, respectively, more positive than that of the first wave and, finally, two one-electron reduction waves remain after the complete disappearance of the original two waves. Therefore, it is to be expected, in the case of 6-chloroquinoline also, that two waves, (A_1) and (A_2), will appear, but that wave (A_2) might overlap wave (D_1). Thus, the apparent wave (D_1) includes the component of wave (A_2) of equivalent height to wave (A_1). When excess phenol is present, wave (D_1) disappears, although the apparent wave remains (see Fig. 5).

If the reaction at waves (A_1) and (A_2) is assumed to be the same as in the case of quinoline[1], the following mechanism is proposed.

For wave (A_1):

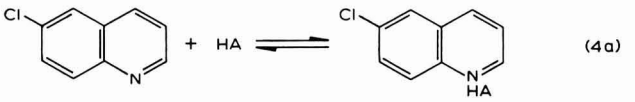

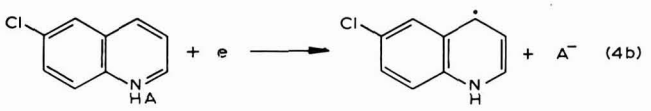

(4b)

For wave (A_2):

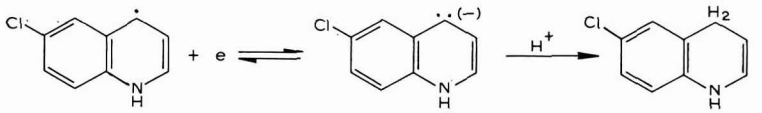

(5)

Since the total wave height at the potential of wave (C) decreases to practically one-half of its original value with increasing phenol concentration, it can be expected that the electrolytic reduction proceeds to the formation of 6-chloro-1,4-dihydroquinoline as shown by eqns. (4a)–(5) and does not include the dechlorination process which occurs at a more negative potential (wave D_2). The dechlorination of dihydrochloroquinoline, formed in the presence of phenol or other proton donors, is much more difficult than that of the original chloroquinoline. The extreme easiness of dechlorination of 6-chloroquinoline might be due to the presence of resonance between Cl and N atoms as shown below.

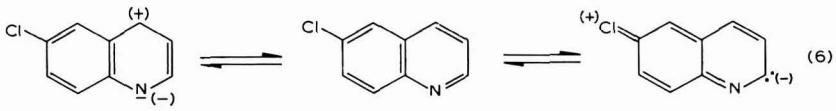

(6)

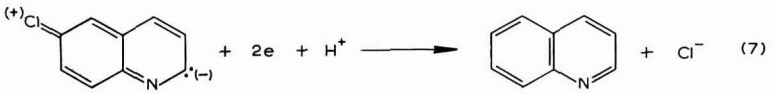

(7)

In conclusion, in the presence of large amount of phenol, two one-electron reduction waves, (A_1) and (A_2), appear, followed by the two-electron reduction wave, (D_2). Therefore, the total wave height at the potential of wave (D_2) corresponds to a four-electron reduction independent of the presence or absence of phenol, see Fig. 5.

III. Effect of water

The effect of the addition of a small amount of water closely resembles that of the addition of phenol. With increase in water content, the total wave height at wave (D_2) remains constant (corresponding to a four-electron reduction), but the height at wave (C) or (B) decreases, although the height at wave (D_1) remains constant. This, together with the surprising fact that the limiting current decreases with increasing cathode potential (curve d in Fig. 2), indicates the following reaction mechanism. For wave (B):

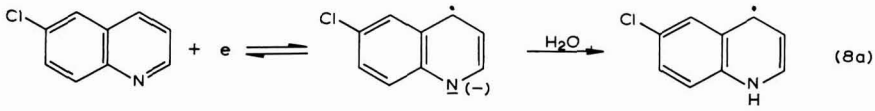

(8a)

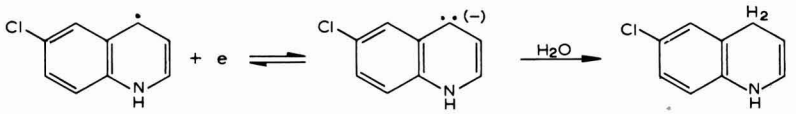

For wave (C):

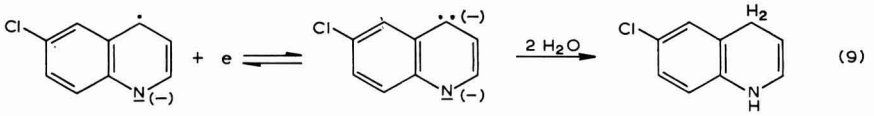

For wave (D_2):

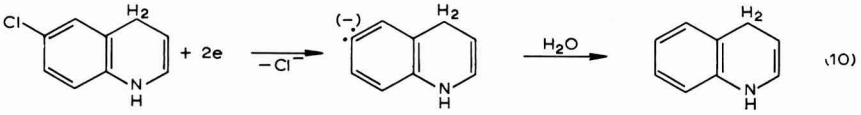

As mentioned previously, in 100% DMF the electrode reactions correspond to eqns. (1), (2) and (3). With increasing water content, wave (B) (eqn. (8)) shifts to more positive potentials, the potential finally exceeding that of wave (D_1) (eqn. (1)) in solutions of water content above 5%. Therefore, with solutions of intermediate water content, first, reaction (1) takes place and then, with increase in negative potential, it is gradually replaced by reactions (8a) and (8b), because reaction (8) is more rapid than reaction (1) (*cf.* Ref. 2). Once the former reaction has proceeded, the reaction product, hydrogenated chloroquinoline, is stabilized and the dechlorination wave (D_2) appears at about -2.6 V, instead of (D_1) (see Section II). Therefore, as is shown in Fig. 8, the unusual drop in the limiting current is observed in wave (B). It is apparent from the mechanism proposed above that the current at the minimum never falls below that of a two-electron reduction. The limiting current at any potential of the descending portion has been proved to be diffusion-controlled, see Expt. No. 3 in Table 1.

When the solution contains 10% of water, wave (D_1) is completely replaced by wave (B), followed by wave (D_2).

With solutions of water content greater than 20%, the final electrolyte discharge interferes with the observation of wave (D_2). The electrode reaction in this case can be represented as follows, as in the case of quinoline[1].

For wave (B_1):

$$R + e \rightleftharpoons \dot{R}^- \quad (R: \text{6-chloroquinoline}) \tag{11a}$$

$$\dot{R}^- + H_2O \rightarrow \dot{R}H + OH^- \tag{11b}$$

$$\dot{R}H + e \rightleftharpoons RH^- \tag{11c}$$

$$RH^- + \underset{\cdot}{R} \rightarrow RRH^- \tag{11d}$$

For wave (B_2):

$$RRH^- + 2\,e + 3\,H_2O \rightarrow 2\,RH_2 + 3\,OH^- \tag{12}$$

The scheme of eqns. (11) and (12) is also supported by the experiments using the

addition of perchloric acid (Fig. 6). The behaviour resembles that of quinoline. Hence, the electrode reaction is given by:
For wave (A):

$$R + H^+ \rightarrow RH^+ \quad (13a)$$

$$RH^+ + e \rightleftharpoons \dot{R}H \quad (13b)$$

$$\dot{R}H + e \rightleftharpoons RH^- \quad (13c)$$

$$RH^- + R \rightarrow RRH^- \quad (13d)$$

Since the electro-active dimer, RRH^-, thus formed, behaves similarly to that produced according to eqn. (11d), the total polarographic processes can be fully explained using eqns. (13), (11) and (12).

Wave (A) divides into two waves in the presence of concentrations of perchloric acid greater than 0.5 mM, as shown in Fig. 6. This phenomenon was investigated by changing the concentration of 6-chloroquinolinium cation, RH^+, prepared with equimolar $HClO_4$ and chloroquinoline. The result is shown in Fig. 9. As the phenomenon

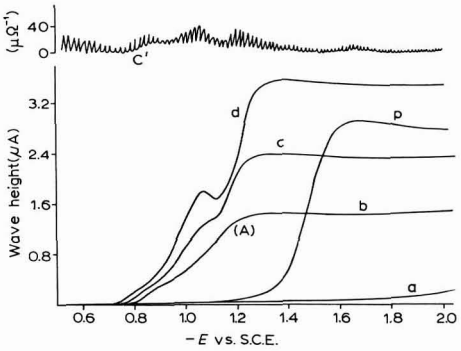

Fig. 9. Polarograms of 6-chloroquinolinum cation in 60% water content. Concn. RH^+: (b), 0.6; (c, c'), 1.0; (d), 1.5 mM; (a), residual current; (p), 1 mM $HClO_4$ only.

is not seen at concentrations below 0.6 mM (curve b) and the kink is more pronounced at concentrations greater than 1 mM (curve d), it can be ascribed to the adsorption of RH^- (or RH_2, chlorodihydroquinoline) at the electrode surface, similar to the abnormal depression in the height of wave (B_1) in solutions containing more than 80% of water.

Ref. 1

The controlled-potential electrolysis of a solution of 6-chloroquinoline in DMF containing 0.1 M NEt_4ClO_4 was carried out at a stirred mercury cathode separated by a sintered-glass disk from a spiral platinum anode. The set potential was chosen as the potential corresponding to the top of wave (D_1) (−2.0 V *vs.* S.C.E.) with the Yanagimoto Controlled-Potential Electrolyser Model VE-3.

The number of electrons transferred at wave (D_1) is two. The amount of chloride ion produced, determined by the mercurous nitrate–diphenylcarbazone method[4], corresponds to 85% equivalent on the basis of the 2-electron change.

Ref. 2

The reaction processes can be explained on the basis of the following two competitive reactions:

$$R + 2\,e \underset{}{\overset{k_1'}{\rightleftarrows}} Q^-Cl^- \xrightarrow[H_2O]{k_1''} QH + Cl^- \quad (14)$$

$$R + 2\,e \underset{}{\overset{k_2'}{\rightleftarrows}} R^{2-} \xrightarrow[2H_2O]{k_2''} RH_2 \quad (15)$$

where R, QH and RH_2 denote 6-chloroquinoline, quinoline and 6-chloro-dihydroquinoline, respectively, and k_i is the rate constant. When a voltage, E, is applied

$$\vec{k}_1' = k_{01} \exp(-\alpha_1 nFE/RT) \quad (16)$$

$$\vec{k}_2' = k_{02} \exp(-\alpha_2 nFE/RT) \quad (17)$$

where k_{01} is the rate constant in the solution at $E = 0$, and α_i is the transfer coefficient. Since reaction (14) is less reversible than reaction (15) (see curve b' in Fig. 2) it follows that $\alpha_1 < \alpha_2$. Therefore $\vec{k}_2'$ increases more rapidly than $\vec{k}_1'$ with increase of E, and since $\vec{k}_1' > \vec{k}_2'$ at about $E_{1\frac{1}{2}}$ this could be reversed at more negative potentials making $\vec{k}_1' < \vec{k}_2'$ at about $E_{2\frac{1}{2}}$.

Thus, reaction (14) takes place at $E_{1\frac{1}{2}}$ and reaction (15) is predominant at $E_{2\frac{1}{2}}$. The fact that reaction (14) is replaced by reaction (15) with increase of water, can be explained by the rapid shift in the reduction potential of the pyridine ring to more positive potentials (see Fig. 3).

ACKNOWLEDGEMENT

This work was partly supported by a grant from the Scientific Research Expenditure Department of the Ministry of Education for which the authors are grateful.

SUMMARY

The polarographic behavior of 6-chloroquinoline in DMF solutions containing 0–90% water, and the effects of phenol and perchloric acid indicate the following mechanism for the reduction of 6-chloroquinoline at the dropping mercury electrode (the reactions are arranged in order of half-wave potentials).

In the presence of less than 20% of water:

Wave (A_1) $R + HA \rightarrow RHA + e \rightarrow \dot{R}H$ (when phenol is added).

Wave (A_2) $\dot{R}H + e \rightleftharpoons RH^- + H_2O \rightarrow RH_2$ (when phenol is added).

Wave (D_1) $R + 2\,e \rightarrow Q^- + H_2O \rightarrow QH$ (water content $< 5\%$).

Wave (B) $QH + e \rightleftharpoons \dot{Q}H^- + H_2O \rightarrow \dot{Q}H_2 + e \rightleftharpoons QH_2^- + H_2O \rightarrow QH_3$, and $R + e \rightleftharpoons \dot{R}^- + H_2O \rightarrow \dot{R}H + e \rightleftharpoons RH^- + H_2O \rightarrow RH_2$ (water content $> 0.4\%$).

Wave (C) $\dot{Q}H^- + e \rightleftharpoons QH^{2-} + 2\,H_2O \rightarrow QH_3$ (water content $< 1\%$), and $\dot{R}^- + e \rightleftharpoons R^{2-} + 2\,H_2O \rightarrow RH_2$ (water content $< 1\%$),

Wave (D_2) $RH_2 + 2\,e \rightarrow QH_2^- + H_2O \rightarrow QH_3$.

In the presence of more than 20% of water:

Wave (A) $R + H^+ \rightleftharpoons RH^+ + e \rightleftharpoons \dot{R}H + e \rightleftharpoons RH^- + R \rightarrow RRH^-$ (when perchloric acid is added).

Wave (B_1) $R + e \rightleftharpoons \dot{R}^- + H_2O \rightarrow \dot{R}H + e \rightleftharpoons RH^- + R \rightarrow RRH^-$.

Wave (B_2) $RRH^- + 2\ e + 3\ H_2O \rightarrow 2\ RH_2$.

where R, RH_2, QH and QH_3 denote 6-chloroquinoline, 6-chlorodihydroquinoline, quinoline and dihydroquinoline, respectively.

REFERENCES

1 T. FUJINAGA, K. IZUTSU AND K. TAKAOKA, *J. Electroanal. Chem.*, 12 (1966) 203.
2 K. TAKAOKA, *Review of Polarography*, 14 (1966) 63.
3 T. FUJINAGA, T. ARAI AND C. KITAZAWA, *J. Chem. Soc. Japan, Pure Chem. Sect.*, 85 (1964) 811.
4 T. MATSUO, *J. Chem. Soc. Japan, Ind. Chem. Sect.*, 56 (1953) 70.
5 T. FUJINAGA, K. IZUTSU AND K. TAKAOKA, *J. Electroanal. Chem.*, 16 (1968) 89.

Elsevier Sequoia S.A., Lausanne – Printed in The Netherlands

SHORT COMMUNICATIONS

Der Einfluss eines Fremdelektrolyten auf die natürliche Konvektion bei der Oxydation der (Pd-H)-Elektrode

Die anodische Oxydation einer (Pd–H)-Elektrode entspricht dem Transport des Wasserstoffes aus der Elektrode in die Lösung in Form von Wasserstoffionen, die sich in der der Elektrode anliegenden Transportgrenzschicht anhäufen. In einer Säurelösung führt die Anhäufung der Wasserstoffionen zu einer Erhöhung der Säurekonzentration in der Transportgrenzschicht, denn zur Bewahrung der elektrischen Neutralität werden durch Ionenwanderung Anionen an die Elektrode herantransportiert. In diesem Fall findet der Stofftransport in der Grenzschichte durch Diffusion und Ionenwanderung statt. Ist der Konzentrationsunterschied, bzw. der Dichteunterschied, zwischen der Grenzschichte und der Masse der Lösung gross, so tritt eine natürliche, absteigende Konvektion auf, die zusätzlich zum Stofftransport beiträgt.

Der Zusatz eines Fremdelektrolyten, in Überschuss gegenüber der Säurekonzentration, kann durch eine entsprechende Änderung der Dichte der Lösung in der Elektrodennähe zu einer Umkehrung der Konvektionsrichtung führen, wobei diese aufsteigend wird.

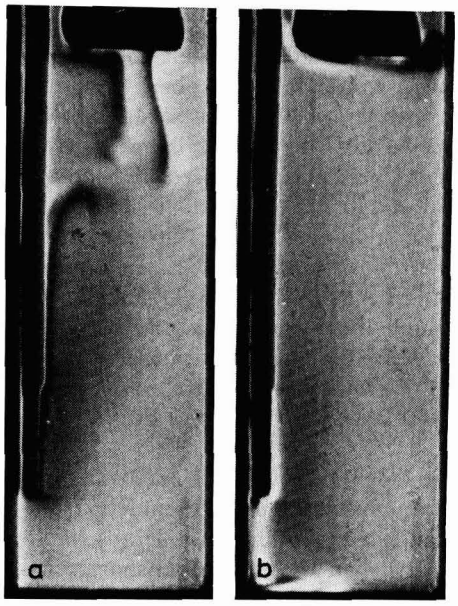

Abb. 1. Schlierenaufnahmen der Konvektion bei der Oxydation der (Pd–H)-Elektrode, 45 sec nach Beginn der Elektrolyse, für $I_{cc}=5$mA cm^{-2}, $T=24.6°$. (a) H_2SO_4 0.01 M; (b) H_2SO_4 0.01 M + K_2SO_4 0.6 M.

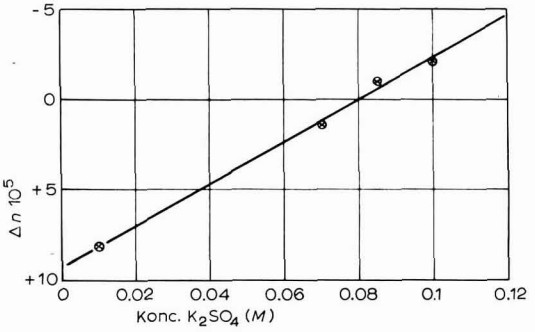

Abb. 2. Änderung der Differenz des Brechungsindexes mit der K_2SO_4-Konzentration in einer H_2SO_4 0.01 M-Lösung 10 Minuten nach Beginn der Elektrolyse, für $I_{cc}=5$ mA cm^{-2}, $T=24.6°$.

Diese zwei Möglichkeiten sind in Abb. 1 im Falle einer H_2SO_4 0.01 M-Lösung und einer H_2SO_4 0.01 M + K_2SO_4 0.6 M-Lösung durch Fotografien veranschaulicht. Die Bilder wurden mit einem Schlierenaufnahmegerät Typ 80 der Firma Carl Zeiss Jena aufgenommen[1], die Foucaultsche Schneide war dabei senkrecht.

Die 10 × 20 × 2 mm grosse (Pd–H)-Anode war mit der Phasengrenze nach unten gerichtet und hatte alle andern Flächen durch Apiezonwachs W isoliert. Die Kathode bestand aus einem 1 mm dicken, senkrechtstehenden Palladiumdraht. Dieser war seitlich von der Anode untergebracht, und bis auf 15 mm vom Ende ebenfalls isoliert, um durch Konvektionsströme den Stofftransport in der Anodennähe nicht zu stören, denn bedingt durch die Symmetrie der Elektrodenprozesse, findet an den zwei Elektroden die Konvektion in entgegengesetzter Richtung statt. Die anodische Oxydation wurde in beiden Fällen bei 24.6°, mit einem konstanten Strom I_{cc} = 5 mA cm^{-2} durchgeführt; die Bilder wurden 45 sec nach Beginn der Elektrolyse aufgenommen.

Die Umkehrung der Konvektionsrichtung ist auf das Vorhandensein der K^+-Ionen zurückzuführen. In der Transportgrenzschichte an der Anode steigt die Dichte der Lösung infolge der Anhäufung der H^+-Ionen weniger an als sie infolge des Abtransportes der K^+-Ionen durch Ionenwanderung verringert wird. So findet global eine Verringerung der Dichte der Lösung durch die Entfernung von K_2SO_4 aus der Anodennähe statt.

Dieser Effekt ist von der Konzentration des Fremdelektrolyten abhängig. In Abb. 2 wurde die mit der Differenz der Dichte proportionelle Differenz des Brechungsindexes zwischen der Phasengrenze und dem Innern der Lösung in Abhängigkeit von der K_2SO_4-Konzentration dargestellt. Dabei wurde von der Gesamtbreite (10 mm) eine Breite von 2 mm in Betracht gezogen, die 1/3 von dem der Kathode entgegengesetzten Rand der Anode gelegen ist. Die Messung wurde mit dem oben benützten Gerät vorgenommen, wobei zur Erzeugung des Interferenzbildes des Simultaninterferenzgerät nach Rayleigh–Svensson eingesetzt wurde[2]. Aus Abb. 2 ist zu ersehen, dass durch Zunahme der K_2SO_4-Konzentration der Unterschied des Brechungsindexes das Vorzeichen ändert. Für die Werte $\Delta n < 0$ ist an der Phasengrenze die Dichte der Lösung kleiner als im Innern der Lösung und es entsteht eine Aufwärtsströmung; bei $\Delta n > 0$ dagegen ist es umgekehrt und die Konvektion ist absteigend. Einer Konzentration von 0.08 M K_2SO_4 entspricht $\Delta n = 0$; hier hört die Konvektion auf und der Transport in der Lösung geht ausschliesslich durch Ionenwanderung und Diffusion vor sich, da die Bedingung $\Delta n = 0$ für bestimmte Werte der Konzentrationsgradienten der H^+-, K^+- und SO_4^{2-}-Ionen verwirklicht wird. Es muss noch betont werden, dass der Wert der K_2SO_4-Konzentration für den $\Delta n = 0$ Wert von der Dichte des Anodenstromes abhängig ist.

Aus diesen geht hervor, dass in dem untersuchten Fall die Umkehrung der Dichteänderung der Lösung in der Anodennähe durch Zusatz eines Fremdelektrolyten zur Änderung des Transportmechanismus der Substanz führt. Zur Veranschaulichung dieser Tatsache wurde die Änderung der örtlichen Dicke der Transportgrenzschichte gegen die Dichte des Anodenstromes aufgetragen (Abb. 3), wobei die Dicke δ_L interferometrisch bei 24.6° in H_2SO_4 0.01 M- und H_2SO_4 0.01 M + K_2SO_4 0.6 M-Lösung, 10 Minuten nach Beginn der Elektrolyse bestimmt wurde. Es ist ersichtlich, dass in der H_2SO_4-Lösung, wegen der Anhäufung der Säure in der Anodennähe, δ_L mit steigender Stromdichte zunimmt und bei I_{cc} = 2mA cm^{-2} einen Grenzwert von

$\delta_L = 0.803$ mm erreicht. Schlierenaufnahmen haben gezeigt, dass für Stromdichten unter diesem Wert die absteigende Konvektion stabil ist, während sie für höhere Stromdichten unstabil wird und δ_L auf den gegebenen Wert begrenzt. In der H_2SO_4 0.01 M + K_2SO_4 0.6 M-Lösung dagegen wird die Lösung in der Anodennähe an Elektrolyten verdünnt, die aufsteigende Konvektion findet senkrecht zur Elektroden-

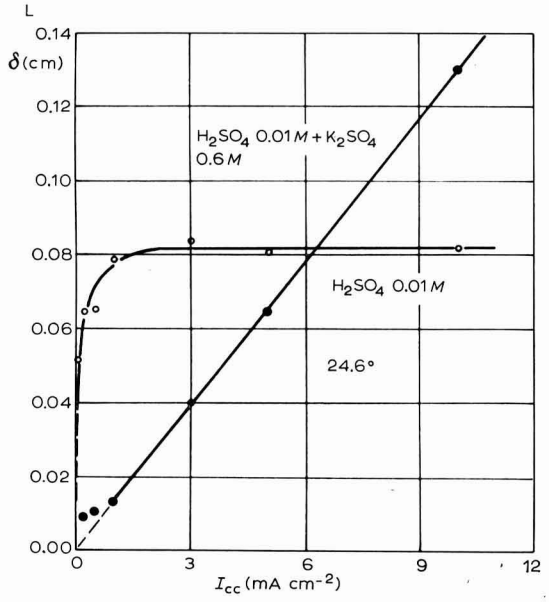

Abb. 3. Abhängigkeit der örtlichen Dicke δ der Transportgrenzschichte von der Stromdichte bei 24.6°. (a) H_2SO_4 0.01 M; (b) H_2SO_4 0.01 M + K_2SO_4 0.6 M.

oberfläche und ausserhalb ihres Querschnittes statt. Dadurch kann die Dicke δ_L mit wachsender Stromdichte stetig wachsen und weist in dem untersuchten Gebiet eine lineare Abhängigkeit auf. In diesem Fall findet der globale Transport des Elektrolyten von der Anode zur Kathode ausschliesslich durch Diffusion und Ionenwanderung statt.

Wir danken Herrn V. MORARU für die bei den Messungen gegebene Hilfe.

Institut für Atomphysik,
Sektion Cluj (Rumänien)

R. V. BUCUR
JUDITH MERCEA

1 W. NEBE, *Jenaer Rundschau*, 3 (1958) 108.
2 W. NEBE, *Jenaer Rundschau*, 5 (1960) 74.

Eingegangen am 17. März 1967, reviziert 1. Mai 1967.

Polarography of inorganic substances in dimethylformamide

In a recent paper, McMASTERS and co-workers[2] have reported half-wave potentials and reversibility data for eleven inorganic species in dimethylformamide, and have summarised the results of earlier work on inorganic compounds in this solvent. Quite independently of McMASTERS, we have also been making a more thorough study of this solvent than has hitherto been done, and the results and discussions of our observations on twenty-six inorganic species in dimethylformamide are now reported.

Experimental

Dimethylformamide was purified in the following way: It was allowed to stand overnight over anhydrous potassium carbonate and then distilled *in vacuo* from the solid. It was then kept overnight over calcium hydride, refluxed for 3 h over this solid at atmospheric pressure, and distilled *in vacuo* from the solid. The first quarter of the distillate was rejected as it contained an amine impurity which complexed with certain transition-metal ions. The water content of the dimethylformamide was less than $3 \cdot 10^{-3}$ *M*, as determined by Karl Fischer titration.

Potassium, magnesium and barium perchlorates were obtained from B.D.H. Ltd. and dried in a vacuum oven at 100°. Other perchlorates were prepared by well-established methods and dried *in vacuo* at room temperature. The amalgams were also prepared by orthodox methods.

All solutions were prepared and added to the polarographic cell in a glove-box. The concentrations of all electroactive ions in the solutions studied were approx. $5 \cdot 10^{-4}$ *M*. The concentration of ferrocene was approx. $2 \cdot 10^{-4}$ *M*. The concentrations of the amalgams were approximately as follows: indium $5 \cdot 10^{-5}$ *M*; bismuth, and gallium $2 \cdot 10^{-4}$ *M*; thallium $4 \cdot 10^{-4}$ *M*; and cadmium, lead and zinc, 10^{-3} *M*.

All potentials are referred to the silver–silver chloride–saturated tetraethylammonium chloride reference electrode. $E_{\frac{1}{4}}$-, $E_{\frac{1}{2}}$- and $E_{\frac{3}{4}}$-values are corrected for potential drop across the cell.

Base electrolytes—0.1*M* solutions of sodium and tetraethylammonium perchlorate—were prepared by dissolving the respective salts in dimethylformamide. Sodium perchlorate was prepared from sodium carbonate and perchloric acid (both of analytical-reagent grade) recrystallised from water, and dried at 200°. Tetraethylammonium perchlorate was obtained from Eastman Kodak and dried in a vacuum oven at 60°.

Apparatus

A Sargent model XV d.c. recording polarograph was used.

A Meites-type H-cell was employed. The reference electrode was a sheet of silver (2 cm × 5 cm) coated with silver chloride and immersed in dimethylformamide saturated with silver chloride, tetraethylammonium chloride and methyl cellulose. The horizontal cross-arm contained a gel of 25% (w/v) tetraethylammonium perchlorate in dimethylformamide containing 5% (w/v) of methyl cellulose. The solution compartment was fitted with a sintered-glass dispersion tube for bubbling dry, oxygen-free nitrogen through the dimethylformamide solutions.

The cell was immersed in a bath of water, the temperature of which was thermostatically controlled at 25.0°. The resistance of the cell was 500 Ω and 750 Ω with

0.1 *M* sodium perchlorate and 0.1 *M* tetraethylammonium perchlorate in the solution compartment, respectively.

Results

Polarographic data for the inorganic species in dimethylformamide are given in Table 1.

The polarographic range using 0.1 *M* sodium perchlorate and 0.1 *M* tetraethyl-

TABLE 1

Species	*Base electrolyte (0.1 M)*	$E_{\frac{1}{2}}(V)$	$E_{\frac{1}{4}}-E_{\frac{3}{4}}(mV)$
Ferrocene*	$NaClO_4$	+0.88	−65 R
Copper(II)	$NaClO_4$	+0.41	33 R
Bismuth amalgam	$NaClO_4$	+0.38	−114
Indium amalgam	$NaClO_4$	+0.03	−32
Lead amalgam	$NaClO_4$	−0.03	−32 R
Lead(II)	Et_4NClO_4	−0.03	40
Thallium amalgam	$NaClO_4$	−0.07	−63 R
Thallium(I)	$NaClO_4$	−0.07	60 R
Cadmium(II)	Et_4NClO_4	−0.17	33 R
Cadmium amalgam	$NaClO_4$	−0.17	−28 R
Gallium amalgam	$NaClO_4$	−0.37	−27
Cobalticinium ion	$NaClO_4$	−0.47	55 R
Nickel(II)	$NaClO_4$	−0.53	64
Zinc(II)	Et_4NClO_4	−0.59	38
Zinc amalgam	$NaClO_4$	−0.59	−30 R
Cobalt(II)	$NaClO_4$	−0.81	89
Manganese(II)	Et_4NClO_4	−1.12	34 R
Barium(II)	Et_4NClO_4	−1.62	33 R
Sodium(I)	Et_4NClO_4	−1.63	54 R
Caesium(I)	Et_4NClO_4	−1.62	57 R
Rubidium(I)	Et_4NClO_4	−1.65	55 R
Potassium(I)	Et_4NClO_4	−1.67	54 R
Strontium(II)	Et_4NClO_4	−1.80	44
Lithium(I)	Et_4NClO_4	−1.92	66 R
Calcium(II)	Et_4NClO_4	−1.95	45
Magnesium(II)	Et_4NClO_4	−2.05	105

* Voltammetry with a rotating platinum electrode.
R Reversible wave. A wave was considered to be reversible if $E_{\frac{1}{4}}-E_{\frac{3}{4}}$ lay within $\pm (56 \pm 14)/n$ mV.

ammonium perchlorate as base electrolytes was + 0.8 V to −1.5 V and + 0.8 V to −2.4 V *vs.* the reference electrode, respectively. The voltammetric range using 0.1 *M* sodium perchlorate as base electrolyte was + 2.1 to −1.5 V *vs.* the reference electrode.

Discussion

These polarographic data were required by the authors for the compilation of a detailed list of formal electrode potentials in 0.1 *M* perchlorate solutions of various non-aqueous solvents, to aid them in their selection of the best solvents for the stabilisation of ions of unusual lower oxidation states such as indium(I) and thulium(II). This work will be reported later, but, in the meanwhile, it is felt that the data obtained may be of interest to analytical and physical chemists. LE GUILLANTON[1] has stated that the non-aqueous solvents most widely used for the polarographic analysis of organic compounds are acetonitrile and dimethylformamide.

Where a comparison of polarographic results can be made, our results are in reasonable agreement with those of McMASTERS *et al.*[2] and BROWN AND AL-URFALI[3], except that McMASTERS obtained two reduction waves for copper(II) while BROWN and we obtained one two-electron reduction wave. The presence of a trace of complexing agent such as chloride, which is known to form stable complexes with transition-metals ions in dimethylformamide[4], could explain the second copper(II) wave on McMASTERS' polarogram. The order of the oxidations and reductions is similar to that for aqueous solutions.

The application of dropping amalgam electrodes in dimethylformamide has supplied useful information, the oxidation waves for lead, thallium, cadmium and zinc amalgams being reversible in 0.1 *M* sodium perchlorate base electrolyte. Dropping amalgam electrodes should be of particular value for obtaining formal electrode potentials in solvents of low solvating ability, where the polarographic reduction of hydrated perchlorates is to be avoided if possible, since water is a complexing agent in such solvents.

Acknowledgement

We are indebted to Mr. I. R. GAULT of this department for the data on ferrocene.

Department of Chemistry,
The University,
Sheffield 10 (England)

J. B. HEADRIDGE
M. ASHRAF
H. L. H. DODDS*

1 G. LE GUILLANTON, *Bull. Soc. Chim. France*, (1963) 2359.
2 D. L. McMASTERS, R. B. DUNLAP, J. R. KUEMPEL, L. W. KREIDER AND T. R. SHEARER, *Anal. Chem.*, 39 (1967) 103.
3 G. H. BROWN AND R. AL-URFALI, *J. Am. Chem. Soc.*, 80 (1958) 2113.
4 A. CIANA AND C. FURLANI, *Electrochim. Acta*, 10 (1965) 1149.

Received April 13th, 1967

* (in part)

Differential capacitance measurements with the dropping mercury electrode in solutions of low conductivity

Introduction

A method was recently described[1] for the measurement of double-layer differential capacities in media of low conductivity. Measurement involves the determination of the change of potential of a hanging mercury drop electrode caused by injection of a known charge under coulostatic conditions. This technique is adapted here to the dropping mercury electrode to eliminate, or at least greatly minimize,

errors resulting from electrode contamination by traces of adsorbable impurities. The modification required the addition of a compensating circuit and also limited application to cells having a resistance not exceeding 1 MΩ.

Experimental

Instrument for coulostatic charging. A schematic representation of the electrical system is shown in Fig. 1. The dropping mercury electrode (DME) was polarized

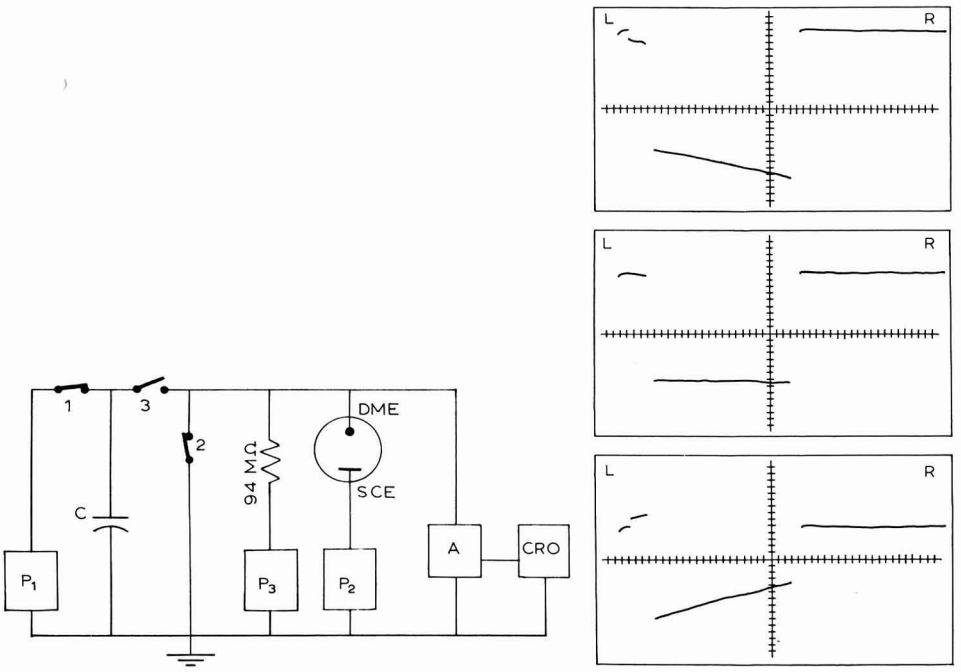

Fig. 1. Schematic circuit.

Fig. 2. Typical oscilloscope traces observed with various settings of compensating current for 10^{-3} *M* sodium fluoride at a potential of −0.8 V *vs.* SCE. Charging capacitor: 0.001 μF charged at 3 V. Ordinate scale, 2.4 mV/square; abscissa scale, 20 msec/square (1 square = 5 divisions). Compensating current: top (undercompensation), 3.9×10^{-8} A; middle (correct compensation), 4.9×10^{-8}; bottom (overcompensation), 6.25×10^{-8} A. Note that the step-variation of potential upon charge injection (to the left) is the same for the three traces. Read from left to right.

with respect to the reference electrode (SCE) by means of a continuously variable potentiometer (P_2). A coulostatic pulse was furnished to the DME by discharge of the precision capacitor C (General Radio 505), which had been charged to a measured potential (typically, 3 V) by the voltage source, P_1. Values of C ranged from 200–2000 pF, and were selected in such a way as to result in a voltage increment at the DME of the order of 5–10 mV. This increment was measured by the differential electrometer amplifier A (Keithley 603) with readout observed on the storage oscilloscope CRO (Tektronix 549 with 1A7 plug-in unit).

The shielded relays 1, 2 and 3 (Clare HG 1035) were actuated by the same pulse generator (Tektronix 160A, 161 and 162) that triggered the hammer used to dislodge a drop from the DME. Since this pulse generator could not provide sufficient current to drive all three relays, the pulse actuated another relay which connected the three relays to a 45-V dry-cell battery. Similarly, the hammer (Clare #39 E.C.) was actually driven by a pulse from a 180-V dry-cell which was switched by means of a fifth relay actuated by the pulse generator. This provided a more positive knock by the hammer, insuring the removal of a drop each time the hammer struck.

It was essential that switches 1 and 2 were fully opened prior to the closing of switch 3. To accomplish this, the coils of the three switches were connected in parallel, and a variable resistor was placed in series with the coil of switch 3. Thus, the larger current passing through coils 1 and 2 caused these switches to open slightly before switch 3 was closed. A resistance of 1000 Ω was sufficient to provide a delay of approximately 10 msec between the opening of switches 1 and 2 and the closing of switch 3.

The continuously variable potential source P_3 (0–20 V) provided a constant current to the DME to maintain the potential of the growing mercury drop constant on open circuit for at least 0.1 sec after the opening of relay 2. This current was the algebraic sum of any spurious faradaic current and the double-layer charging current. The latter was nearly constant during at least 0.1 sec when relay 2 was opened a few seconds after the beginning of drop life. The proper compensating current was easily adjusted by trial and error until a horizontal trace was observed (Fig. 2).

The ohmic drop across the cell was determined from the compensating current and the cell resistance. The compensating current was computed from the ohmic drop as measured by means of a differential voltmeter (Fluke 825A), across the 94 ± 1 MΩ resistor. The cell resistance was measured with a conventional bridge (General Radio 1650A).

The high value (94 MΩ) of the resistance in the compensating circuit insured minimal loss of the coulostatic pulse through this resistor, but to eliminate this as a possible source of error, a calibration procedure was used wherein a series of precision capacitors (General Radio 505) were substituted for the electrochemical cell and, with potentiometers P_2 and P_3 set at 0, the scope trace "jump" corresponding to each capacitor was measured. A plot of trace height *versus* dummy cell capacitance was then made, and subsequent electrochemical measurements were then referred to this graph. Such a procedure also eliminated the capacitance of electrical leads, etc., as a possible source of error, since the same leads were used in connecting the dummy cell and actual cell to the instrument.

Switches 1, 2 and 3 were kept activated for a period of 100 msec by the pulse generator. Readings on the oscilloscope (time base, 20 msec/cm) were taken some 20 msec after the pulse and extrapolated back to the time at which the pulse was applied. This was necessary to eliminate the temporary overloading of the amplifier and also because of the relatively slow discharge of the pulsing capacitor. The latter factor became critically important for solutions of very high resistance (greater than 3 MΩ). Hum pick-up was minimized by enclosing the instrument in a grounded steel cage.

Cell. The cell was constructed entirely from Pyrex and consisted of three compartments separated by fritted disks of fine porosity. Each was filled with the solution being studied and was then de-aerated by bubbling N_2 through the solution

for at least 20 min. The N_2 was purified in the usual way by passing it through a solution of V(III) in contact with zinc amalgam. Water bubblers were used to provide an exhaust route for the N_2 while preventing passage of air into the cell compartments. During measurements, nitrogen was passed over the solution in compartment 1 and through the solution in compartments 2 and 3.

The dropping mercury electrode was inserted in the first cell compartment, and the saturated calomel reference electrode was placed in the third compartment. The calomel electrode, fitted with a fine tip, made contact with the solution in the third compartment *via* filter paper and another fritted disk. The middle compartment served only to minimize contamination of solution in the first compartment. Electrodes were placed in the solution just prior to making measurements.

The area of the mercury drop was calculated by assuming a spherical drop shape and a constant volume flow rate during the course of a run. Flow rates were

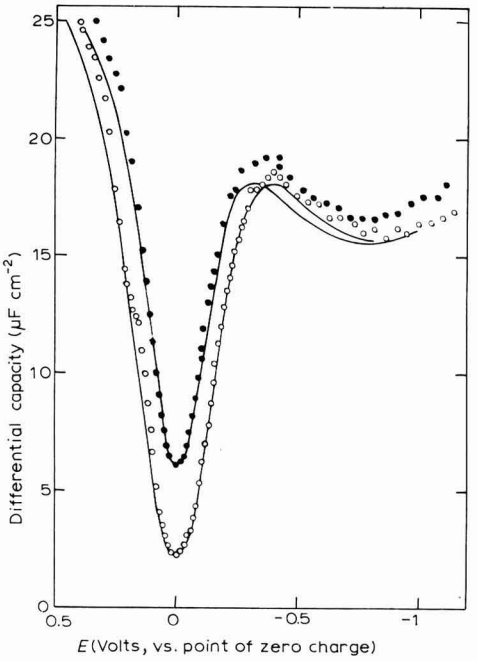

Fig. 3. Differential capacity *vs.* potential for: (●), 10^{-3} and (○), 10^{-4} *M* sodium fluoride. Points are experimental values; curves represent calcd. capacities.

measured for each run by weighing the mercury expelled over the measured time of the run. Pulsing occurred 4.00 sec after a drop was removed by the hammer.

Reagents. Solutions were prepared from Baker Analyzed Reagent sodium fluoride. Water was twice-distilled. Mercury was triple-distilled (Bethlehem Apparatus Company, Inc., Hellertown, Pennsylvania).

Results and discussion

Experimental results for 10^{-3} and 10^{-4} *M* sodium fluoride are shown in Fig. 3

and are compared with values expected on the basis of GRAHAME's data for higher concentrations. These curves were prepared as described in the earlier publication[1]. The potential of zero charge was taken to be the minimum of the capacitance–polarization curve, and occurred at -0.485 V with respect to the saturated calomel electrode (ignoring junction potentials). All data was obtained at $23 \pm 2°$. Results for 10^{-5} *M* sodium fluoride were poor because the high cell resistance prevented a sufficiently accurate extrapolation of potential–time curves to determine the potential increment resulting from charge injection.

Agreement between experimental and calculated capacities is very good in the region of the point of zero charge but is not as good at the more positive and negative potentials. The discrepancy possibly results from experimental errors, although the inadequacy of the Gouy–Chapman theory[2] cannot be excluded.

Acknowledgement

This investigation was supported by the National Science Foundation.

Department of Chemistry,
New York University,
New York 10003 (U.S.A.)

P. DELAHAY
D. J. KELSH*

1 P. DELAHAY, R. DE LEVIE AND A.-M. GIULIANI, *Electrochim. Acta*, 11 (1966) 1141.
2 H. D. HURWITZ, A. SANDFELD AND A. STEINCHEN-SANDFELD, *ibid.*, 9 (1964) 929.

Received May 8th, 1967

* On leave from Gonzaga University, Spokane, Washington.

The storage of iron samples for hydrogen analysis

In a previous paper[1] the results of the coulometric method of analysis for hydrogen absorbed in iron were shown to agree with the volume of gas evolved from iron in a nitrogen atmosphere. Since then a study has been made of the desorption of absorbed hydrogen from iron in the presence of carbon dioxide.

Experimental

The iron samples used were reagent-grade iron wires, 0.235 mm in diameter, cut to such a length that 2.0–11.0 cm would be exposed to the solutions. After being degreased in acetone, the iron wires were dipped in 6 *N* nitric acid and then rinsed with distilled water. The wire was then placed in 2 *N* sodium hydroxide solution as one electrode and a large platinum gauze was used as the other electrode. The iron wire was cathodically charged with hydrogen for 180 sec using constant currents that ranged from 0.9 mA to 0.3 A. The hydrogen on the electrode was then oxidized with a polarograph by sweeping the voltage over the range for oxidation of hydrogen. The generation of hydrogen and its oxidation were repeated until the polarographic curves

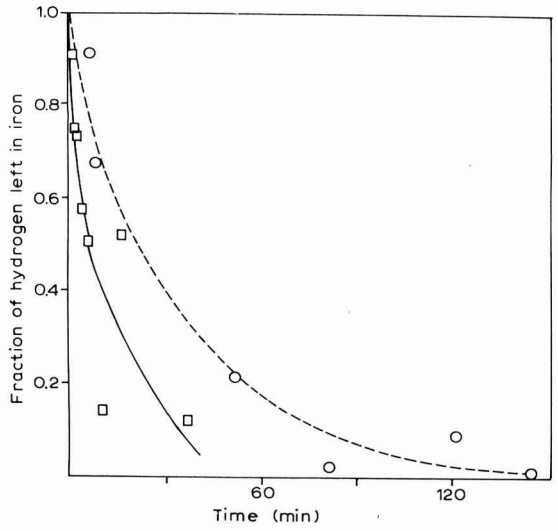

Fig. 1. The desorption of hydrogen from iron. (○), In nitrogen; (□), in air.

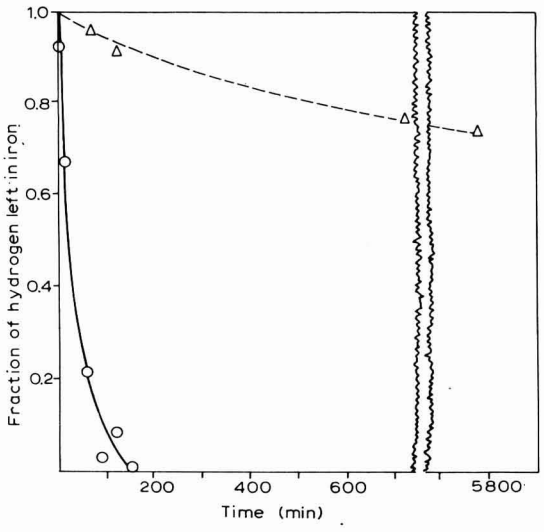

Fig. 2. The desorption of hydrogen from iron. (○), In nitrogen; (△), in carbon dioxide.

were approximately the same. As previously described[2], the area under the polarographic curve is a coulometric measure of the hydrogen adsorbed on and in iron.

The electrode was again charged with hydrogen with the same current for the same length of time. This sample was immediately transferred to a test-tube filled with either air, nitrogen or carbon dioxide. The system was flushed with the gas and sealed. After standing for varying lengths of time the sample was removed, replaced

in the polarographic cell and once more analyzed coulometrically for the amount of hydrogen remaining in the iron.

The test-tube was attached to a U-tube and levelling bulb containing mercury so that qualitative observations could be made on changes in volume of gas that might occur. The nitrogen was commercial tank nitrogen and the carbon dioxide was obtained from dry ice.

Results

Figures 1 and 2 summarize the results. The nitrogen and air curves include all of the points taken. The data taken in carbon dioxide showed a good deal of scatter and each point shown is the average of 2–6 experiments. The average deviation of the results in carbon dioxide was 177 parts/thousand.

It is obvious that the rate of removal of hydrogen from iron decreases in the order air > nitrogen ≫ carbon dioxide. The rapid removal of hydrogen in air is caused by the reaction between oxygen and the hydrogen. This reaction can be readily followed by observing the decrease in volume of air during the time of the experiment.

The removal of hydrogen in a nitrogen atmosphere involves merely the desorption of the hydrogen[1]. The removal of the hydrogen in carbon dioxide atmosphere involves also a reaction with the carbon dioxide. This is shown by a decrease in volume of carbon dioxide during the time of the experiment. The slow rate of removal of hydrogen is probably caused by a tight film of the reduction product on the surface of the iron. The existence of this film was indicated in the oxidation polarograms taken immediately after the hydrogen-saturated iron wires were removed from carbon dioxide. An oxidation wave was obtained at a potential more anodic than the hydrogen region. This probably corresponds to the reduced carbon dioxide peak observed by GINER[3] on platinum.

The data indicate that iron samples to be analyzed for mobile hydrogen are probably best stored in a carbon dioxide atmosphere. However, it should be recognized that samples stored in carbon dioxide do undergo a surface reaction.

This research has been supported by the Robert A. Welch Foundation of Houston, Texas.

Chemistry Department,
Baylor University,
Waco, Texas (U.S.A.)

THOMAS C. FRANKLIN
NELLY F. FRANKLIN

1 T. C. FRANKLIN AND N. F. FRANKLIN, *J. Electroanal. Chem.*, 8 (1964) 310.
2 F. MATSUDA AND T. C. FRANKLIN, *J. Electrochem. Soc.*, 112 (1965) 767.
3 J. GINER, *Electrochim. Acta*, 9 (1964) 63.

Received March 31st, 1967

Elsevier Sequoia S.A., Lausanne – Printed in The Netherlands

BOOK REVIEWS

Electronic Electrochemical Measuring Instruments, by D. DOBOS, Akademiai Kiado, Publishing House of the Hungarian Academy of Sciences, Budapest, 1966, 449 pages, $14.70.

This book falls into two roughly equal parts. The first is an introduction to electronic components, circuits, and applications to electrochemical measurements. The second describes some commercially-available instruments. The scope of the book illustrates by default the rapid progress of the applications of electronics to electrochemistry as well as of electronics itself. Thus, potentiostats are mentioned twice but not discussed; operational amplifiers are not mentioned; only classical polarography is discussed; field effect transistors are said to be still in development.

In Chapter 1 there is a clear, elementary description of the elements of electronic circuits, while the following chapter describes the basic circuits for amplification, oscillation, etc. In Chapter 3 these are applied to electrochemical measurements, mostly in general terms, although practical circuits are given for a vacuum tube and a transistorized voltameter for potentiometric titration, a conductance meter, a dielectric constant meter and a number of high-frequency titrator circuits. The first half of the book concludes with two short chapters on handling electronic instruments and on simple calculations; *e.g.*, calculation of cathode bias resistor.

Chapter 6, which takes up the second half of the book, is a partial trade catalogue of commercially-available instruments, each with a photograph, many with operating instructions, and a few with component lists and circuit diagrams. The principle of selection is not clear. Fifty-odd pH-meters from nine countries are included as well as automatic titrators, conductometers, oscillometric titrators, dielectrometers, and polarographs. The only East European instruments are those from Hungary. It is particularly surprising that polarographs from Czechoslovakia and the U.S.S.R. are not described. Most of the instruments are from Western Europe although a few from the United States are included. While this section of the book might be of use in selecting a suitable instrument to buy, it is not clear that anything has been added to the manufacturers' specifications which are readily obtained by a prospective purchaser and are kept up-to-date. The aim of this section of the book would have been more effectively served by a more comprehensive list of manufacturers with addresses and simply the names of the instruments made by each.

The English translation is excellent and the production of the book equally good.

ROGER PARSONS, California Institute of Technology

Advances in Magnetic Resonance, Vol. 2, edited by J. S. WAUGH, Academic Press, Inc., New York, 1966, 269 pages, 96 s.

Like its predecessor, this volume contains a mixture of experimental and theoretical articles on magnetic resonance, with a strong bias towards N.M.R. A high standard has again been achieved, and the reviews will be useful to specialists in the appropriate fields.

ERNST has contributed a long (135 pages) and general account of signal-to-noise problems in magnetic resonance; he has considered a wide variety of techniques for enhancing sensitivity. Theories of the chemical shift are developed and discussed in articles by LIPSCOMB (40 pages) and MUSHER (48 pages). These are timely since it is becoming clear, particularly through measurements of shielding anisotropies, that our understanding of chemical shifts is rudimentary. LIPSCOMB's review is principally concerned with the calculation of proton shielding constants in simple hydrides. MUSHER's is aimed at providing a "physical understanding" of chemical shifts; however, he is unconvinced of the validity of much of the work that has been done, and includes a statement that the key equation in LIPSCOMB's article has "no non-trivial character"! Finally, there is a detailed theoretical account by DEUTCH and OPPENHEIM (38 pages) of nuclear relaxation in gaseous and liquid hydrogen.

There are author and subject indexes, and a list of forthcoming articles. The series will be of the maximum usefulness to research workers in magnetic resonance only if publication is rapid and the price kept down (Vol. 2 costs over 20% more/page than Vol. 1).

A. D. BUCKINGHAM, University of Bristol

CALENDAR OF FUTURE SCIENTIFIC MEETINGS

Date	*Place*	*Subject*	*Secretary*
17–21 June, 1968	University of California, Berkeley	4th International Materials Symposium: The structure and chemistry of solid surfaces, including: lattice dynamics, scattering by surfaces, electron and neutron scattering techniques, optical and emission studies, atomic and ion beam interaction, fundamental surface reactions	Mr. C. V. PETERSON, Inorganic Materials Research Div., Lawrence Radiation Laboratory, Bld. 62, Room 205, University of California, Berkeley Calif. 94720

Vol. 16 No. 1 JOURNAL OF ELECTROANALYTICAL CHEMISTRY JANUARY 1968
AND INTERFACIAL ELECTROCHEMISTRY

CONTENTS

Countercurrent Separation Processes

by H. R. C. Pratt

Chief, Division of Chemical Engineering, C.S.I.R.O., Melbourne, Australia

6 × 9″, xxii + 537 pages, 30 tables, 173 illus., 415 lit.refs., 1967, Dfl. 95.00, £9.10.0, US$34.00

The countercurrent separation processes represent, in terms of invested capital, the most important single group of operations in the chemical and process industries. Such operations, which must be clearly distinguished from mechanical separations such as continuous countercurrent decantation and leaching, are normally restricted in the chemical engineering texts to distillation in its various forms (including azeotropic and extractive distillation), absorption and stripping, liquid-liquid extraction, and sometimes adsorption.

Since the 1940's, chemical engineers have become increasingly concerned with isotopic and other difficult separations. Furthermore, newer techniques, such as liquid thermal diffusion, etc. enable separations to be accomplished which are difficult or unobtainable by other means. It became evident therefore that a text should be available which generalises the treatment to cover all types of separation process, and this is in fact what the author hopes to have achieved here. The list of processes dealt with in the various chapters does not exhaust all possibilities. However, most of the remaining known processes are either of very limited application, or are as yet relatively undeveloped.

Although the book is fairly advanced in coverage, selected material can be used as the basis for a course for final year chemical engineering students. It should also be of particular interest to research workers, both in stimulating applications of the various processes to hitherto unachieved separations, and in development of entirely new types of separation process. Although not intended to be used as a design manual, it should prove of great value to practising chemical engineers and plant designers in providing a basic understanding of the principles involved in the design of equipment for these processes.

ELSEVIER PUBLISHING COMPANY

AMSTERDAM LONDON NEW YORK